BIOCHEMICAL AND STRUCTURAL STUDIES OF p62/SQSTM1 AND THE BECLIN1-UVRAG INTERACTION IN AUTOPHAGY AND ENDOSOMAL TRAFFICKING

WU SHUAI

Ph.D

The Hong Kong Polytechnic University

2017

The Hong Kong Polytechnic University

.

Department of Applied Biology and Chemical Technology

Biochemical and Structural Studies of p62/SQSTM1 and the Beclin1-UVRAG Interaction in Autophagy and Endosomal Trafficking

WU Shuai

A thesis submitted in partial fulfillment of the requirements for the degree of Doctor of Philosophy

April 2016

CERTIFICATE OF ORIGINALITY

I hereby declare that this thesis is my own work and that, to the best of my knowledge and belief, it reproduces no material previously published or written nor material which has been accepted for the award of any other degree or diploma, except where due acknowledgement has been made in the text.

----------(Signed)

WU Shuai (Name of student)

Abstract

Autophagy is an evolutionarily conserved cellular process that traffics cytosolic contents to lysosomes for degradation and recycling. This process plays a critical role in maintaining cellular homeostasis and its malfunction has been implicated in the pathogenesis of multiple human diseases. There is intense interest to understand the molecular mechanism of autophagy execution and regulation with the long-term goal to target this process for novel disease-modifying therapies.

My thesis reports the biochemical and structural studies of two important components of the autophagy machinery, i.e. the autophagy receptor protein p62/SQSTM1 and the Beclin1-UVRAG interaction within the VPS34 lipid kinase complex.

The first part of my thesis focuses on p62/SQSTM1, a scaffolding protein that serves as a receptor in the selective autophagy process by binding to ubiquitinated substrates. This activity relies on its C-terminal ubiquitin-associated (UBA) domain, a small motif that binds to ubiquitin with moderate affinity. Cell biology study from our collaborator's lab reveals that ULK1, a serine/threonine kinase critical for autophagy induction, phosphorylates the UBA domain at S409. Such phosphorylation enhances p62's association with ubiquitinated substrates to promote their clearance

through autophagy. My thesis has summarized our biochemical and structural studies to delineate the molecular details of how S409 phosphorylation leads to enhanced UBA- ubiquitin (Ub) binding. Our data reveal that the phosphorylation mimicking mutation S409E destabilizes the UBA dimer interface and promotes its transition to the monomeric form that suitable for Ub binding. Furthermore we have identified K422 as another critical residue for UBA dimer interface and our preliminary data shows that post-translational modification at this site may lead to enhanced Ub binding in similar manner to S409 phosphorylation. Thus modulating the UBA dimer stability may be a strategy to regulate p62-dependent selective autophagy.

The second part of my thesis reports our work on the Beclin1-UVRAG interaction. These two proteins are tightly associated to form the regulatory arm of the mammalian Vps34 Complex II. They serve to stabilize the otherwise structurally dynamic Vps34-Vps15 catalytic arm and up-regulate its lipid kinase activity to promote autophagosome biogenesis. Our structural study of the Beclin1-UVRAG complex reveals a tightly packed coiled coil interface that is strengthened by complementary features on Beclin1 and UVRAG respectively. The notable high affinity of the Beclin1-UVRAG interaction is further confirmed by *in vitro* and *in vivo* studies. The functional significance of this strong association in regulating autophagy and endosomal trafficking has been investigated by cell-based autophagy assays and EGFR degradation experiment. Our results show that the affinity of the Beclin1-UVRAG interaction is particularly important for the endosomal trafficking process.

Furthermore, using the Beclin1-UVRAG structure as guidance we designed a series of stapled peptides with the aim to promote the Beclin1-UVRAG interaction and to enhance autophagy and endosomal trafficking. Our data show that these rationally designed stapled peptides can bind to Beclin1 *in vitro*, enhance autophagic flux and accelerate EGFR degradation in cell-based assays. These findings highlight the exciting possibility that modulating the Beclin1-UVRAG interaction can potentially serve as a novel approach in quest for autophagy-targeting therapies.

Publications arising from the thesis

Lim J, Lachenmayer ML, **Wu S**, Liu WC, Kundu M, Wang R, et al. (2015) Proteotoxic Stress Induces Phosphorylation of p62/SQSTM1 by ULK1 to Regulate Selective Autophagic Clearance of Protein Aggregates. PLoS Genet 11(2): e1004987.

Wu S, He YJ, Yang WC, Liu WC, Li XH, Qiu XX, Li Y, Shen HM, Wang RX, Yue ZY, and Zhao YX. Potent Beclin1-UVRAG interaction via coiled coil region is critical to promote Vps34-dependent endocytic trafficking and can be targeted for modulation. (Paper submitted)

Wu S, Liu WC, Lim J, Yue ZY and Zhao YX. p62/SQSTM1 UBA phosphorylation and its implication in cancer. International Symposium on "Frontiers in Cancer Biology and Drug Development", The Hong Kong Polytechnic University, Hong Kong, March 12th-13th, 2015.

Wu S, Liu WC, Lim J, Lachenmayer ML, Yue ZY and Zhao YX. S409 Phosphorylation in p62 UBA domain by ULK1 enhances its interaction with ubiquitin by destabilizing the dimer interface. Autophagy (E6) of Keystone Symposia on Molecular and Cellular Biology. Beaver Run Resort, Breckenridge, Colorado, USA, June 19th-24th, 2015 (Barrie Hesp Scholarship winner).

Acknowledgements

My foremost and deepest gratitude goes to my supervisor Dr. Zhao Yanxiang for professional guidance, generous support and warmly encouragement given to me throughout the whole course of my PhD studies. Her respect and passion for science, enthusiasm at work, and way of logical and creative thinking have greatly impacted me and I am grateful for what I have learned from her.

I would like to thank all the teammates who worked or still work in the lab. Special thanks to Dr. Li Xiaohua and Dr. Liu Wenchao for helping me to get used to the lab and life in Hong Kong, and teaching me useful experimental techniques. Many thanks to Dr. He Yunjiao and Dr. Pan Xuehua for helping me and sharing of valuable experiences. Thanks to Mrs Sun Lu, who used to serve the lab as a part-time lab manager. It is really pleasure to have Ms. Qiu Xianxiu, Ms. Li Na, Dr. Yang Wenchao, Mr. Yeung Saifeng, Ms. Zhang Xiaozhe and Ms. Gurung Shilpa join and extent our lab family with enthusiasm and energy. My appreciation to Ms. Qiu Xianxiu and Ms. Li Na for helping with much of lab routine work.

I am grateful to Dr. Shen Hanming for giving me the great opportunity to study autophagy assays in his lab at National University of Singapore. Three months of study in Singapore is full of happy memories. Special thanks to Ms. Shi Yin for helping me to get familiar with the lab. Many thanks to Mr. Yeong Bin, Mr. Zhang Jianbin, Mr. Wang Liming, Mr. Ren Yi, Ms Xu Jian, Mr. Cui Jianzhou, Mrs. Zhou Zhihong and

Mrs Yang Naidi for valuable suggestion and help.

Thanks to labmates in Y1208, with whom we shared the lab and worked together for more than two years before we moved to Y704. Many thanks to Dr. Cuiwei, Dr. Hu Shengquan, Mr. Marvin Mark for help.

Finally, I would like to thank my parents and younger brother for generous support and endless love.

Table of contents

CERTIFICATE OF ORIGINALITY i

Abstract ii

Publications arising from the thesis v

Acknowledgements vi

List of Figures xi

List of Tables xiii

List of Abbreviations xiv

Chapter 1. Background introduction 1

1.1. The cellular process of autophagy 1

1.1.1. The initial discovery of autophagy 2

1.1.2. The cellular process of autophagy 6

1.1.3. Classification of autophagy 7

1.1.4. Autophagy in other eukaryotic systems 19

1.2. Molecular machineries that execute the mammalian autophagy process 22

1.2.1. The mTOR complex as a master regulator of autophagy 23

1.2.2. The ULK1 complex to initiate the autophagy process 25

1.2.3. The Atg12-Atg5-Atg16 conjugation system for autophagosome formation 25

1.2.4. Lipidated LC3 as an important marker for autophagosomes 26

1.3. Function of autophagy and its implication in human diseases 27

1.3.1. Autophagy's dual-natured role in cancer 28

1.3.2. Autophagy in neurodegenerative diseases 29

1.3.3. Autophagy in innate immunity 30

1.3.4. Autophagy in development 31

Chapter 2. Biochemical and structural studies of p62/SQSTM1 UBA-Ub interaction 34

2.1. Introduction 34

2.1.1. Selective *vs.* non-selective autophagy 34

2.1.2. The molecular events of selective autophagy 34

2.1.3. p62/SQSTM1 is a crucial receptor for selective autophagy 35

2.1.4. The p62/SQSTM1-Ub interaction is mediated by its UBA domain with dimer-to-monomer transition 36

2.1.5. Casein Kinase 2 phosphorylates p62/SQSTM1 UBA domain on S405 37

2.2. Results 38
2.2.1. S409 is a novel ULK1-mediated phosphorylation site in p62 UBA domain 38
2.2.2. S409 phosphorylation leads to enhanced association between p62 and Ub *in vivo* 41
2.2.3. ULK1-mediated pS409 and CK2-mediated pS405 impact p62-Ub interaction in biochemically distinct ways 42
2.2.4. K422 in UBA domain is a potential novel post-translational modification site to modulate p62-Ub association 50
2.2.5. Super UBA and its interaction with Ub 57
2.3. Discussion 58
2.4. Materials and Methods 61
2.4.1. Plasmid construction 61
2.4.2. Protein Expression and Purification 73
2.4.3. Isothermal Titration Calorimetry (ITC) 84
2.4.4. Size exclusion chromatography (SEC) 84
2.4.5. Static light scattering (SLS) 85
2.4.6. Differential Scanning Calorimetry (DSC) 85
2.4.7. NMR (HSQC) 86
2.4.8. Ub binding assay 86
2.4.9. Crystallization and structure determination 87
Chapter 3. Potent Beclin1-UVRAG interaction via coiled coil region is critical to promote Vps34-dependent endocytic trafficking and can be targeted for modulation 89
3.1. Introduction 89
3.1.1. Atg14L and UVRAG are mutually exclusive binding partners of Beclin1 mediated by their respective coiled coil domains 89
3.1.2. Beclin1 coiled coil domain is a metastable homodimer with an imperfect interface 90
3.1.3. Beclin1 coiled coil domain undergoes dimer-to-monomer transition upon interaction with Atg14L and UVRAG to form heterodimeric coiled coil assembly 91
3.1.4. The Beclin1-UVRAG interaction is critical for autophagy and endocytic trafficking 92
3.1.5. UVRAG impacts endocytic trafficking via interaction with the HOPS complex 95
3.1.6. Functional roles of UVRAG beyond autophagy 96
3.2. Results 97

3.2.1. The Beclin1-UVRAG complex structure reveals a parallel coiled coil assembly 97

3.2.2. The Beclin1-UVRAG interface is significantly stabilized by hydrophobic pairings and electrostatically complementary interactions 98

3.2.3. Potent Beclin1-UVRAG interaction via coiled coil domains is required to promote lysosomal degradation of EGFR but not critical for autophagy 104

3.2.4. Structure-based rational design of Beclin1-targeting stapled peptides 110

3.2.5. Rationally designed stapled peptides promote autophagy and enhance EGFR degradation 119

3.3. Discussion 129

3.4. Materials and Methods 133

3.4.1. Cell Lines and Cell Culture 133

3.4.2. Reagents and Antibodies 134

3.4.5. Immunoblot analysis 135

3.4.6. EGFR degradation assay 136

3.4.7. Autophagy assay by LC3 137

3.4.8. Autophagy assay by p62/SQSTM1 141

3.4.9. Isothermal titration calorimetry (ITC) 141

3.4.9. Static light scattering (SLC) 142

3.4.10. Cell viability assay 143

Chapter 4. Concluding remarks and future perspectives 144

4.1. Further effort to determine the structure of the UBA-Ub complex 144

4.2. Future effort to optimize the potency of the stapled peptides and to test *in vivo* efficacy in EGFR-related cancer models 145

References 147

..... 149

List of Figures

Figure 1.1 Molecular machineries that execute the mammalian autophagy process

Figure 2.1 Schematic representation of p62 and its interacting partners

Figure 2.2 ULK1 phosphorylates p62 at Ser409

Figure 2.3 P-Ser409 is prerequisite for ULK1-mediated p-Ser405

Figure 2.4 S409 phosphorylation promotes p62-Ub association *in vivo*

Figure 2.5 Isothermal Titration Calorimetry (ITC) analysis of binding between UBA S405 or S409 and mono-Ub

Figure 2.6 Crystal structure of UBA S405E

Figure 2.7 Modeling of UBA S405E-Ub interaction

Figure 2.8 S409E does not impact overall folding of UBA in binding to Ub

Figure 2.9 p62 UBA S409E destabilizes p62 UBA dimer thermostability

Figure 2.10 Crystal structure and schematic representation of p62 UBA domain

Figure 2.11 Crystal structure of UBA S409E revealed K422 is important for intermolecular interaction

Figure 2.12 Isothermal Titration Calorimetry (ITC) analysis of binding between UBA K422 mutant and Ub

Figure 2.13 UBA K422A is an Ub-binding monomer

Figure 2.14 K422 is a potential acetylation site in p62 UBA

Figure 2.15 Diagram of phosphodiester bond between nucleotides

Figure 2.16 Diagram of first round PCR in PCR-based cloning

Figure 3.1 Crystal structure of Beclin1-UVRAG coiled coil complex

Figure 3.2 Key residues for Beclin1-UVRAG interaction

Figure 3.3 UVRAG mutations with reduced Beclin1 affinity

Figure 3.4 Co-immunoprecipitation results to characterize the association between Beclin1 and UVRAG Leu-to-Glu mutants *in vivo*

Figure 3.5 Competitive co-immunoprecipitation experiments to compare the *in vivo* potency of Beclin1 association between UVRAG mutants and Atg14L

Figure 3.6 The potent Beclin1-UVRAG interaction is not essential for autophagy

Figure 3.7 The potent Beclin1-UVRAG interaction is important for EGFR degradation in HEK293T cells

Figure 3.8 The potent Beclin1-UVRAG interaction is important for EGFR degradation in A549 non-small cell lung cancer cells

Figure 3.9 The design principle of Beclin1-specific α-helical stapled peptides

Figure 3.10 ITC profile show that Beclin1 with mutation in the C-terminal region of its CC domain (mBeclin1) binds to UVRAG stronger than wild-type

Figure 3.11 Structure-based rational design of stapled peptides to target the Beclin1 coiled coil domain

Figure 3.12 Stapled peptides bind to Beclin1 and make Beclin1 monomeric

Figure 3.13 Peptides on viability of HEK293T and A549

Figure 3.14 Stapled peptide co-localizes with Beclin1

Figure 3.15 Partial co-localization of peptide with LC3

Figure 3.16 Tat-stapled peptide induced GFP-LC3 puncta formation

Figure 3.17 Stapled peptide induced LC3 lipidation

Figure 3.18 Stapled peptide promotes EGFR degradation in HEK293T cell

Figure 3.19 Scheme analysis of autophagy assay by LC3 turnover

Figure 3.20 GFP-LC3 puncta formation under starvation

Figure 4.1 Crystals of UBA K422A- (GS)*6-Ub

List of Tables

Table 2.1 Statistics of diffraction data and structure refinement

Table 2.2 Expression vectors in the lab for protein expression in *E.coli*

Table 2.3 Expression vectors for transient over expression

Table 2.4 PCR reaction composition

Table 2.5 PCR reaction condition

Table 2.6 Purified protein storage

Table 3.1 Computational modeling optimized staple peptides

Table 3.2 Peptide components and stapled peptide

List of Abbreviations

Amp	Ampicillin
ATG	Autophagy-related genes
ATG14L	Autophagy gene 14 like
Bcl-2	B-cell lymphoma/leukemia-2
BH3	Bcl-2 homology 3
β-ME	β-Mercaptoethanol
CCD	Coil-coiled domain
CD	Circular Dichroism
CMA	Chaperone-mediated autophagy
CQ	Chloroquine
DMEM	Dulbecco's Modified Eagle's Medium
DSC	Differential Scanning Calorimetry
DTT	Dithiotheretol
ECD	Evolutionarily-conserved domain
EBSS	Earle's Balanced Salt Solution
EGF	Epidermal Growth Factor
EGFR	Epidermal Growth Factor Receptor
E.coli	*Escherichia coli*
FBS	Fetal Bovine Serum

GFP	Green fluorescence protein
GST	Glutathione-S-Transferase
HRV	Human Rhinovirus
HEK293T	Human Embryonic Kidney 293 cell
HEPES	4-(2-hydroxyethyl)-1-piperazineethanesulfonic acid
hsc70	Heat shock cognate 70
IPTG	Iso-propyl thio-galactoside
ITC	Isothermal Titration Calorimetry
LAMP-2A	Lysosome-associated membrane protein type 2A
LC3	Microtubule associated protein light chain 3
LIR	LC3 interaction region
MCS	Multiple Cloning Site
MW	Molecular Weight
mTOR	Mammalian Target of Rapamycin
MS	Mass Spectrometry
NMR	Nuclear Magnetic Resonance
PAS	Pre-autophagosomal structure
PBS	Phosphate Buffered Saline
PB1	Phox and Bem 1p domain
PCR	Polymerase Chain Reaction
PEG	Polyethylene Glycol
PMSF	Phenylmethanesulfonyl Fluoride

PE	Phosphatidylethanolamine
PI3KC3	Class III Phosphatidylinositol 3-Kinase
PI3P	Phosphatidylinositol 3-phosphate
PS	Penicillin-Streptomycin
p62/SQSTM1	Nucleoporin 62 / Sequestosome 1
RPMI1640	Roswell Park Memorial Institute 1640 medium
SAP	Shrimp Alkaline Phosphatase
SDS-PAGE	Sodium Dodecyl Sulfate Polyacrylamide Gel Electrophoresis
SEC	Size Exclusion Chromatography
SLS	Static Light Scattering
SNAREs	soluble N-ethylmaleimide-sensitive fusion protein attachment receptors
Tris	Tris(hydroxyethyl) Aminomethane
TEMED	N,N,N′,N′ -Tetramethylethylenediamine
TRX	Thioredoxin
UBA	Ubiquitin-associated domain
ULK1	Uncoordinated 51-like kinases
UVRAG	UV irradiation resistance-associated gene
VPS	Vacuolar Protein Sorting
WT	Wild Type

Chapter 1. Background introduction

1.1. The cellular process of autophagy

To survive and maintain homeostasis, cells rely on two distinct cellular processes to degrade and recycle dysfunctional or excessive cellular material, namely the ubiquitin-proteasome pathway and lysosome-autophagy pathway (Korolchuk et al., 2010; Lilienbaum, 2013). Ubiquitin-mediated proteasomal degradation is responsible for breaking down and recycling majority of the short-lived or abnormally folded proteins to maintain healthy protein turnover in cells (Ding et al., 2007; Glickman and Ciechanover, 2002). Autophagy, on the other hand, is mainly responsible for the lysosomal degradation of bulk and long-lived proteins, protein aggregates, damaged organelles, and other cytoplasmic components (Mizushima, 2007). Autophagy is evolutionarily conserved throughout all eukaryotes, including yeast, plants and mammalian cells. In lower eukaryotes such as yeast, autophagy mainly serves as a survival mechanism during starvation (Reggiori and Klionsky, 2013). However, in higher eukaryotes such as mammals, the role of autophagy has extended beyond this classical aspect. Autophagy helps cells to cope with harsh external environment ranging from nutrition deprivation, temperature fluctuations, radiation and toxic chemical reagents to invading pathogen, as well as internal stresses such as accumulation of aggregated proteins and damaged organelles (Di Bartolomeo et al., 2010). The process responsible for delivering and recycling those diverse cytoplasmic cargos to lysosome for degradation is collectively defined as autophagy.

1.1.1. The initial discovery of autophagy

The word “autophagy” is derived from Greek words “auto” and “phagy”, which means “self” and “to eat” respectively. Early studies on autophagy are mainly based on morphological observations. Lysosome, the most important organelle in autophagy, was discovered by Christian de Duve during the studies on mechanisms of protein degradation (Duve et al., 1955), which uncovered the mystery of intracellular protein degradation process. Soon later, mitochondrion in mouse kidney was found in membrane compartments termed “dense bodies”, which were subsequently presented to lysosome (Clark, 1957; Novikoff, 1959). Several years later, semi-digested mitochondrial and endoplasmic reticulum were observed in membrane-bound structures in hepatocytes of rats with glucagon administration(Ashford and Porter, 1962). Very soon, Christian de Duve at the Ciba Foundation Symposium on Lysosomes used the term “autophagy” to describe the single-membrane or double-membrane vesicles that containing cytoplasm or organelles, and speculated that the smooth endoplasmic reticulum is the origin of membrane (de Duve and Wattiaux, 1966; Duve, 1963). Autophagy was later found to be enhanced in the liver of staved animals (Novikoff AB, 1964) and autophagy-inducing effect of glucagon was also confirmed (Deter et al., 1967; Novikoff AB, 1964). In contrast to glucagon as an autophagy inducer, insulin was demonstrated as autophagy inhibitor(Pfeifer, 1977). 3-methyladenine (3-MA) was also identified later to inhibit autophagy (Seglen and Gordon, 1982). Later on, autophagy was for the first time proved to be regulated by phosphatases and protein kinases (Holen et al., 1992). More discoveries on autophagy

as a versatile degradation pathway were made by studies in yeast and higher eukaryotes onwards.

Although autophagy was initially identified in mammals and has been studied for almost six decades, insights into the molecular mechanism of autophagy has only been made in the past two decades, which was mainly carried out through mutagenesis-based genetic screens in yeast *Saccharomyces cerevisiae*. Ohsumi's group discovered the similarity in morphologic change of yeast vacuoles during autophagy induction induced by various nutritional constituent deprivation (Takeshige et al., 1992). Autophagy-defective mutants in yeast were isolated and their functions in protein degradation upon nitrogen starvation were characterized and confirmed. *Atg1* mutant yeast was found to exhibit impaired protein degradation and loss of cell viability (Tsukada and Ohsumi, 1993). Later, *Atg1* was identified as the first autophagy related gene (*ATG*) in *Saccharomyces cerevisiae* and the encoded ATG1 protein as a novel protein kinase involved in the regulation of autophagic process (Matsuura et al., 1997).

The discovery of *ATG* genes in yeast shed light on the identification and characterization of their counterparts and functional role in higher eukaryotes. In contrast to ATG proteins in yeast that is encoded by a single gene, ATG proteins in higher eukaryotes are often with duplication, which confer increased regulatory complexity of autophagy in mammals. In 1998, Mizushima in Ohsumi's laboratory identified ATG12-ATG5 as a protein conjugation system in human that is well

conserved throughout eukaryotes (Mizushima et al., 1998). Mizushima also found hATG16L as the counterpart of yeast Atg16, which is characterized by a long carboxyl terminal WD repeats. Similar to the function in yeast, hATG16L targets autophagic isolation membrane with ATG12-ATG5 conjugates by forming a dimer (Mizushima et al., 2003). Meanwhile, ATG12-ATG5-ATG16L complex was found only resides on the surface of autophagosome membrane during autophagosome formation and leaves the membrane once the autophagosome formation is completed (Mizushima et al., 2001; Mizushima et al., 2004). These work also suggested that GFP-ATG5 could be served as a marker to track the process of autophagosome formation. In 2000, Yoshimori and colleagues identified microtubule-associated protein 1A/1B-light chain 3 (LC3), a mammalian homologue of the first identified ubiquitin like Atg protein Atg8 that is essential for autophagy in yeast, as another conjugation system in mammals. LC3 is post-translationally processed into cytosolic form LC3-I and subsequently become membrane-bound form LC3-II by hATG4; LC3-II is present in both inside and outside membrane surface of autophagosome and its amount is positively correlated with number of autophagosomes (Kabeya et al., 2000). Therefore, LC3 is used as a marker in autophagy assay.

More *Atg* genes in mammals have been identified in addition to those belongs to the aforementioned two conjugation systems. These include the discovery of two *Atg1* homologues, *ULK1* and *ULK2* in complex with *Atg13* and *FIP200* to mediate autophagy initiation through mTOR signaling (Jung et al., 2009). Target of rapamycin

(Tor) is a serine/threonine kinase in yeast involved in cellular response to nutrition deprivation. Tor phosphorylates protein Tap42 to reduce enzymatic activity of phosphatase 2A (PP2A). Rapamycin inhibition of Tor result in dephosphorization of Tap42 and render it dissociates form PP2A. The free PP2A then dephosphorylates its targets and lead to autophagy induction (Beck and Hall, 1999). mTOR is the mammalian orthologue of Tor, which regulates autophagy activity through similar mechanism (Holen et al., 1992).

Genetic manipulation of *Atg* genes in animal provides a convenient way to study autophagy in mammals. Shortly after the discovery of mice ATG5-ATG12 conjugation system, transgenic mouse expressing green fluorescent protein tagged LC3 (GFP-LC3) was generated to monitor and track autophagosomes formation in animals in response to nutrient starvation (Mizushima et al., 2004). The first *Atg* gene knock-out mouse, the *Atg5* knock-out mouse, was able to survive the embryonic stage but the newborns died in 24 hours after birth (Kuma and Mizushima, 2010). On the contrary, transgenic mouse with Atg5 overexpression showed enhanced autophagy and extended lifespan (Pyo et al., 2013). Beth Levine identified *Beclin 1* as a mammalian homologue of *Atg6*. Studies on *Atg6* suggested that autophagy is involved in tumor progression (Liang et al., 1999). Up to now, at least 9 *Atg* genes have been manipulated in genetically modified mice. The phenotypes of *Atg7*, *Atg9*, *Atg3 and Atg16L* knock-out mice are similar to that of *Atg5*, with newborn died soon after birth. Other genetically modified mice with homozygous knockouts like *Beclin 1*, *FIP200*

and *Ambra1* were unable to have offspring as the embryo died during early embryonic stage (Levine and Kroemer, 2008).

1.1.2. The cellular process of autophagy

The process of macroautophagy (autophagy) is known to be controlled by a series of autophagy-related –genes (Atgs) encoded proteins in a coordinated manner. These Atg proteins are involved in three conservative stages of autophagy process, namely 1) the early stage, where autophagy is initiated; 2) the middle stage, in which the autophagosome with engulfed contents is formed through nucleation, expansion and elongation steps; 3) the late stage, where autophagosomes are fuse with lysosomes and 4) the last stage, where contents are degraded for recycling. Nutrition starvation is the most typical and strong trigger of autophagy, and any types of essential nutrient starvation could induce autophagy. Nitrogen starvation is the most potent stimuli in yeast. Depletion of total amino acids in mammals strongly induced autophagy. Central to autophagy is the formation of double-membrane vesicles known as autophagosomes. In yeast, autophagosomes is likely to be initiated at phagophore assembly site (PAS) and controlled by the Atg1: Atg13: Atg17 complex (Cheong et al., 2008). In mammals, there is no clear evidence for mammalian equivalent of PAS so far, but the autophagy initiation process is under control of ULK1:Atg13:FIP200 complex (Ganley et al., 2009; Jung et al., 2009). Macroautophagy and other types of autophagy will be discussed in detail in the following section.

1.1.3. Classification of autophagy

Autophagy is a major cellular degradative process that delivers damaged organelles, aggregated proteins, invading pathogens, nucleotides and other cytosolic materials into lysosome for degradation. Autophagy serves as a housekeeper through which cytosolic aged and aggregated proteins, or damaged intracellular organelles are delivered to lysosome for degradation. Depending on the way the cytosolic materials reached lysosome for degradation, autophagy can be classified into three types, namely macroautophagy, microautophagy and chaperone-mediated autophagy (CMA) (Mizushima, 2007). Macroautophagy is characterized by the formation of double-membrane organelles that engulf cytosolic contents and passed to lysosome for degradation. Unlike macroautophagy, microautophagy is an autophagic process characterized by direct engulf and invagination of cytosolic materials into lumen by lysosome/vacuole for degradation without the formation of autophagosome. In contrast, CMA is collectively known as the degradative processes mediated by chaperones and lysosomal-associated membrane protein type 2A (LAMP 2A) on lysosome (Kaushik and Cuervo, 2012). The macroautophagy and other two types of autophagy will be introduced in detail in this section.

1.1.3.1. Macroautophagy

Macroautophagy is a “self-eating” process that is characterized by the formation of double-membrane autophagosome with engulfed cytosolic materials for lysosomal degradation. It is the primary and most extensively studied autophagic pathway that is

evolutionally conserved from yeast to plants and animals (Mizushima and Komatsu, 2011; Reggiori and Klionsky, 2013; Suzuki and Ohsumi, 2007). The term “autophagy” is used to describe macroautophagy unless otherwise noted. The balance between biosynthesis and degradation of cellular components, as well as invading pathogens is of great importance for cellular homeostasis and health (Mizushima and Komatsu, 2011). Under starvation conditions, autophagosomes enclose a portion of the cytoplasm and subsequently fuse with lysosome to be degraded. Autophagy is widely involved in diverse physiological processes including cell growth, differentiation and development, and pathological conditions like neurodegeneration diseases, myopathies, aging and cancer (Choi et al., 2013). Autophagy has a large number of substrates ranging from aggregated proteins, lipid droplets and dysfunctional organelles like damaged mitochondrial, to invading microbes. Autophagy encompasses both nonselective bulk degradation of cytoplasmic contents as well as selective degradation of specific cellular components (Suzuki, 2013; Weidberg et al., 2011). The nonselective bulk degradation role of autophagy was indicated by the observation that hepatocytic cytosol enzymes with different half-life were sequestered for degradation at the same rate (PO et al., 1990). Growing body of evidence suggested that autophagy specificity could be achieved by a variety of autophagy receptor proteins. Depending on the specific cargos to be degraded, selective autophagy can be sub-divided based on the type of the cargos. Mitophagy is used for the selective degradation of damaged or stressed mitochondrial that was firstly described more than 10 years ago (Lemasters and J., 2005), and was recently reported to be linked to

PINK1-Parkin pathway (Vincow et al., 2013). Lipophagy is the specific lysosomal clearance of lipid droplets by autophagy (Singh et al., 2009). Ribophagy is the selective degradation of ribosomes that was firstly described in *Saccharomyces cerevisiae* that requires catalytic activity of Ubp3p/Bre5p and ubiquitin protease for fully functioning (Kraft et al., 2008). Many more selective autophagy has been reported on clearance of protein aggregates (aggrephagy), peroxisomes (pexophagy), bacterial (xenophagy), etc (Shaid et al., 2013).

1.1.3.2. Chaperone-mediated autophagy

Chaperone-mediated autophagy (CMA) is a lysosomal degradation pathway through which soluble cytosolic proteins are specifically selected by chaperones and targeted to lysosome membrane for direct translocation into the lysosomal lumen for degradation (Kaushik and Cuervo, 2012). Unlike microautophagy, which pass proteins by vesicles that formed through the invagination of lysosomal membrane, CMA targets specific cytosolic proteins through a motif within their amino acid sequence (Fred Dice, 1990) and pass the lysosomal membrane without vesicle formation. These unique features of CMA allows selective removal of individual proteins, not only for damaged proteins but also for physiologically active proteins such as enzymes and transcription factors (Kaushik and Cuervo, 2012).

Discovery and steps of CMA

Selective degradation of cytosolic proteins in lysosome was initially observed

with different rates (Dice et al., 1978). This phenomenon was further confirmed by the findings that starvation increased the lysosomal degradation of some proteins micro-injected into the cytosol of human diploid fibroblasts, but not other proteins (Auteri et al., 1983). Later, enzymatic fragmentation of a protein susceptible to starvation-induced lysosomal degradation led to the finding of a penta-peptide within the protein that is required for degradation (Agarraberes and Dice, 2001; Backer et al., 1983; Backer and Dice, 1986). This penta-peptide was found as the binding site within the protein for interaction with cytosolic chaperone hsc70 (Chiang and Dice, 1988), and the binding was proved as required for the lysosomal degradation of the protein (HL et al., 1989). What further make CMA distinct from other lysosomal degradation pathways is the substrate of CMA could get across the lysosome membrane directly without formation of autophagosomes (as in macroautophagy) and invagination of lysosome membrane (as in microautophagy) (Cuervo et al., 1994; Terlecky et al., 1992). These findings indicate that CMA might represent a new type of lysosomal degradation pathway. Isolated lysosome is a useful tool for *in vitro* study of CMA and identification of lysosomal proteins that mediated substrate binding and uptake. Extensive studies by using isolated lysosome found that CMA can be saturated by substrates and requires special proteins on lysosomal membrane (Cuervo et al., 1995; Cuervo et al., 1994).

CMA is a multi-step process, including substrate recognition, lysosomal targeting, substrate binding and unfolding, substrate translocation and substrate degradation in

lysosome. Substrate recognition is carried out in cell cytosol with the help of chaperone hsc70 (heat shock-cognate protein of 70KDa), which binds to the penta-peptide motif within the substrate proteins (HL et al., 1989). The amino acid constitutions of the pent-peptide motif possess some distinct features. Among the five residues, the first or the last amino acid in the sequence should be glutamine (Q); The motif should also contain one of two positively charged residues lysine (K) or arginine (R); one of the two negatively charged residues aspartic acid (D) or glutamic acid (E), one of the four hydrophobic residues leucine (L), isoleucine (I), phenylalanine (F) or valine (V), and the last residues should be either positive or hydrophobic residues listed above (Fred Dice, 1990). It is the amino acid charge that made the CMA penta-peptide motif special. Based on that, it is possible to create a complete penta-peptide motif out of incomplete four-amino acid peptide by posttranslational modifications such as acetylation, phosphorylation or even mutation. The discovery of acetylation modification of glycolytic enzymes promotes its lysosomal degradation via CMA might support this speculation (Lv et al., 2011).

Once bound to chaperone hsc70，the substrate is targeted to the cytosolic tail of lysosome-associated membrane protein type 2A (LAMP-2A) located on the surface of the lysosome membrane (Cuervo and Dice, 1996). Substrate-binding drives LAMP-2A undergoing oligomerization and also in association with other proteins to form a complex for substrate translocation (Bandyopadhyay et al., 2008). Although how multimerization of LAMP2A contributes to substrate internalization is not fully

understood, a GXXG motif in transmembrane region of LAMP-2A protein was regarded as necessary for this process as mutations on this motif blocked multimerization and CMA (Bandyopadhyay et al., 2008). The formation of the complex is dynamic and the complex stability is maintained through its interaction with hsp90 located inside lysosome (Bandyopadhyay et al., 2008). In order to get cross the lysosomal membrane, CMA substrates needs to undergo unfolding, although it is not required for substrate binding to LAMP-2A (Salvador et al., 2000). The substrate unfolding is likely to be mediated by hsc70 and some co-chaperones located on the lysosomal membrane, and the unfolding process is completed before the fully formation of the LAMP-2A translation complex. Sooner after the substrates be translocated into the lysosomal lumen, LAMP-2A disassembles from the translocation complex as monomers. Lysosomal hsc70 (lys-hsc70), which functions inside lysosome, was reported to be required for the substrate protein translocation (Agarraberes and Dice, 2001). Lys-hsc70 itself is a CMA substrate but its presence in the lysosome is not likely due to CMA, as CMA blockage does not affect the level of hsc70 in lysosome. It is possible that hsc70 reaches lysosome by internalization as multi-vesicular bodies from late endosomes through endosomal-lysosomal fusion. After the substrate proteins been translocated into the lysosomal lumen, they are subjected to proteolysis for degradation and recycling.

Physiological functions of CMA

The dependence of LAMP-2A for translocation of substrate proteins from cytosol

to lysosomal lumen makes CMA special. The activity of CMA is directly relied on the availability of LAMP-2A on the lysosomal membrane. CMA was firstly proposed to be important for protein recycling during long term starvation(Cuervo et al., 1995). CMA activation requires prolonged starvation (8-10h) and the elevated CMA activity is last for up to three days after starvation withdraw (Cuervo et al., 1995; Massey et al., 2006). CMA also functions in quality control for the cell. CMA activity is up regulated under oxidative stress, through which the oxidatively damaged proteins are degraded (Kiffin et al., 2004). Other conditions that lead to protein damage and cell stress like toxic compounds exposure or hypoxia can also induce CMA (Cuervo et al., 1995; Dohi et al., 2012). Chemical enhancer of CMA has also been reported, which might serves as a potential therapy in cell dysfunction and disease result from reduced CMA activity (Anguiano et al., 2013). Limited progress has been made in identification of specific inhibitors of CMA. To date, in order to block CMA, the best way is to down regulate LAMP-2A by knock-down or knock-out, as LAMP-2A is currently found to be dedicated in CMA.

Pathology of CMA

Malfunction of CMA contributes to the progression of several human disorders. Both reduced and enhanced CMA activities have been proved to cause diseases. Neurodegenerative diseases are often related to diminished function of CMA. The reduced activity of CMA fails to timely and efficiently elimination of pathogenic proteins, thus lead to the precipitation of protein aggregates that easily cause neuronal

demise.

Parkinson's disease (PD) is closely related to malfunction of CMA. PD is characterized by the selective loss of dopaminergic neurons and related motor deficits. The mutation of α-synuclein genes in familial PD, together with the aggregation of α-synuclein in Lewy bodies in sporadic PD, placed α-synuclein at the center of PD pathogenesis. In familial PD, CMA-targeting motifs are mutated in α-synuclein (A30P and A53T mutants), which prevents its translocation into lysosomal lumen for degradation (Cuervo et al., 2004; Orenstein et al., 2013). Although mutated α-synuclein can be recognized by hsc70 and successfully delivered to the lysosomal membrane for LAMP-2A binding, the abnormally high affinity of the pathogenic α-synuclein and lysosomal surface LAMP-2A result in failed translocation of α-synuclein across the lysosomal membrane (Cuervo et al., 2004). This abnormal high affinity and failed translocation not only prevents its own degradation but also occupied CMA transporter LAMP-2A, thus inhibits clearance of other proteins through CMA. Sporadic PD, which accounts for the majority of the PD cases, has also been reported to link with alterations in CMA function. Unfavorable post-modifications on α-synuclein by cellular stress and other environmental factors result in reduced degradation of α-synuclein through CMA. Dopamine-modified α-synuclein is also abnormal in degradation by CMA. The tight binding of dopamine-modified α-synuclein with LAMP-2A and inefficient translocation of it across the lysosomal membrane lead to accumulation of toxic α-synuclein on lysosome membrane and

inhibited degradation of other CMA substrates. Some recent studies found that even abnormal high level of α-synuclein without noticeable post-translational modifications has inhibitory effect on CMA (Orenstein et al., 2013). Malfunction of CMA in the pathogenesis of PD is further proved by studies on expression level of CMA components. In advanced stage of PD, reduced level of LAMP-2A and hsc70 have been observed in the dopaminergic neurons of human brain (Alvarez-Erviti et al., 2010). Two novel sequence variants were identified on the promoter region of LAMP-2A gene in sporadic PD patients, which might contribute to PD onset through reduced LAMP-2A protein expression (Pang et al., 2012). It is also reported that the deregulation of microRNA underlies the down regulation of CMA components, including LAMP-2A (Alvarez-Erviti et al., 2013).

Alzheimer disease (AD) is another neuronal disease linked to CMA activity. It is a chronic neurodegenerative disease that is characterized by symptoms like impaired memory and disturbances in language, reasoning and perception. The disease is closely associated with amyloid plaques and neurofibrillary tangles in the brain (Ballard et al., 2011). AD pathogenesis is triggered by over production or failure of clearance of amyloid-β peptide, which self-aggregates into oligomers that cause modification of Tau proteins and dysregulation of other neuronal related signaling pathways. Tau protein aggregation and cleavage are two hallmarks for AD. CMA plays a role in delivery of normal Tau protein across lysosomal membrane for degradation. However, mutated Tau protein bound to the LAMP-2A is cleaved but

only partially translocated into lysosomal lumen, leaving smaller Tau fragments oligomerized directly on the lysosomal membrane, which lead to disruption of lysosomal membrane integrity and blocks CMA degradation of other proteins (Ballard et al., 2011). Released mutant toxic Tau fragments oligomers could serve as nucleation center to induce further Tau aggregation in cytosol.

While CMA deficiency and malfunction underlie many neurodegenerative diseases, up regulation of CMA has been implicated in the progression of cancer (Kon et al., 2011; Lv et al., 2011; Saha, 2012). Basal CMA activity in different types of breast cancer cells was consistently up-regulated, regardless the status of macroautophagy (Kon et al., 2011). The increased CMA activity is mostly due to aberrant up-regulation of LAMP-2A expression in these cancer cells. For cancer cells, the up-regulated LAMP-2A expression and CMA activity is able to sustain glycolysis to provide energy for rapid cancer cell proliferation. Although the mechanism for CMA up-regulation in cancer development is not clear, microRNA deregulation of CMA components in neurodegeneration may underlie LAMP-2A over-expression in cancer (Alvarez-Erviti et al., 2013). Breast cancer cells with LAMP-2A deficiency exhibit increased sensitivity to drug treatment. Knockdown of LAMP-2A in cancer cells reduced cancer cell proliferation and metastasis (Kon et al., 2011). Blockage of CMA can either reduces at the transcriptional level of some rate-limiting glycolytic enzymes, or decreases those enzymes at protein level directly, thus suppress cancer cell growth. In breast cancer, CMA blockage promotes generation of ROS, which

subsequently induced apoptosis in cancer cells. Blockage of CMA in mice implanted with human lung cancer xenograft not only delayed xenograft growth and reduced cancer metastasis, but also induced regression of existing xenografts (Kon et al., 2011). At the same time, there are side effects of CMA blockage in cancer treatment, part of the negative effects is reduced cytosol quality control, which might lead to accumulation of oxidized and aggregated proteins normally degraded by CMA (Ali et al., 2011; Saha, 2012). In summary, the relationship between CMA and cancer development is complicated. The dependence of CMA in cancer development suggests a pro-oncogenic role of CMA, while effective CMA ability is beneficial in normal cells and patient with neurodegenerative diseases.

1.1.3.3. Microautophagy

The term microautophagy was proposed by Christian de Duve and Wattiaux in 1960s (Duve and Wattiaux, 1966). It was firstly used to describe the hypothetical notion back then that tiny part of the mammalian cell cytoplasm could be directly engulfed by lysosomes membrane and digested in lysosome. Later, researchers used microautophagy to describe non-selective lysosomal/vacuolar uptake and degradation of cytosolic components. In the past two decades, much understanding on microautophagy has been gained through the studies of yeast mutants, including proteins involved in the micro-autophagic formation and subsequent events. Microautophagy is usually described in four sequential stages and they are summarized as follow.

Microautophagic invagination and autophagic tubes formation

Microautophagic invagination process is started with bulge of membrane on the surface of lysosome/vacuole that initiates by lateral segregation of lipids or exclusion of large transmembrane protein. Although invagination is a constitutive process, its activity is greatly enhanced by starvation. The highly extension of membrane invagination exhibit a characteristic tubular shape that termed as “autophagic tube”, from which vesicles bud off into the lumen of lysosome/vacuole (Müller et al., 2000). The composition of the lysosomal/vacuolar membrane changes as the vesicles consumes portion of the lysosomal/vacuolar membrane (Li et al., 2012a). Atg7-dependent ubiquitin-like conjugation (Ublc) pathways are involved in the formation of autophagic tubes (Doelling et al., 2002). In addition, the vacuolar transporter chaperone (VTC) complex plays an important role in autophagic tube formation in yeast (Uttenweiler et al., 2005). However, the driving force behind the vacuolar membrane invagination is still unclear.

Vesicle formation

High density of lipids and low density of proteins induced the invagination of autophagic tubes through the lateral sorting mechanism (Müller et al., 2000), which facilitates vesicle formation (Müller et al., 2000). Vesicle in microautophagy is the functional equivalent of autophagosome in macroautophagy. Unlike other conventional SNARE-mediated fusion, which requires the involvement of SNARE

proteins, vesicle formation in microautophagy is generally independent of those proteins.

Vesicle expansion and scission

After the vesicles are formed on the top of the autophagic tubes, they further grow to form pre-vesicular structure that is highly dynamic. The vesicle expansion is mediated by binding to enzymes located at the inner surface of unsealed vesicle without the involvement of SNARE proteins (Tian et al., 2010). The subsequent scission and release of vesicle from the tube into the vascular lumen is driven by the GTPase activity and membrane potential (Müller et al., 2003). V-ATPase pumps H^+ into the lumen to acidify the vacuolar lumen and establishes membrane potential across the vacuolar membrane, which is indispensable for membrane fusion.

Vesicle degradation and recycling

The released vesicles into the lumen are degraded by Atg15p and other hydrolyses (Epple et al., 2001) and the nutrients and energy are recycled by permease Atg22p (Yang and Klionsky, 2007).

1.1.4. Autophagy in other eukaryotic systems

1.1.4.1. Autophagy in yeast

Yeast is one of the simplest eukaryotic organisms but possess many essential

cellular processes similar to human. Yeast is the first eukaryotic organism to have its genome sequenced, which paved the way to study all the information encoded in the organism's genetic blueprint. Therefore it is an important organism to study the basic molecular processes in humans, including autophagy. Autophagy in yeast involves the delivery of cytoplasmic components into vacuole for degradation and recycling of the resulting degradation products. While nitrogen starvation is the strongest stimuli to induce rapid and robust autophagy in yeast, deprivation of carbon source, auxotrophic amino acids or nucleic acids can also induce autophagy, albeit in a much lower extent.(Takeshige； et al., 1992). Upon autophagy induction, portion of the cytoplasm is sequestered into double-membrane vesicles called autophagosomes that is synthesized from *de novo* synthesis (Baba et al., 1994). The completed autophagosomes are subsequently docked and fused with vacuoles to release the single-membrane vesicles or autophagic bodies for hydrolase degradation. Finally, the content is degraded and recycled. While the morphology of autophagy was first characterized in mammals, almost all the *ATG* genes were initially isolated in yeast, such as *Saccharomyces cerevisiae*, *Hansenula polymorpha*, and *Pichia pastoris.* The relative simplicity of genetic manipulation on them (Fry et al., 2006), shed light to the identification of their mammals orthologues later on (Levine and Klionsky, 2004). Analyses of yeast atg mutants lead to characterization atg involving in different autophagic process, such as Atg1 in regulation of autophagy induction, Atg19, Atg11 and Atg8 in cargo packaging, Vps34 in vesicle nucleation, Atg8 and Arg12-Atg5 conjugation systems in vesicle expansion, Atg9, Atg 2 and Atg18 in components

retrieval and Atg15 in vesicle breakdown (Levine and Klionsky, 2004; Wang and Klionsky, 2003).

1.1.4.2. Autophagy in plants

Autophagy is a highly evolutionarily conserved cellular degradation mechanism in eukaryotes, including mammals, yeast, drosophila and plants, whereby cytoplasmic components are engulfed in double-membraned autophagosome and are delivered to lysosome (mammals) and vacuoles (yeast and plants) for degradation and recycling (Kwon and Park, 2008). Recently, studies uncovered the involvement of autophagy in multiple aspects of plant life, including seeding establishment, plant development, stress resistance, metabolism and reproduction (Michaeli et al., 2015). The flowering plant *Arabidopsis thaliana* is an important model system for identifying genes and determining their functions in plants due to the unique feature of genome, such as a short generation time, small size, large number of offspring, and a relatively small nuclear genome (initiative, 2000). *Arabidopsis thaliana* is the first plant to have its genome sequenced and is widely used as a model system for autophagy study. The model plant used in autophagy study has expanded from *Arabidopsis thaliana* to more photosynthetic organisms, such as aquatic photosynthetic eukaryotes (Pérez-Pérez et al., 2010; Ramundo et al., 2014; Shemi et al., 2015), gymnosperms (Minina et al., 2013) and angiosperms (Yue et al., 2015). There are also new evidence regarding the role of autophagy in plant cell survival (Avin-Wittenberg et al., 2015) and cell death (Minina et al., 2014). In plants, ATG1/13 complex was shown to be important for the

existence of autophagic bodies in the vacuole, but not for ATG5 and ATG8 modification, suggesting the complex is involved solely in autophagosome enclosure, the advanced steps of autophagy (Li et al., 2014). Crosstalk has been found between metabolic enzymes and autophagy in plants, as glyceraldehyde-3-phosphate dehydrogenase (GAPDH) was shown to play a role in restraining autophagy in addition to glycolysis (Henry et al., 2015). Most selective autophagy processes in metazoans act in plants as well. Nevertheless, autophagy in plant is also involved the clearance of plant-specific compartments, such as chloroplasts (Xie et al., 2015). While NBR1 and p62 function independently as cargo receptor for selective autophagy in mammals, *Arabidopsis* cargo receptor AtNBR1 is a functional hybrid of NBR1 and p62. Effort to discover additional plant cargo receptors led to the characterization of TSPO pathway, plastid ATI1 pathway and RPN10 pathway and their role as new plant cargo receptors (Michaeli et al., 2015).

1.2. Molecular machineries that execute the mammalian autophagy process

The molecular machineries of autophagy in mammalian cells are under the control of three systems. The first system is centered upon the mammalian homologue of Atg1, the ULK1/ULK2, which is under the control of the upstream nutritional regulator mTOR and cellular energy sensor/regulator AMPK (Egan et al., 2011) The second system is represents by two important ubiquitin-like conjugation systems, the Atg12 conjugation system and LC3/GABARAP conjugation system, through which

Atg12 and LC3 are conjugated to targets via several sequential enzymatic processes similar to protein ubiquitination (Mizushima et al., 2011). The third system is centered on Beclin1, which functions as a scaffold protein to interact with many proteins such Vps34, Atg14L, UVRAG, et al (He and Levine, 2010).

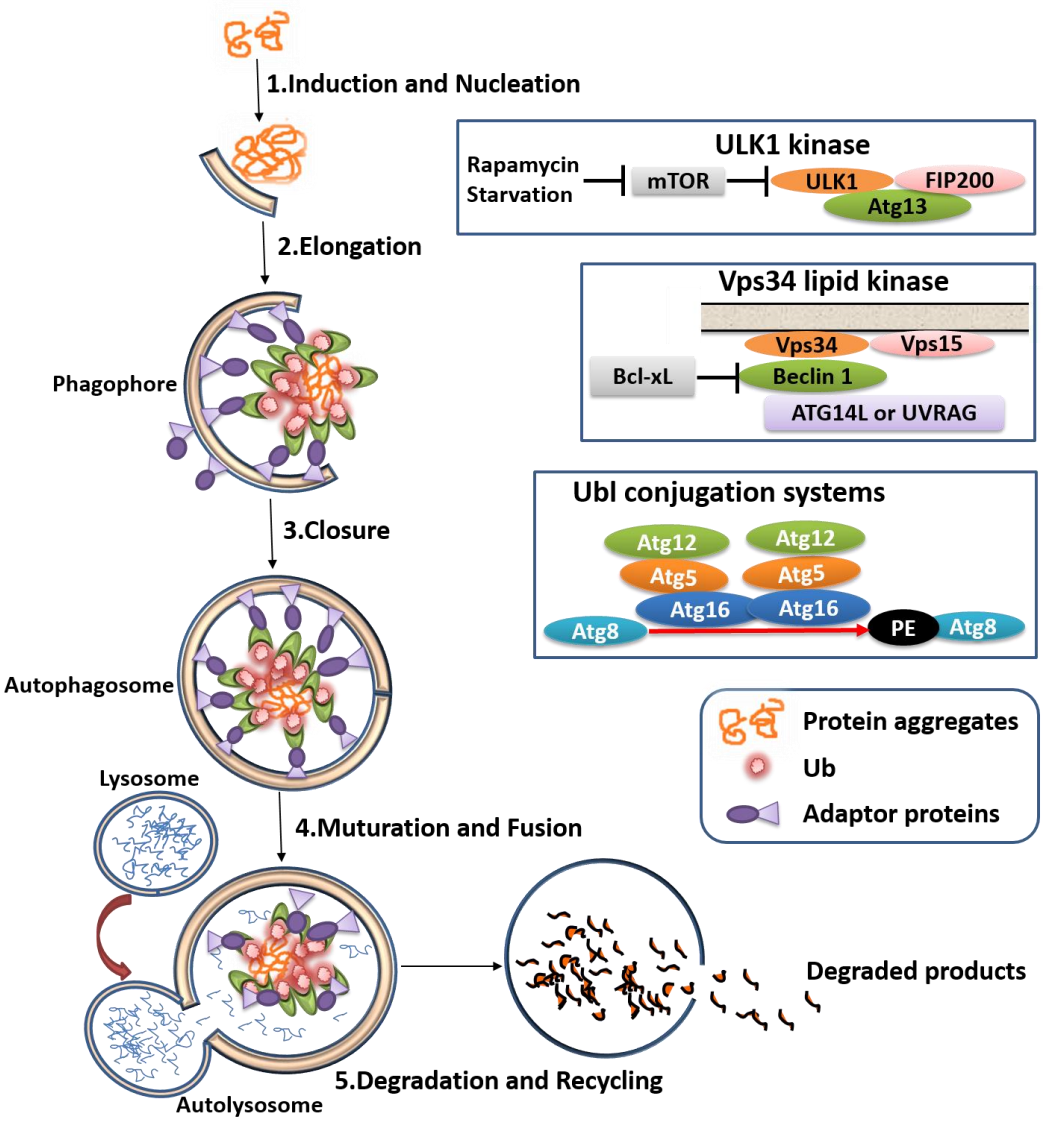

Figure 1.1 Molecular machineries that execute the mammalian autophagy process

1.2.1. The mTOR complex as a master regulator of autophagy

mTOR or mammalian target of rapamycin, a evolutionarily-conserved

serine/threonine protein kinase with molecular size near 300kDa, is a master regulator of cellular metabolism and promotes cell growth in response to environmental cues. The activity of mTOR is inhibited under nutrient starvation, which is crucial for autophagy induction in eukaryotes (Noda and Ohsumi, 1998; Scott et al., 2004). mTOR forms two distinct signaling complexes, mTOR complex 1 (mTORC1) and mTORC2, by binding with multiple companion proteins. RAPTOR and PRAS40 are specific to mTORC1 (Haar et al., 2007; Hara et al., 2002; Sancak et al., 2007; Thedieck et al., 2007; Wang et al., 2007) whereas RICTOR, mSin1, and PROCTOR1/2 are specific to mTORC2 (Dos et al., 2004; Frias et al., 2006; Jacinto et al., 2006; Pearce et al., 2007). Both complexes have distinct substrate preference and therefore carry out specific downstream signaling events to modulate cellular function. Most of the autophagy induction conditions, such as nutrition deprivation or low cellular energy levels have been shown to inhibit mTORC1 activity (Kim and Guan, 2015). Amino acids are crucial regulator of mTORC1. Rag proteins (RagA/B/C/D) are key mediators of amino acid–induced mTORC1 activation by interacting with key component RAPTOR of mTORC1 (Kim et al., 2008; Sancak et al., 2008). The mammalian ULK1/2 complex are the major autophagy initiator. The complex contains ULK1/2 (mammalian homologs of Atg1), ATG13 (a mammalian homolog of Atg13), RBC1CC1/FIP200 (focal adhesion kinase family interacting protein of 200 kDa, a putative mammalian homolog of Atg17) and ATG101 (not conserved in *S.cerevisiae*) (Hara et al., 2008; Hosokawa et al., 2009a; Hosokawa et al., 2009b; Mercer et al., 2009; Mizushima, 2010). Among them, ULK1/2 and ATG13 are regarded as direct effectors

of mTORC1.

1.2.2. The ULK1 complex to initiate the autophagy process

mTORC1 phosphorylates both ULK1/2 and ATG13 under nutrient-enriched conditions to inhibit autophagy initiation. On the contrary, upon amino acid starvation mTORC1 is released from ULK1/2 complex, leading to dephosphorylation of ULK1/2 and ATG13, which in turn initiates autophagy. The dephosphorylation of ULK1/2 by phosphatase, such as PP2A-B55α complex upon starvation condition (Wong et al., 2015), activates ULK1/2, which subsequently phosphorylates RBC1CC1/ATG13, and presumably AMBRA1 and Beclin1 to promote autophagy (Alers et al., 2012). Moreover, activated ULK1/2 phosphorylates FIP200, which is required for autophagosome formation in mammalian cells (Hara et al., 2008) (Jung et al., 2009). Under glucose starvation conditions, AMPK induced autophagy by direct phosphorylation on ULK1. In glucose-rich conditions, mTORC1 inhibits ULK1 and ATG13 through phosphorylation, which disrupts interaction between ULK1 and AMPK, so as to inhibit autophagy (Kim et al., 2011a).

1.2.3. The Atg12-Atg5-Atg16 conjugation system for autophagosome formation

The ubiquitin-like (Ubl) protein conjugation systems are conserved from yeast to mammals. There are two Ubl conjugation systems, namely Atg12-Atg5 conjugation

system and Atg8 lipidation system. Atg12 is the first identified ubiquitin-like protein and synthesized as active (Mizushima et al., 1998). E1 enzyme Atg7 activates Atg12 and transfer it to E2 enzyme Atg10 before conjugated with Atg5 to form Atg12-Atg5 conjugate. Atg16 forms a dimer and is essential for dimerization of Atg12-Atg5 conjugates through interaction with Atg5 (Kuma et al., 2002; Shintani et al., 1999). Unlike Atg12, Atg8 is synthesized as a precursor, which is processed by protease Atg4 to expose carboxyl terminal glycine. To carry out lipidation function, the processed Atg8 is firstly activated by E1 enzyme Atg7, and then transferred to E2 enzyme Atg3 before conjugated with membrane lipid phosphatidylethanolamine (PE) to form Atg8-PE (Kirisako et al., 2000). The Atg12-Atg5-Ath16 conjugate is reported to possess E3- activity and functions as an E3 enzyme to mediate Atg8 conjugation reaction with lipid PE (phosphatidylethanolamine) (Hanada et al., 2007). In addition, the Atg12-Atg5-Atg16 conjugate is also reported to enhance the E2 activity of Atg3 and specifies the site of Atg8-PE production to the autophagy-related membranes.(Nakatogawa, 2013; Sakoh-Nakatogawa et al., 2013).

1.2.4. Lipidated LC3 as an important marker for autophagosomes

Microtubule-associated light chain 3 (LC3), a mammalian homolog of yeast Atg8 that ubiquitously distributed in mammalian tissues and cultured cells, is the most commonly used autophagy marker. The cytosolic unconjugated form of LC3 proteins are specifically cleaved at the carboxyl terminal by Atg4 to form LC3-I, which has an exposed carboxyl terminal that conjugates to phosphatidylethanolamine (PE) to form

LC3-II. Autophagy is accompanied with the redistribution of LC3-II to autophagosome to form cytoplasmic puncta, which is finally degraded in autolysosomes.

Autophagy is a dynamic process. Autophagy flux is the flow of autophagosome formation, maturation, and the subsequently fusion with lysosome to breakdown cytoplasmic material and organelles and release of macromolecules. There are basically two means to monitor autophagy flux by LC3, one is to measure LC3-II protein level by Western blot, as induced autophagy is accompanied with rapid transition of LC3-I to LC3-II; the other way is to count the number of GFP-LC3 puncta, which denotes the formation of autophagosome during autophagy induction. What is important in autophagy flux assay is that the lysosome inhibitor has to be added in order to rule out the false positive caused by failure of autophagosome-lysosome fusion or lysosome malfunction (Mizushima et al., 2010). Bafilomycin A1 (Baf) blocks autophagosome-lysosome fusion by inhibiting vacuolar H^+ ATPase. Chloroquine (CQ) accumulation prevents acidification of lysosome that fuse with autophagosome, thereby preventing autolysosome formation and degradation.

1.3. Function of autophagy and its implication in human diseases

Given the facts that autophagy is an essential mechanism for survival through

recycling of a variety of cellular components including but not limited to proteins, organelles, lipids, carbohydrates, nucleic acids and infecting microbe, the dysregulated autophagy can be easily linked to diseases. Increasing reports have emerged regarding autophagy dysfunction in diseases, such as cancer, neurodegenerative diseases, infectious diseases, aging and metabolic disease (Levine et al., 2011; Mizushima and Komatsu, 2011; Nixon, 2013; Rubinsztein et al., 2011; White, 2012). Autophagy in cancer, neurodegenerative disease, innate immunity and development will be briefly discussed in the following paragraphs.

1.3.1. Autophagy's dual-natured role in cancer

Cancer is caused by the successive acquisition of mutations and epigenetic changes that override cell failsafe mechanisms such as cell death and cell cycle arrest (Hanahan and Weinberg, 2000; Rosenfeldt and Ryan, 2011). Autophagy has an evolutionarily conserved role in coping with metabolic stress caused by limited nutrients or oxygen. The role of autophagy in various stages of cancer development is different. Studies suggest that autophagy mainly functions as a tumor suppressor in the early stage of tumorigenesis, but once tumor has been developed, solid tumor can utilize autophagy for energy production and survival (Janku et al., 2011; Levine et al., 2011). The mostly studied autophagy related protein in cancer is Beclin1. Beclin1 is the mammalian homologue of yeast Atg6/Vps30 that interacts with class III PI3K. It functions as scaffold protein to recruit downstream autophagic proteins for autophagosomes formation (He and Levine, 2010; Liang et al., 1999). Studies using

genetically engineered mice established a link between autophagy and cancer development. For example, *BECN1* has been reported to be monoallelically deleted in several types of human cancers, such as breast cancer, ovarian cancer and prostate cancer (Aita et al., 1999; Gao et al., 1995; Liang et al., 1999; Qu et al.; Saito et al., 1993). In contrast, abnormal high level of Beclin1 expression in tumor tissues is an indication of poor prognosis (Giatromanolaki et al., 2011; Koukourakis et al., 2010; XB et al., 2010; Xia et al., 2013; YH et al., 2009). In addition, the Beclin1-binding protein UVRAG is often monoallelically mutated in human colon cancer (Liang et al., 2006a). Moreover, autophagy protein ATG5 has been reported as over-expressed in prostate cancer but down regulated in the development of early-stage cutaneous melanoma (Kim et al., 2011b; Liu et al., 2013).

1.3.2. Autophagy in neurodegenerative diseases

Neurons in brain are heavily rely on autophagy for clearance of cellular waste and stress. Some unique features of neuron make it susceptible to autophagy function disturbance. Neuron cell are usually big in size compared with other cells and with huge expansion of dendritic and axonal cytoplasm, which make the long distance transportation of autophagosomes to lysosome that mainly concentrated in cell body a burden (Lee et al., 2011b). Unlike mitotic cells that divide and renew by itself, neurons seldom divide. This made neurons more susceptible to the toxicity of waste accumulation caused by slowdowns in proteolytic clearance (Lee et al., 2011b). Parkinson's disease (PD) is a progressive neurodegenerative disorder caused by

reduced dopaminergic transmission in the basal ganglia (Fahn, 2003; Trinh and Farrer, 2013). *PARK2/Parkin* and *PARK6/PINK1* are reported to be involved in Parkinson's disease. PTEN-induced putative kinase protein 1 (PINK1) is encoded by *PARK6/PINK1* and functions at the upstream of Parkin that encoded by *PARK2/Parkin.* Parkin is an E3 ubiquitin ligase that functions in mitophagy (Narendra et al., 2008; Valente et al., 2004; Valente et al., 2001). The accumulation of excessive damaged mitochondrial has been linked to Parkinson's disease(Schapira, 2008). PINK1 recruits Parkin to damaged mitochondrial to ubiquitinate mitochondrial membrane proteins in selective autophagy. Autophagy defect is likely to cause accumulation of damaged mitochondrial and lead to pathogenesis of PINK1/Parkin-related Parkinson's disease. Alzheimer's disease (AD) is another prevalent neurodegenerative disease that characterized by aggregation of amyloid beta (Aβ) inside neurons and extracellular Aβ plague accumulation. The mechanisms of autophagy related Alzheimer's disease include the failure of autophagosomes formation and lysosomal degradation

1.3.3. Autophagy in innate immunity

Autophagy has been recognized to play a wide array of roles in immunological processes. Autophagy acts as an evolutionarily conserved microbial clearance mechanism to protect the eukaryotic cells from invading pathogens and is intimately intertwined with nearly all aspects of innate immunity. The link between autophagy and innate immunity includes the responses of autophagy to microorganisms, damage

associated molecular patterns (DAMPs) such as HMGB1,IL-1β, pattern recognition receptors (PRR) including Toll-like receptors (TLRs), Nod-like receptors (NLRs) and RIG-I-like receptors (RLRs), sequestosome 1 (p62)-like receptors (SLRs) and immunity related GTPase IRGM, et al (Deretic, 2011). The impact of autophagy on the function of immune system can be categorized into three principal types. The first type mainly functions at the cellular level by recognition, capture and degradation of intracellular pathogens through xenophgy. The recognition of microbial is enhanced by stimulation of innate immunity receptors, such as TLRs, NLRs and RLRs or DAMPs such as HMGB1, as autophagy is a downstream specialized effector mechanism to them (Lee et al., 2010). The second type is actually the generic role of autophagy in cellular homeostasis. Autophagy helps to maintain immune cell's cellular viability, fitness and functionality. Some immune cells, such as T cells, are more dependent on autophagy to survive when growth factors are limited (Li et al., 2006; Pua et al., 2007). The third type includes the non-autophagy role of Atg factors as they function as coordinator between different functional systems that independent of their roles in canonical autophagy (Virgin and Levine, 2009).

1.3.4. Autophagy in development

Essential role of autophagy in development was initially revealed through genetic knock-out studies of *ATG* genes in lower eukaryotes. The systematic and tissue-specific knock-out of *ATG* genes in mice has led to greatly increased understanding the role of autophagy in mammalian development (Mizushima and Levine, 2010).

Autophagy pathway is a dynamic and highly inducible catabolic process that responses to environmental and chemical cues. It drives the rapid, precise and in time changes necessary for proper development(Mizushima and Levine, 2010). The deficiency in autophagy might result in inefficient lysosomal degradation or inadequate or failure of energy production (Zhang et al., 2009). Autophagy in mammal development was initially characterized in fertilized oocytes, which discovered *ATG5* as essential in the onset of preimplantation development (Tsukamoto et al., 2008). Autophagy activity is at low level in unfertilized oocytes, but can be massively accelerated within 4 hours after fertilization (Tsukamoto et al., 2008). The "reprogramming" after fertilization utilizes autophagy to rapidly degrade maternal mRNA and proteins, which in turn prepared for synthesis of new mRNA and proteins encoded by the zygotic genome (Merz et al., 1981; Stitzel and Seydoux, 2007). The next massive wave of autophagy in mice development was observed at the early neonatal stage (Kuma et al., 2004). After birth, the supply of nutrients through placenta is terminated, which demand increased autophagy activity to provide enough energy (Komatsu et al., 2005). Different *ATG*-gene knockout mouse models are vary in phenotypes. Conventional *Atg3*$^{-/-}$, *Atg5*$^{-/-}$, *Atg7*$^{-/-}$, *Atg9*$^{-/-}$and *Atg16L1*$^{-/-}$ embryos survived the whole embryonic period, which suggest that those genes are not essential for embryogenesis. *Beclin1*$^{-/-}$ mice shown early embryonic lethality and abnormally small embryos. In contrast, Beclin1$^{-/-}$ embryonic stem cells are viable, suggesting that Beclin1 is important for development *in vivo* but dispensable *in vitro* (Qu et al., 2003; Yue et al., 2003). Further studies are required to

investigate whether the autophagy pathway itself or merely several autophagy-involving components with autophagy-independent functions are essential for embryonic development (Mizushima and Levine, 2010).

Chapter 2. Biochemical and structural studies of p62/SQSTM1 UBA-Ub interaction

2.1. Introduction

2.1.1. Selective *vs.* non-selective autophagy

Autophagy is initially discovered as a bulk non-specific degradation process, by which a portion of the cytoplasm is indiscriminately sequestrated by a membranous organelle called phagophore. The resulting autophagosome is subsequently fused with lysosome for degradation. Growing body of evidence suggested that autophagy is a more selective process than originally anticipated. Autophagy specificity is achieved through a variety of autophagy receptor proteins, such as p62/SQSTM1, NBR1, OPTN and NDP52, for the degradation of ubiquitinated proteins.

2.1.2. The molecular events of selective autophagy

Autophagy receptor proteins are key players in selective autophagy, which always harbor both the Ub-association domain (UBA domain) and the LC3-interacting region (LIR). Selective autophagy is achieved through the domain coordination of autophagy receptors, which recognize cargos labeled with degradation signals, usually cargos with ubiquitination, by UBA domain, and LC3 on autophagosomal membrane through their LIR, leading to the engulfment of cargo by autophagic membrane (Kirkin et al., 2009; Stolz et al., 2014). The resulting autophagosomes formed are further fused with lysosome and followed by

degradation of both the cargos and the autophagy receptors.

2.1.3. p62/SQSTM1 is a crucial receptor for selective autophagy

p62/SQSTM1 is a multifaceted protein implicated in diverse cellular events (Moscat et al., 2007). In mammals, p62/SQSTM1 is one of the most important cargo receptors in selective autophagy to bridge the ubiquitinated proteins and autophagy marker LC3 for lysosomal degradation. p62/SQSTM1 has multiple domains such as a PhoxI and Bem1p (PB1) domain, a zinc finger (ZZ) domain, two nuclear localization signals (NLS1 and NLS2), a tumor necrosis factor receptor-associated factor 6 (TRAF-6) binding domain, a nuclear export signal (NES), a LC3-intaracting region (LIR), a Keap-interacting region (KIR), and a ubiquitin-associated (UBA) domain at the very carboxyl terminal (Katsuragi et al., 2015) (Figure 2.1). Among those domains, the N-terminal PB1 domain, the middle LIR domain and the C-terminal UBA domain are critical for selective autophagy.

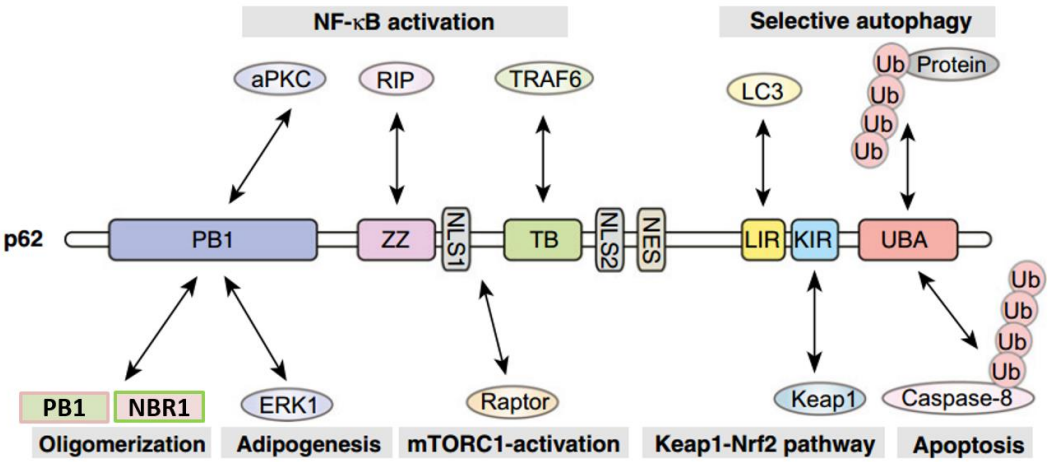

Figure 2.1 Schematic representation of p62 and its interacting partners

The N-terminus PB1 domain contains a basic cluster formed by conserved lysine residues and acidic OPCA motif made up of a loop and a helix. The OPCA motif was reported to interact with the basic cluster of other p62 PB1 domain to form oligomers (Lamark et al., 2003), which is important in p62 mediated selective autophagy. On the other hand, LIR consists of an acidic cluster and hydrophobic residues (Ichimura et al., 2008; Pankiv et al., 2007), which is responsible for LC3 interaction. LC3 localizes to the isolation membrane/phagophore and the interaction of LIR and LC3 incorporated ubiquitinated proteins to autophagosome-lysosome pathway. Knockdown of LC3 can lead to accumulation of p62 positive inclusion bodies made up of ubiquitinated protein aggregates (Kirkin et al., 2009; Shvets et al., 2008). The C-terminal of p62 ubiquitin associated (UBA) domain plays a pivotal role in selective autophagy by interacting with ubiquitinated proteins.

2.1.4. The p62/SQSTM1-Ub interaction is mediated by its UBA domain with dimer-to-monomer transition

The direct p62-Ub interaction is mediated through the p62 C-terminal UBA domain, which adopts a dimeric form (Shin Isogai, 2011). UBA interacts with Ub as monomer with relatively low affinity in part due to UBA homo-dimerization, which was reported as mutually exclusive and incompatible with mono-Ub binding (Long et al., 2010b; Shin Isogai, 2011) . p62 self-oligomerization through its PB1 domain confers high avidity to Ub by forming clustered p62, which counteracts the self-association of UBA domain, so as to stabilize the otherwise weak individual p62-Ub

interaction (Wurzer et al., 2015). Although p62 is important for ubiquitinated proteins degradation, loss of p62 seems does not impair selective autophagy (Komatsu and Ichimura, 2010), suggesting that other receptor proteins might also play the role.

2.1.5. Casein Kinase 2 phosphorylates p62/SQSTM1 UBA domain on S405

The UBA domain is conserved among Ub-binding proteins. Casein kinase 2 (CK2) was reported to phosphorylate p62 UBA at serine 405 (S405), which greatly increased the binding affinity between UBA and Ub (Lim et al., 2015; Matsumoto et al., 2011b). This report demonstrates that p62 can be post-translational modified to regulate autophagic clearance of ubiquitinated proteins.

2.2. Results

2.2.1. S409 is a novel ULK1-mediated phosphorylation site in p62 UBA domain

Cell biology studies by our collaborator (Prof. Zhenyu Yue, Icahn School of Medicine at Mount Sinai, New York, NY, USA) discovered the interaction between ULK1 and p62 through their kinase domain and UBA domain respectively (Lim et al., 2015). *In vitro* phosphorylation assay with ^{32}P-ATP revealed that ULK1 WT but not ULK1 kinase inactive (KI) mutant generate radioactivity labeling on p62. Further studies by mass spectrometry analysis identified serine 409 in p62 UBA domain as a potential phosphorylation site by ULK1. To confirm the phosphorylation, serine 409 was substituted with alanine (S409A), which serves as a phosphorylation-null mutant. Purified MBP-p62 S409A and Myc-ULK1 were subjected to *in vitro* phosphorylation assay. The ^{32}P-radioactivity labeling of S409A mutant by ULK1 is markedly reduced compared to that of the p62 WT (Figure 2.2 a), suggesting that S409 is one of the ULK1 targeting sites. To further confirm the site specificity of S409 phosphorylation, antibody against the phosphorylated S409 of p62 (p-S409) was raised and used to detect S409 phosphorylation of purified p62 by ULK1. The results show that, incubation of p62 with ULK1 (but not ULK1 kinase inactive mutant, KI) results in the detection of a strong band with right molecular weight by anti-p-S409 antibody (Figure 2.2 b) and this band is abolished in the presence of alkaline phosphatase (AP). These data demonstrate that p62 S409 is a novel phosphorylation target site of ULK1.

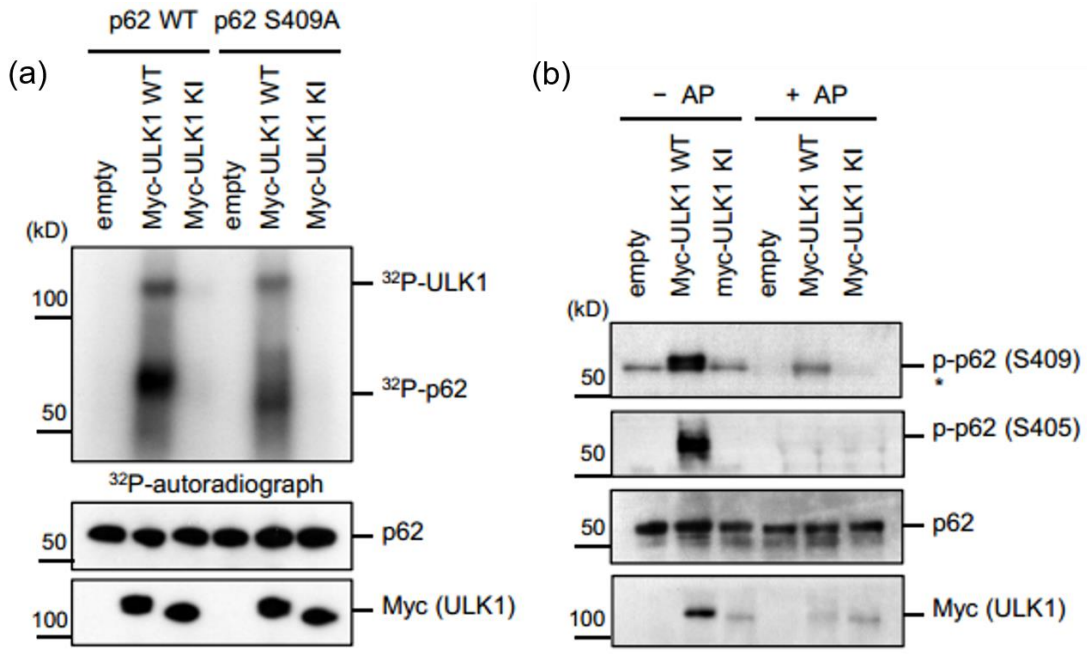

Figure 2.2 ULK1 phosphorylates p62 at Ser409

(a) ULK1 phosphorylates p62 at Ser409 *in vitro*. Purified MBP-p62 WT or S409A proteins were subjected to *in vitro* ULK1 kinase assay in the presence of ^{32}P-ATP.
(b) ULK1 phosphorylates p62 at Ser405 and Ser409. Purified MBP-62 WT protein was subjected to *in vitro* ULK1 kinase assay and dephosphorylation by alkaline phosphatase (AP). Asterisk indicates nonspecific bands. p-S405 and p-S409 were detected with each phospho-specific antibody, respectively.

Previous report showed that p62 S405 (human p62 S403 equivalent) can be phosphorylated by Casein kinase (CK2) (Matsumoto et al., 2011). Prof. Zhenyu Yue' lab found that p62 S405 can also be phosphorylated by ULK1. Purified p62 protein was incubated with co-immunoprecipitated Myc-ULK1, p-S405 was detected by anti-p62 pS405 antibody via immunoblot analysis and phosphatase treatment abolished the signal (Figure 2.2 b). Next, to understand the relationship of ULK1-mediated p62 phosphorylation at S405 and S409, FLAG-p62 WT, S405A, or S409A along with empty vector, Myc-ULK1 or Myc-ULK1 KI mutant were co-expressed into HEK293T cells and performed immunoprecipitation with FLAG antibody. The result shows that,

Myc-ULK1, but not KI mutant, induces the phosphorylation at p62 S405 as well as S409, suggesting that ULK1 phosphorylates both S409 and S405 of UBA (Figure 2.3). Interestingly, while p62 S405A retains p-S409, p62 S409A completely abolished p-S405, suggesting that p-S409 is a pre-requisite for p-S405, while p-405 has no impact in p-S409. Thus it is likely that p-S409 may precede p-S405 or p-S409 is required for the stability of p-S405.

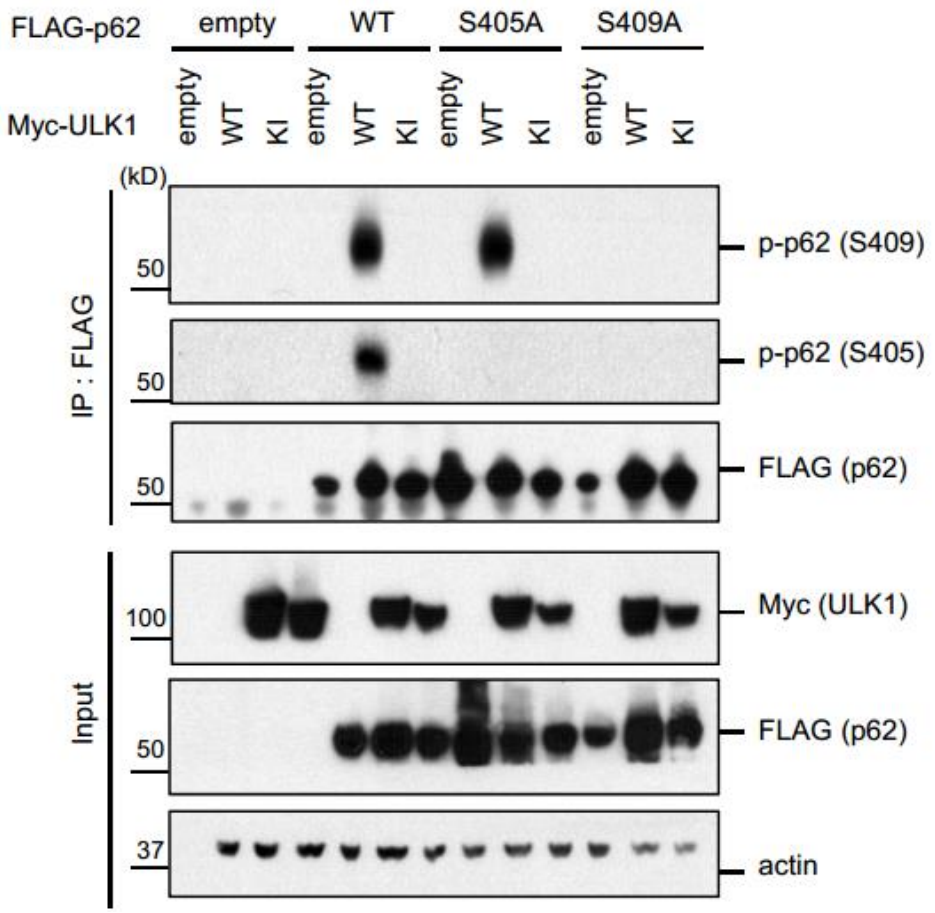

Figure 2.3 P-Ser409 is prerequisite for ULK1-mediated p-Ser405

HEK293T cells were transfected with indicated plasmids. Immunoprecipitation with anti-FLAG antibody was performed and Western blot assay with indicated antibodies was followed.

2.2.2. S409 phosphorylation leads to enhanced association between p62 and Ub *in vivo*

S409 resides in p62 UBA domain near S405 and phosphorylation of S405 has been reported to enhance the p62–Ub interaction (Matsumoto et al., 2011a). We tested if p-S409 shown the similar effect. We used p62 KO MEF cell lines stably expressing FLAG-p62 WT, S409A and phosphorylation-mimicking mutant S409E. To minimize the interference of p62 self-ubiquitination, we incubated cell lysates from p62 KO MEF treated with MG132 (providing enriched poly-ubiquitinated proteins) with MEF lysates stably expressing FLAG-p62 variants (providing bait), followed by immunoprecipitation with FLAG antibody. The result shows that, S409E pulled down significantly higher levels of poly-ubiquitinated (poly-Ub) proteins compared with p62 WT; in contrast, S409A pulled down less amount of poly-Ub proteins than p62 WT (Figure 2.4 a and b). These data collectively demonstrate that phosphorylation of p62 S409 promotes p62-Ub association.

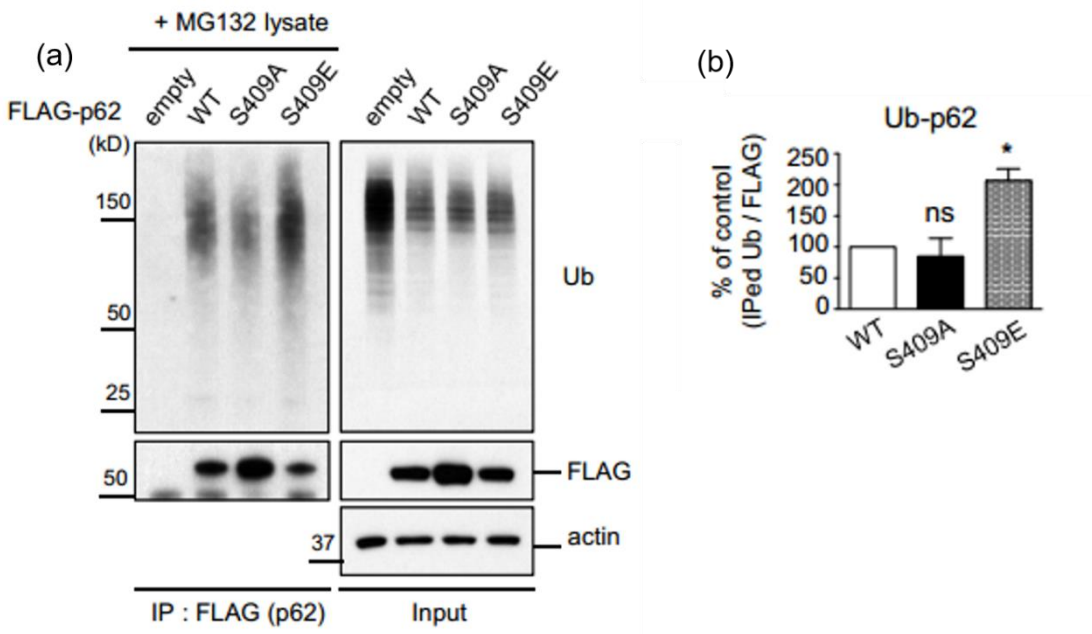

Figure 2.4 S409 phosphorylation promotes p62-Ub association *in vivo*

(a) P-Ser409 (S409E) enhances binding between p62 and poly-Ub proteins. Cellular lysates of p62 KO MEFs stably expressing empty vector, FLAG-p62 WT, S409A, or S409E were incubated with p62 KO MEFs lysates treated with MG132 and subsequently subjected to immunoprecipitation using anti-FLAG antibody. Immunoblot assay with indicated antibodies were followed.
(b) Quantification of the results from Figure 2.3 a were obtained by normalizing levels of co-immunoprecipitated Ub to FLAG blots; then S409A and S409E were normalized to WT. One sample t-test was used and data are represented as mean ± SEM (n=3). * $p < 0.05$, ns, not significant

2.2.3. ULK1-mediated pS409 and CK2-mediated pS405 impact p62-Ub interaction in biochemically distinct ways

2.2.3.1. Phosphomimetic mutants S409E and S405E show higher binding to monomeric ubiquitin *in vitro*

We next investigated the binding affinity of p62 UBA to mono-Ub by Isothermal Titration Calorimetry (ITC) assay. Mono-Ub was titrated into UBA WT and different mutants. ITC results showed that the K_d for purified p62 UBA WT is ~ 51.5 μM (Figure 2.4 5), confirming a weak interaction between p62 UBA domain and mono-Ub (Long et al., 2008a). The K_d for S409E mutant, however, is ~ 33.1 μM, suggesting a moderate effect of Ser409 to Glu mutation in enhancing Ub binding (Figure 2.5 C). In contrast, K_d for S405E mutant is ~ 2.8 μM, indicating a much stronger binding compared to both WT and S409E (Figure 2.5 B). To our expectation, the K_d for phosphorylation-null mutant S409A and S405A (~62.3 μM and ~58.6 μM respectively) (Figure 2.5 E and D) are similar to UBA WT (~51.5 μM), further

suggesting the promoting effect of S409 and S405 phosphorylation in Ub binding. These data collectively demonstrate that phosphorylation at S405 or S409 increased UBA-Ub binding.

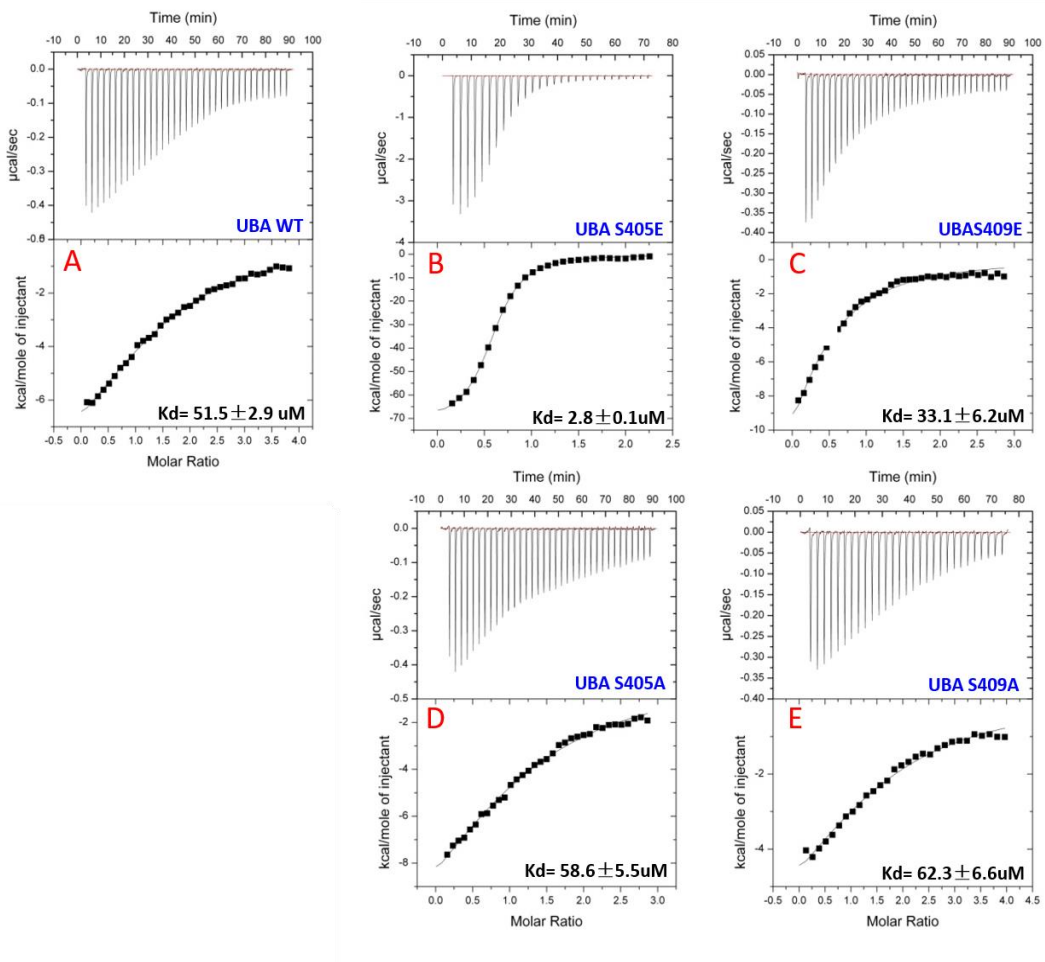

Figure 2.5 Isothermal Titration Calorimetry (ITC) analysis of binding between UBA S405 or S409 mutants and mono-Ub

Top parts of A to E are ITC thermograms for mono-Ub binding of both UBA wild type and mutants (S405E, S409E, S405A, S409A). ITC experiments were performed by titration of concentrated mono-Ub from syringe into cell with UBA. Bottom parts of A to E are plots of corresponding integrated heat values. Each measurement was repeated at least three times. Typical titration profile is shown. *Kd*, dissociation constant.

2.2.3.2. Crystal structure of phosphomimetic mutant UBA S405E resembles the structure to UBA WT

To better explain how p62 S405 phosphorylation-mimicking mutant S405E enhance binding to mono-Ub, we solved the crystal structure of UBA S405E by molecular replacement. The crystal structure reveals that UBA S405E is a dimer, with S405E residue located far away from the dimer interface (Figure 2.6 a). Superimpose of the crystal structure of UBA S405E with the reported UBA WT structure (Shin Isogai, 2011) demonstrated that two structures resembled each other (Figure 2.6 b), which suggest that pSer405 mutation might not interfere with UBA dimerization.

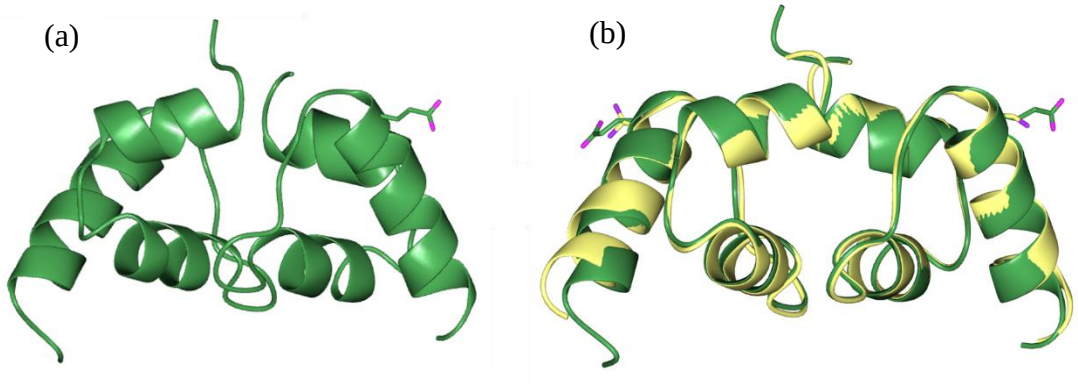

Figure 2.6 Crystal structure of UBA S405E

(**a**) UBA S405E crystal structure (green). Purple color denotes residue S405E. Only one residue S405E is shown (purple).
(**b**) UBA S405E (green) superimposed with UBA wild-type (yellow).

Although the crystal structure of p62 UBA-Ub complex is not available, other UBA-Ub complex has been reported (Chang et al., 2006). The structure of the p62 UBA-Ub complex model reveals that, residue S405 is located at the end of a α-helix (Figure 2.7 and Figure 2.10 of Section 2.2.3.3) that is required for Ub binding,

which excludes the possibility that the strong S405E-Ub binding is due to UBA dimer dissociation. Closely analysis of the modeling complex structure of p62 UBA (green) and Ub (brown) shows that, the negatively charged S405E of p62 UBA interacts with positively charged lysine 6 (K6) and histidine (H68) of Ub (Figure 2.7). Those charged residue interaction might contribute to the strong S405E-Ub interaction.

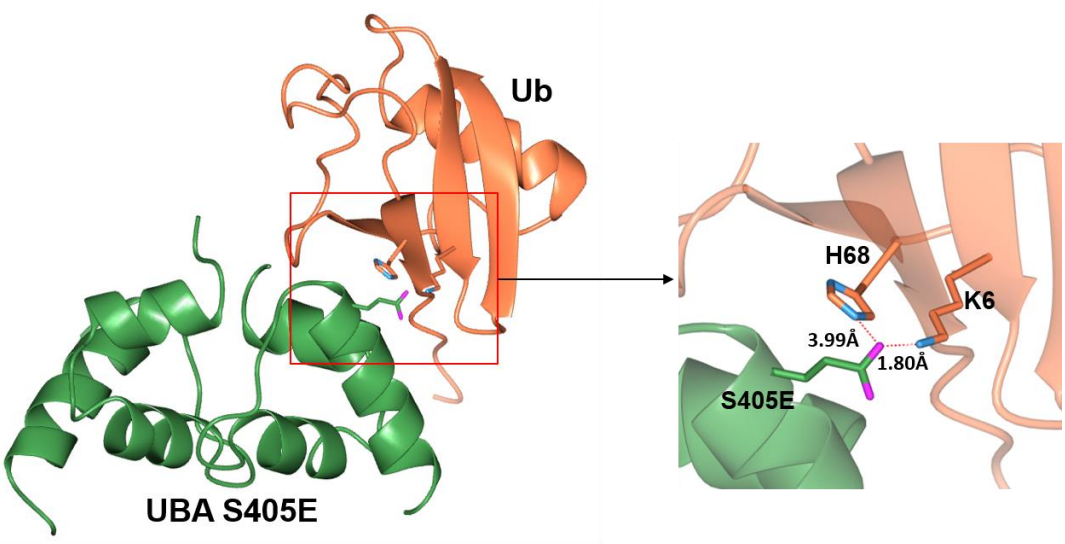

Figure 2.7 Modeling of UBA S405E-Ub interaction

Charged residue interactions exist between negatively charged residue S405E of UBA and positively charged residues K6 and H68 of Ub.

Statistics of diffraction data and structure refinement for UBA S405E are summarized in Table 2.1 (section 2.2.4.1). The coordinates of UBA S405E has been deposited to Protein Data Bank (PDB 5HH2).

2.2.3.3. NMR studies reveal that S409E induce no overall structural changes in p62 UBA-Ub binding

Previous structural studies revealed that while there is a dimer-monomer equilibrium of UBA dimer in solution, there is a dimer to monomer shift of UBA domain upon binding to Ub (Isogai et al., 2011; Long et al., 2010a). To study the structural basis for how p-S409 influences Ub binding, we performed NMR spectrum analysis (HSQC). Firstly, the ^{1}H-^{15}N correlation spectra of the ^{15}N-labeled p62 UBA WT and S409E mutant were collected in the absence of mono-Ub (Figure 2.8 a). The results show that the overall disperse pattern of cross peaks for S409E mutant and WT are similar. However, a few residues are with significant chemical shift. For example, residues D410, G412, W414 and L418 are evidently altered in position using the published WT spectra as reference (Isogai et al., 2011). The shifted residues are located in the vicinity of S409. Thus the S409E mutation might alter these residue's local environment and lead to chemical shift in the HSQC spectra. Noticeably, residues W414 and L418 are both important residues located at the UBA dimer interface in the WT structure. The result suggests that the chemical perturbation by S409E mutation might lead to local destabilization of the UBA dimer interface.

Next, we carried out HSQC by adding six-fold molar ratio excess of unlabeled mono-Ub to the ^{15}N-labeled p62 UBA WT and S409E. The addition of mono-Ub induced a large set of chemical shifts in the spectra of S409E, consistent with the idea that S409E undergoes dimer-monomer transition upon Ub binding as reported in the

previous studies for WT p62 UBA domain (Isogai et al., 2011). The analysis, however, revealed that the disperse pattern of S409E UBA in the presence of Ub is similar to that of WT, with only a few noticeable chemical shifts involving residues such as S409E and W414. (Figure 2.8 b). The data suggest that S409E mutant follows the similar pattern as the WT in the overall folding of UBA structures in the absence or presence of Ub. Collectively, our data suggest that S409E might destabilizes the UBA dimeric structure without impact overall folding of UBA bound to Ub.

(a)

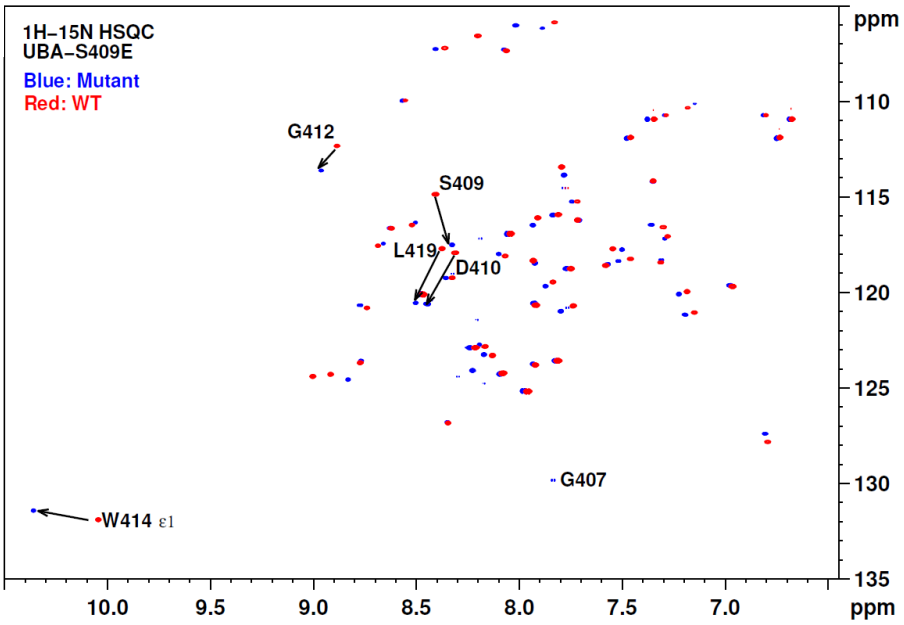

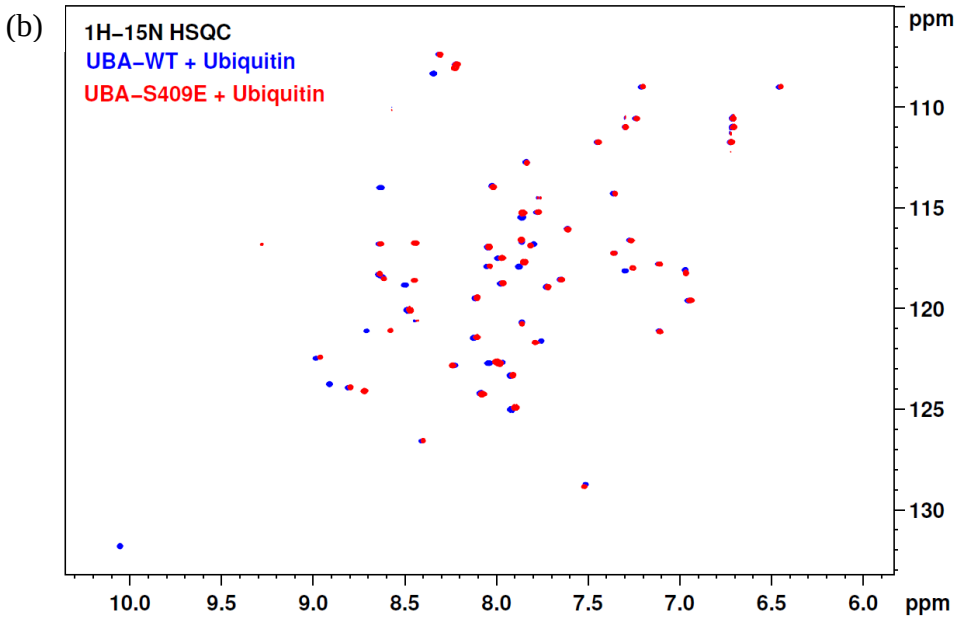

Figure 2.8 S409E does not impact the overall folding of UBA in binding to Ub

(a) S409E does not influence overall folding of UBA. Overlay of ^{1}H-^{15}N HSQC spectra of ^{15}N-labeled p62 UBA WT (red) and S409E (blue) in the absence mono-ubiquitin (Ub). Arrows indicate the significant chemical shifts with the corresponding residues labeled.

(b) Overlay of 1H-15N HSQC spectra of 15N-labeled p62 UBA WT (blue) and S409E (red) in the presence of 6-fold excess unlabeled mono-Ub.

2.2.3.3. S409E weakens the UBA dimer structure as suggested by DSC measurements

We hypothesize that the chemical perturbation by S409E may lead to local destabilization of the dimer interface and overall thermal stability of the dimer conformation. To test this hypothesis, we measured melting temperature (T_m) of p62 UBA WT and S409E by Differential Scanning Calorimetry (DSC). The result shows that, UBA S409E exhibits much lower T_m (61.5 °C) than WT (68.5 °C) (Figure 2.9),

supporting our hypothesis of a less stable dimeric structure for UBA S409E.

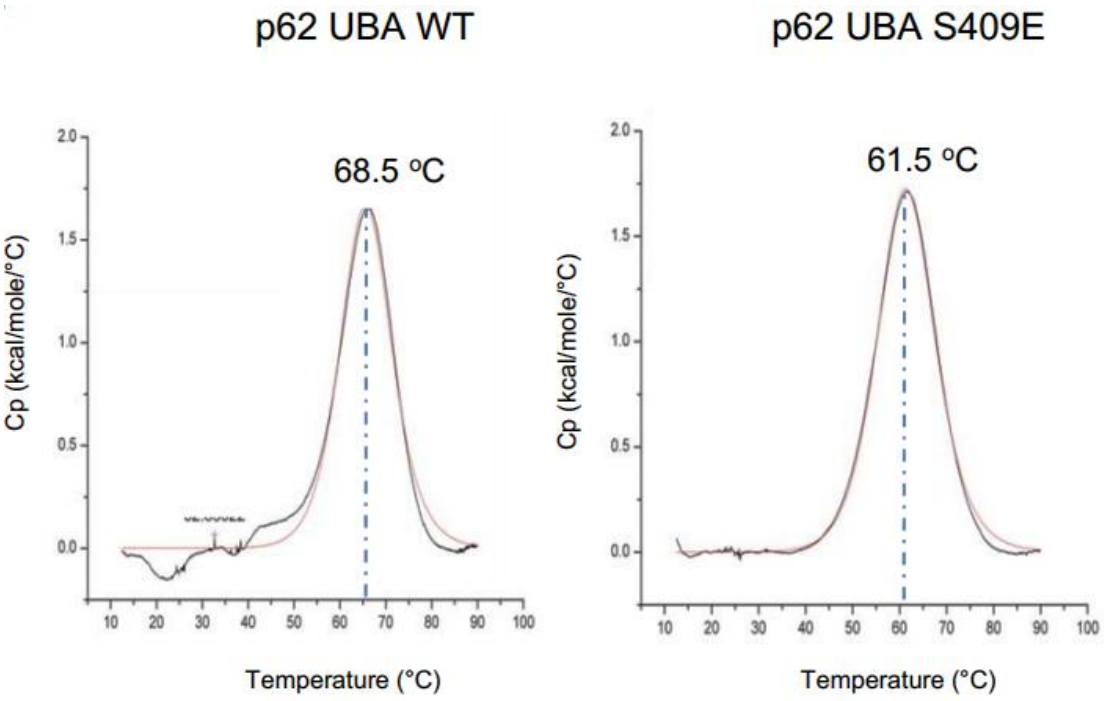

Figure 2.9 p62 UBA S409E destabilizes p62 UBA dimer thermostability

Differential Scanning Calorimetry (DSC) was performed on p62 UBA WT and S409E to measure the melting temperature (T_m) of p62 UBA dimer.

The WT UBA crystal structure revealed a dimerized UBA(Shin Isogai, 2011). Closely looking into the crystal structure of UBA dimer and specially its dimer interface shows that, S409 is outside but near the dimer interface that is mainly formed by α2 helix (Figure 2.10 a and b). It is possible that S409E mutation disturbed the local environment and render dimer unstable, which is favorable for Ub-binding. In living cells, on the other hand, the disturbed local environment by S409E might promote p62 phosphorylation at residue S405, which is located in α1 helix that responsible for direct Ub binding (Figure 2.10 a and b).

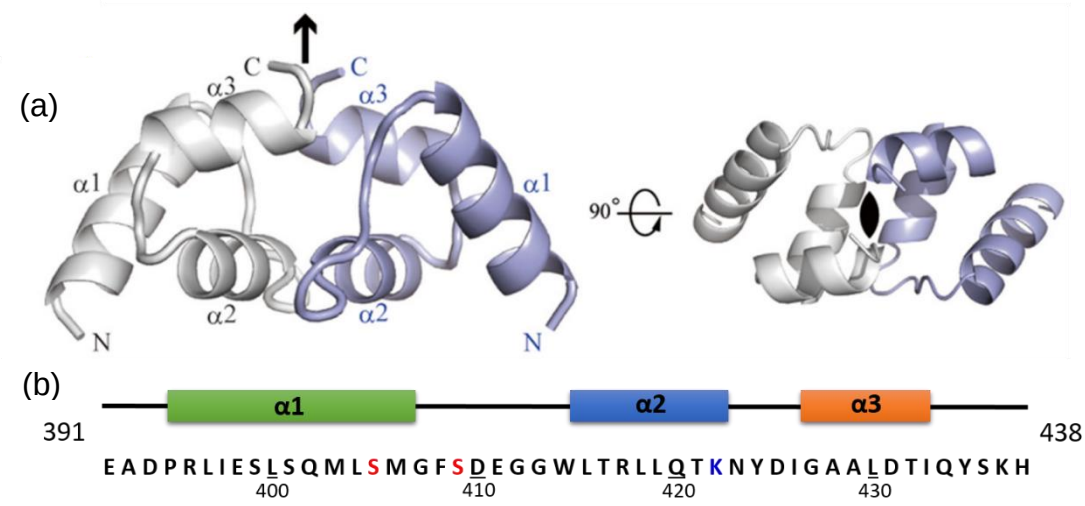

Figure 2.10 Crystal structure and schematic representation of p62 UBA domain

(a) Ribbon representation of crystal structure of p62 UBA domain. The figure is adapted from (Shin Isogai, 2011).
(b) The sequence and schematic representation of p62 UBA domain. N terminal α1 helix is not involved in UBA dimer interface formation. The central α2 helix and C terminal α3 helix are mainly responsible for the dimer interface formation. Location of residues S405 and S409 are marked in red with residues numbered under the sequence. Location of residue K422 is mark in blue.

2.2.4. K422 in UBA domain is a potential novel post-translational modification site to modulate p62-Ub association

2.2.4.1. Crystal structure of UBA S409E mutant reveals K422 as a key residue to mediate inter-molecular association

Dr. Liu Wenchao, who used to work in the lab, solved Crystal structure of S409E. The S409E crystal structure demonstrated a trimer that three copies of S409E interact with each other (Figure 2.11). Close inspection of the modeling structure of UBA S409E-Ub revealed that UBA-A S409E (cyan) and UBA-B K422 (green) forms electrical interaction. At the same time, UBA-C K422 (brown) forms strong

electrical interaction with S409-E411 patch in UBA-B (green). Those interactions mediated by K422 bring three copies of UBA together to form a new trimetric UBA complex.

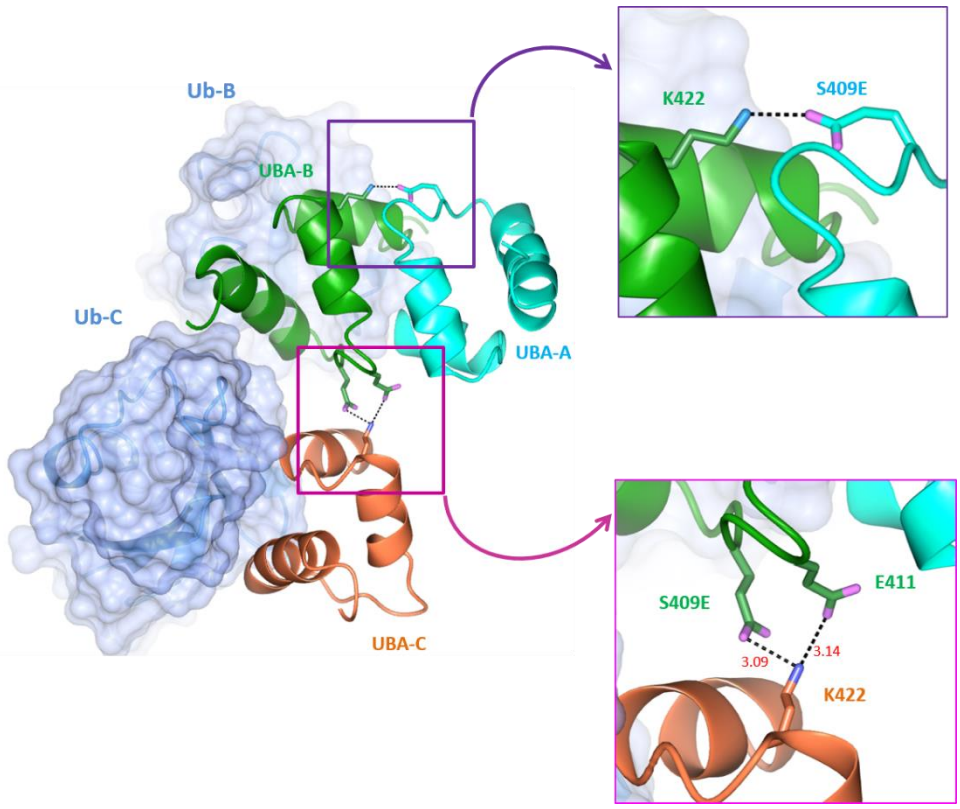

Figure 2.11 Crystal structure of UBA S409E revealed K422 is important for intermolecular interaction

The three UBA molecules in the asymmetric unit are drawn in ribbons style and labeled UBA-A (cyan), UBA-B (green) and UBA-C (brown) respectively. The spheres on these three molecules represent residues S409E, E411 and K422. The two modeled ubiquitin molecules, labeled Ub-B and Ub-C respectively to represent their associate to UBA-B and UBA-C molecules, are drawn in ribbons style with space-filling envelope. The zoom-in picture represents the S409E-E411-K422 electrostatic interaction. The residues are drawn in bond-and-stick model. The distances between the side chain groups are marked with the dashed lines.

The coordinates of UBA S409E has been deposited to Protein Data Bank (PDB 5HGY). Statistics of diffraction data and structure refinement for UBA S409E are summarized in Table 2.1.

Table 2.1 Statistics of diffraction data and structure refinement

	UBA S409E	UBA S405E
Data collection		
Space group	*C222*$_1$	P6$_5$22
Unit cell parameters		
a, b, c (Å)	33.62, 61.37, 129.10	67.95, 67.95, 111.58
α, β, γ(°)	90.00, 90.00, 90.00	90.00, 90.00, 120.00
Resolution (Å)[a]	32.28-1.77 (1.87-1.77)	33.98-2.40(2.53-2.40)
R_{merge}(%)[b]	5.7(11.4)	7.4(30.8)
$I/\sigma I$[b]	21.5 (11.0)	37.3(14.2)
Completeness(%)[b]	96.8 (94.0)	100(100)
Redundancy [b]	7.2 (7.1)	38.9 (40.3)
Structure refinement		
Resolution(Å)	32.27-1.77	33.97-2.40
R_{cryst}/R_{free}(%)	17.86/22.39	23.61/28.24
No. of reflections		
Working set	12271	6036
Test set	637	329
No. of atoms		
Protein atoms	1133	755
Water molecules	59	4
Average B-factor(Å^2)		
Main chain	11.314	37.227
Side chain	15.590	41.949
R.m.s deviations		
Bond lengths (Å)	0.022	0.015
Bond angles (°)	2.098	1.698
PDB ID	5HGY	5HH2

[a] Numbers in parenthesis define the highest resolution shell of data.
[b] Numbers in parenthesis are the statistics for the highest resolution shell of data

2.2.4.2. K422A mutation leads to significantly enhanced interaction with ubiquitin *in vitro* and *in vivo*

The crystal structure of UBA S409E revealed that residue K422 is important for UBA self-association. We hypothesize that this self-association might play a role in UBA-Ub interaction. To test this hypothesis, positive charged UBA K422 was mutated into more neutral alanine (K422A) or negative charged glutamic acid (K422E). The interactions of UBA K422A and UBA K422E with Ub were determined by ITC. Interestingly, the result shows that the *Kd* for UBA K422A mutant is ~9.2 μM (Figure 2.12 A-1 and A-2), indicating stronger binding compared to WT (~51.5 μM). To our surprise, the *Kd* for UBA K422E mutant is ~4.0 μM (Figure 2.12 B-1 and B-2), suggesting a much stronger binding that is comparable to UBA S405E (Kd ~2.8 μM). These ITC data together demonstrate that UBA K422 is crucial for UBA-Ub binding.

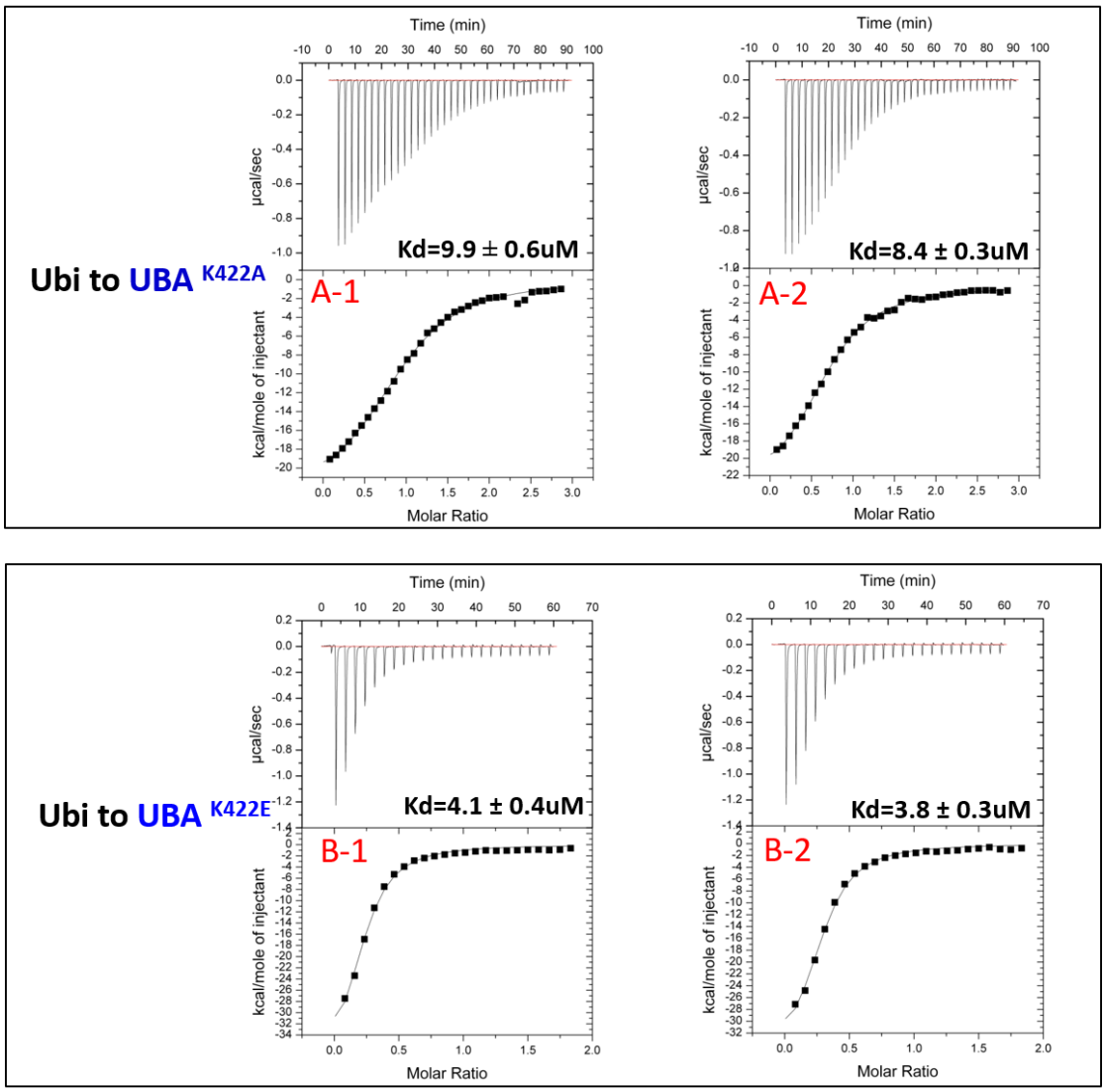

Figure 2.12 Isothermal Titration Calorimetry (ITC) analysis of binding between K422 mutant and Ub

The experiment was performed by titrating concentrated Ub in a syringe to the cell with UBA proteins. ITC thermograms of Ub binding with both K422A (A-1 and A-2) and UBA K422E （B-1 and B-2）(top) and the plots of corrected heat values (bottom) are shown. Each measurement was repeated at least twice. *Kd*, dissociation constant.

Residue K422 is located at the UBA dimer interface. Break of the UBA intermolecular interaction may be the reason for increased K422A/E-Ub binding. To test this hypothesis, we performed size exclusion chromatography (SEC) for

UBA K422A and UBA WT, and compared their retention volume. To our expectation, the retention volume of UBA K422A (84.60 mL) is much larger compared to that of UBA WT (76.05 mL), suggesting smaller size of the UBA K422A due to a single site mutation (Figure 2.13 a). Static Light Scattering show that the observed molecular weight for the purified UBA K422A is ~6000 Dolton, which is quite close to its theoretical molecular weight (~5836 Dolton), supporting the monomeric state UBA K422A mutant (Figure 2.13b). Next, we tested if K422A has the similar effect as S409E to enhance the interaction between p62 poly-ubiquitinated (poly-Ub) proteins. We overexpressed FLAG-p62 WT, S409E, S409A and K422A into the MEF cells. Cells treated with proteasome inhibitor MG132 were lysated and followed by immunoprecipitation with FLAG antibody. As expected, S409E pulled down significantly higher levels of poly-Ub proteins than p62 WT; in contrast, S409A pulled down similar but less amount of poly-Ub protein than WT. To our surprise, K422A pulled down the most amount of poly-Ub proteins, much more than both WT and S409E (Figure 2.13 c), indicating K422 is of great importance for p62-Ub interaction. However, it seems that there is no synergistic effect of S409E and K422A, as double mutation S409E/K422A does not enhance binding compared with K422A alone. One possibility is that the promoting effect of S409E is over saturated by much stronger K422A. Those data together suggest that residue K422 of UBA is important for UBA-Ub binding.

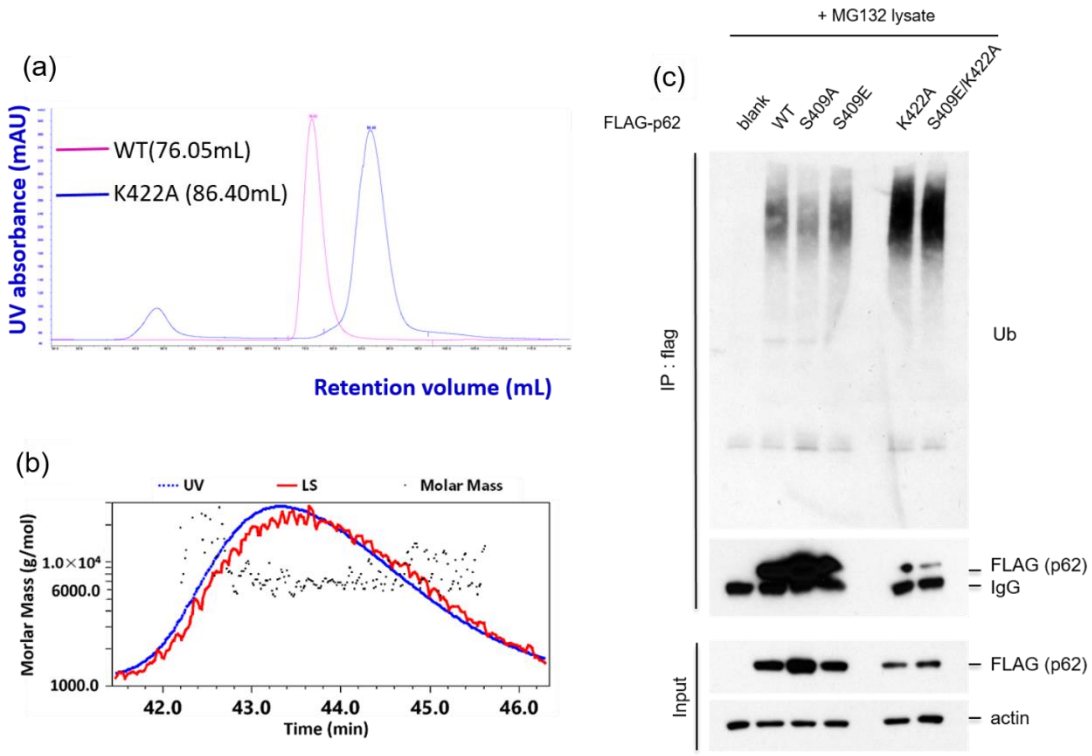

Figure 2.13 K422A is an Ub-binding monomer

(a) K422A has large retention volume than UBA WT. The same amount and volume of UBA WT and K422A were run size exclusion chromatography separately, and their UV absorbance curves were intergraded and compared. The retention time for UBA WT and K422A are 76.05 mL and 86.40 mL, respectively.
(b) Static Light Scattering shows monomeric state of UBA K422A. Static Light Scattering was performed with purified UBA K422A protein to measure the molecular weight. The observed molecular weight is ~6000 Dolton.
(c) K422A enhances binding between p62 and poly-Ub proteins. Cellular lysates of MEFs transiently expressing empty vector, FLAG-p62 WT, S409A, S409E, K422A and S409E/K422A were incubated with p62 KO MEFs lysates treated with MG132 and subsequently subjected to immunoprecipitation using anti-FLAG antibody. Immunoblot assay with indicated antibodies were followed.

2.2.4.3. Preliminary data suggests that K422 can be acetylated *in vivo*

- Based on the above results of UBA K422A, we assume K422 could be a target site for posttranslational modification. To check if there is any modification on K422, we performed mass spectrometry analysis of antibody purified GFP-p62 from HEK293T cells. The result suggests that K422 as a potential target site for

acetylation (Figure 2.14). To confirm the K422 acetylation, we plan to inhibit acetylation by treating cells with acetyltransferases inhibitor, and perform mass spectrometry analysis for antibody-purified p62 protein. Ongoing studies are now in this direction.

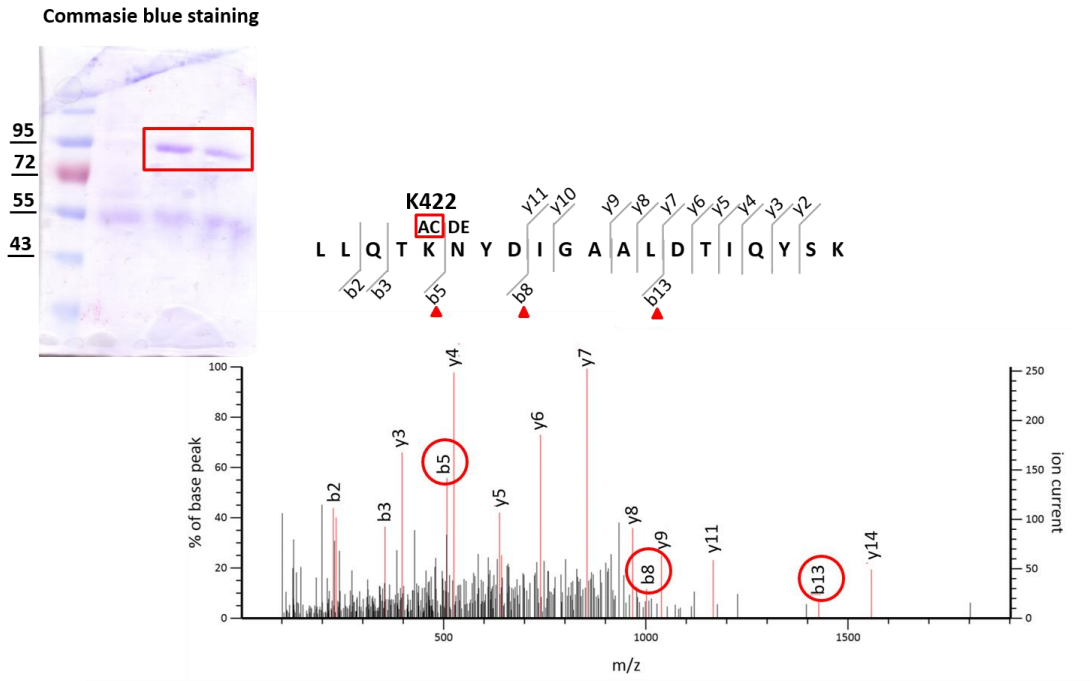

Figure 2.14 K422 is a potential acetylation site in p62 UBA

GFP-tagged mouse p62 full length was transiently over expressed in HEK293T cell and purified by GFP antibody. The purified GFP-p62 sample was resolved by SDS-PAGE and stained with Coomassie brilliant blue. The GFP-p62 band (red box) was excised and prepared for mass analysis.

2.2.5. Super UBA and its interaction with Ub

This section would be discussed in Chapter 4.

2.3. Discussion

Our studies reveal that phosphorylation of autophagy receptor p62/SQSTM1 by ULK1 under proteasome inhibition condition plays an important role in the regulation of selective autophagy. Phosphorylation of p62 UBA S409 leads to enhanced association of p62 and poly-Ub proteins *in vivo*. The enhanced UBA S409E-Ub binding by ITC also supports the stronger association.

Our studies also provide novel structural and functional insights into the role of the novel p62 S409 and the previously identified S405 phosphorylation in regulating ubiquitinated protein binding (Lim et al., 2015; Shin Isogai, 2011). Previous findings showed relatively weak interaction between dimeric UBA WT and mono-Ub (Long et al., 2008b; Shin Isogai, 2011). Modulation of UBA domain dimer-monomer transition is likely to play a role in regulating p62-Ub interaction (Shin Isogai, 2011). S409E mutation alters residues in the local environment around S409, including W414 and L418 at the p62 UBA-UBA dimer interface. HSQC studies further show that S409E mutant follows the similar pattern as the WT in terms of binding to Ub. Moreover, the overall thermal stability of the UBA domain is significantly reduced in the S409E mutant, suggesting a reduced self-association of UBA S409E. Thus we conclude that phosphorylation at S409 destabilizes UBA dimer interface and facilitates dimer–monomer transition in favor of binding to ubiquitinated proteins.

At the same time, UBA S405 phosphorylation greatly increased p62 UBA-Ub binding, consistent with a previous report that Casein Kinase 2 (CK2) directly phosphorylates UBA S405 and increased its binding affinity to polyubiquitin chain (Matsumoto et al., 2011b). S405 resides at a α-helix required for Ub binding but not for dimer interface formation (Figure 2.9 b). Dimeric UBA is reported as incompatible with ubiquitin binding due to C-terminal sterically interfere (Shin Isogai, 2011). Our crystal structure of UBA S405E show a dimeric structure resembling the previously reported structure of UBA WT. So it is not likely that the increased S405E-Ub binding is due to UBA dimer dissociation by S405E mutation. Our modeling of UBA S405E-Ub interaction reveals electrical interactions between residue S405E and Ub residues K6 and H68. Based on the above findings, we conclude that phosphorylation of S405 does not compromise UBA dimer interface, but increase direct S405E-Ub binding through charged residues interaction. What's more, phosphorylation of S409 might be a pre-requisite for S405 phosphorylation, as p62 S409 phosphorylation null mutant S409A completely abolished S405 phosphorylation by ULK1. We thus propose a model in which S409 is phosphorylated first by ULK1 to promote UBA dimer dissociation, followed by the exposure of S405 to ULK1 (or CK2) for further phosphorylation.

Crystal structure of UBA S409E reveals a UBA trimer with intermolecular interactions involving S409E and a new residue K422. Mutation of K422 into alanine

(K422A) or glutamic acid (K422E) greatly increased Ub-binding in both ITC studies and poly-Ub binding assay. Furthermore, size exclusion chromatography and static light scattering suggest monomeric state of UBA K422A. Our finding suggest that K422 is important for maintaining the dimeric structure of p62 UBA WT and is a potential target for modification to regulate p62-Ub interaction. Interestingly, mass spectrometry suggests K422 is a potential target site for acetylation. Our findings provides new insights and possibilities into the mechanism of ULK1-p62 coordinated action in selective autophagy pathway.

In summary, our study reveals a molecular and structural mechanism underlying the autophagy receptor p62-mediated degradation of poly-ubiquitinated proteins through selective autophagy.

2.4. Materials and Methods

2.4.1. Plasmid construction

FLAG-p62 WT, S409A, S409E and K422A were cloned into HindIII and XhoI restriction site of LPC retroviral vector. The UBA domain of mouse WT, S405E, S405A, S409E, S409A, K422A and K422E were cloned into a modified pET32M vector between the restriction sites BamHI and EcoRI with Trx-His×6 tag fused at N terminal. The full length of human ubiquitin was cloned into a modified pETM vector between the restriction sites BamHI and Not I with His×6 tag fused at N terminal. Both pETM and pET32M vectors contain a human rhinovirus (HRV) 3C protease cleavage site between tag and protein. The detailed background, methods and procedures for plasmid construction are as follow.

Prokaryotes and eukaryotes expression vectors

Target gene transcription is always under control of a specific promoter that preferably and tightly controls target gene expression. There are differences on regulation of target gene translation and protein expression between prokaryotes and eukaryotes expression vectors. The characteristics of prokaryotes and eukaryotes expression vectors in the lab will be discussed in details as follow. The eukaryotes expression vectors would contain the Kozak consensus sequence that plays a major role in the initiation of the translation process.

Prokaryotes expression vectors

Different expression vectors have different transcriptional machinery and elements for protein expression. Prokaryotes expression vectors have a Shine-Dalgarno sequence at the translation initiation site for ribosomes binding. The expression vectors used in the lab for prokaryotes expression in *E.coli* and eukaryotes expression in mammalian cell are list in Table 2.2.

Table 2.2 Expression vectors in the lab for protein expression in *E.coli*

Vector	Tag	Fusion protein	Cleavage site	Selection marker
pET-M	N terminal His×6	None	HRV 3C	Ampicillin
pET-32M	N terminal His×6	TRX	HRV 3C	Ampicillin
pET-49M	N terminal His×6	GST	HRV 3C	Kanamycin
pGEX-4T-2	None	GST	Thrombin	Kanamycin

Eukaryotes expression vectors

Eukaryotes expression vectors in the lab are listed in Table 2.3.Among them, pcDNA 3.1-Flag, pEGFP-N3 and pmCherry-N1 were used in experiments.

Table 2.3 Expression vectors for transient over expression

Vector	Tag	Selection marker
pcDNA 3.1-Flag	N terminal Flag	Ampicillin
pcDNA 3.1-HA	N terminal HA	Ampicillin
pcDNA 3.1-Myc	N terminal Myc	Ampicillin
pCMV-Flag	N terminal Flag	Ampicillin
pCMV-Myc	N terminal Myc	Ampicillin
pEGFP-N3	C terminal EGFP	Kanamycin
pEGFP-C3	N terminal EGFP	Kanamycin
pmCherry-N1	C terminal mCherry	Kanamycin
pDsRed-Express-N1	C terminal DsRed	Kanamycin

Basically, two methods were used for sub-cloning the gene of target into expression vectors, namely polymerase chain reaction (PCR) method and ligation method. The gene of target can be obtained from commercialized plasmids or reverse transcription PCR for the cDNA of the target gene. If both sources of target gene are not available, whole gene synthesis service is a good option as the gene sequence can be codon optimized for host expression.

2.4.1.1. Ligation method

Ligation is the most straightforward method for expression plasmid construction. A phosphodiester bond is formed between 5’ phosphate and 3’ hydroxyl of two adjacent DNA fragments with the catalyzation of DNA ligase (Figure 2.15).

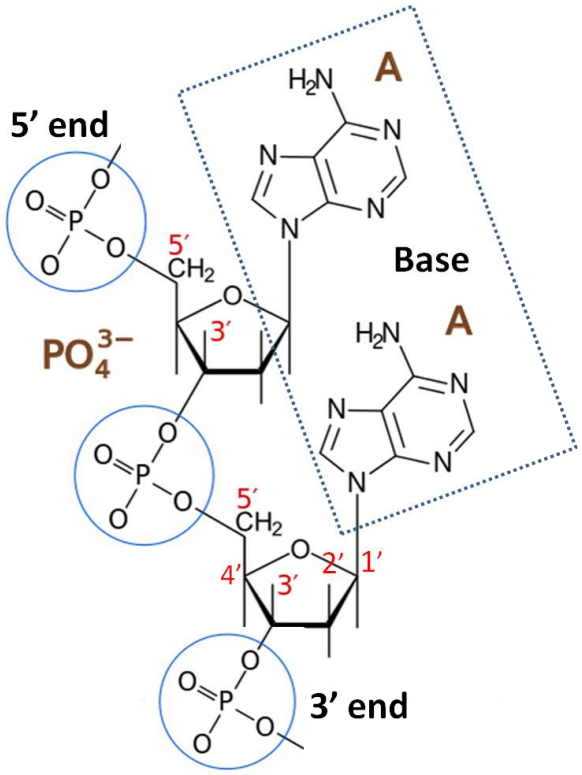

Figure 2.15 Diagram of phosphodiester bond between nucleotides

In nucleic acid, two hydroxyl groups on the phosphoric acid react with hydroxyl group of other two sugar molecules to form a phosphodiester bond. The phosphodiester bond is formed between the 3’ carbon atom of one sugar and 5’ carbon atom of another sugar. Base A represents two molecules of adenine. The 3’ end and 5’ end is also shown. DNA ligase is a type of enzyme that catalyze the formation of phosphodiester bond between nucleic acid fragments in ligation.

DNA digestion

If the target gene is already in a plasmid with the right restriction sites, the plasmid can be directly restriction enzyme digested. Usually digestion of 5-8 μg of donor plasmid and 1ug of recipient plasmid will be enough for one ligation. Otherwise, gene of target is generated by PCR with primers specially designed for ligation. Each end of the PCR product is designed with a suitable restriction site that comes along with the primers. Both the aim vector and target gene were digested with a pair of

restriction enzymes to generate sticky ends. Before gel purification, the digested aim vector with sticky 3’ ends and 5’ ends were treated with shrimp alkaline phosphatase (SAP) (Thermo Scientific), which catalyzed the dephosphorylation of 3’ ends and 5’ ends DNA phosphomonoester. The dephosphorylation by SAP prevents self-ligation of the aim vector.

Insert and aim vector gel purification

The DNA samples were ran on an agarose gel with ladder as standard, and preferably DNA without digestion as control in case of trouble shooting. The gel was illuminated with a UV box (Major Science), and the gel band corresponding to the digested insert and aim vector were cut out. The gel was purified with a gel purification kit and DNA eluted out with 20 μL of elution buffer. The concentration of the purified insert and aim vector were determined.

Ligation

Ligation was conducted by firstly adding insert into recipient vector at a molar ratio of 10:1, then ligase buffer and T4 ligase (Thermo Scientific) in an Eppendorf tube and gently mixed well. The ligation mixture were placed at 16 °C overnight or room temperature 2 hour for the ligation process to complete. Same amount of digested recipient vector was used as negative control.

Transformation

In molecular biology, transformation is a way to introduce foreign genetic materials into cell through cell membrane. The prerequisite of transformation is the bacterial cell undergo the process should be competent in a way that it is able to uptake the exogenous genetic materials. The bacterial used for transformation are therefore named as competent cell, which acquires competence by chemical induction. To perform transformation, add 12 μL of the ligation product or digested recipient vector (negative control) into 200 μL DH5α competent cell each; place the mixture on ice for 30 minutes, heat shock the mixture for 90 seconds at 42°C in a water bath or with a heat block; then immediately cool down on ice for 2 minutes, add 600 μL of fresh LB broth without antibiotics and let the bacterial recover and express antibiotic resistance protein on a shaker of 150 rpm for 45 minutes at 37°C. At the same time, pre-warm 10 cm LB agar plate with suitable selection antibiotics at 37°C. After recover, pellet the cell at 3000 rpm for 5 minutes with a centrifuge. Re-suspend the pellet with 100 uL LB broth and spread it onto the plate. Incubate the plate with plate bottom side up at 37°C for 12 to 16 hours. Agar plate with single colony should be stored at cold room or 4°C refrigerator before picking bacterial colony for screening.

Colony verification

Colonies should grow on the agar surface if the transformation worked out. The colonies grow on the plate transformed with recipient vector should serve as background control. The difference in the number of colonies between the control

plate and the ligation plate is proportional to the chance for successful screen. A large number of colonies on control plate indicates that the vector digestion is incomplete or self-ligation of recipient plasmid. Small number of or no control plate colonies, together with a few or a lot of colonies in ligation plate suggesting high chance to get the positive colony. Pick at least two single colonies and inoculate them in LB for bacterial culture, then aliquot 500 μL of bacterial culture each for sequencing (BGI). Successful colony PCR with the bacterial culture suggest right ligation if the insert is PCR synthesized at the first place, although sequencing is required to confirm the successful ligation. Extract plasmid with the bacterial culture and wait for the sequencing results to confirm the right ligations.

Ligation is easy to perform, usually with no length limitation of the target gene and relatively high efficiency. Special attention should be paid to the following two points. The first point is, for expression vector with tag expressed in front of target gene, the target gene should be in frame with the tag and stop codon should be added at the end of the target gene. The second point is, for expression vector with tag expressed at the end of the target gene, a start codon is need in front of the target gene, while there should be no stop codon at the end of the sequence and the tag should be in frame with the target sequence. Sometimes, the target gene contains the same restriction enzyme sites as those in the multiple cloning site of expression vector. In this circumstance, ligation method might not applicable, and method like PCR would be a nice option.

2.4.1.2. PCR method

PCR method is the most popular method in our lab to make constructs. PCR method is so versatile a method that it is not only convenient in making new constructs but also powerful in making point mutations, deletion mutations or insertion mutations. PCR method begin with primer design, followed by two rounds of PCR, DPNI digestion, transformation and sequencing.

Designing primer

The primers for PCR based cloning consist of the following two parts:

Target gene hybridization sequence: about 18-20 base-pairs long that binds to the ends of the target gene.

Target vector hybridization sequence: about 20 to 25 base-pairs long that binds to or around the multiple cloning site of the target vector.

The general designing principle of the target gene hybridization sequence is the same as designing primers to amplify a gene. This part of primer is mainly working in the first round PCR to amplify the target sequence. The target vector hybridization sequence, which is a part of target vector around MCS, will bind to target vector as primers to initiate second round PCR that amplify the full length of target vector (Figure 2.14).

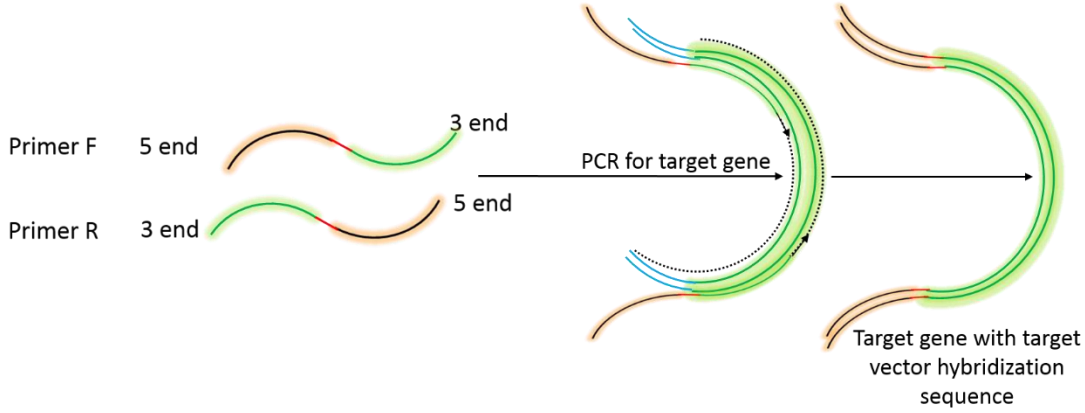

Figure 2.16 Diagram of first round PCR in PCR-based cloning

Run first round PCR

Run first round PCR to amplify the target gene. High fidelity polymerase should be used to minimize the chance of mutation. The general composition and condition for the PCR with Phusion High-fidelity DNA polymerase (Phu) (Thermo Scientific) are listed in Table 2.4 and Table 2.5, respectively. The amount of DNA doubles in each cycle. Template DNA added is the initial source of template for the PCR, as the amplification goes on, the PCR product will be the predominant source of template. The denature step is critical for the successful PCR, as too long the period of

Table 2.4 PCR reaction composition

Components	20µL Reaction	50µL Reaction	Final
H_2O	14.7µL	36.8µL	
5 X Phu buffer	4.0µL	10.0µL	1 X
Template (200 ng/µL)	0.3µL	0.75µL	3.0 µg/µL
Forward primer (100µM)	0.2µL	0.5µL	1.0 µM
Reverse primer (100µM)	0.2µL	0.5µL	1.0 µM
dNTPs (10 mM)	0.4µL	1.0µL	200.0 µM
Phu polymerase	0.2µL	0.5µL	0.1 U/20µL

denaturation at high temperature will compromise the performance of polymerase while inadequate denaturation cannot provide enough template for primer annealing. Both will lead to little PCR product or PCR failure, and this is particular important in genomic DNA, which generally requires much more severe conditions for denaturation. The annealing temperature can be calculated based on the target gene hybridization sequence. The extension time is depending on the polymerase.

Table 2.5 PCR reaction condition

Components	Step	Temperature	Time
Initial denature	1	98 ° C	180 S
Denature DNA	2	98 ° C	30 S
Primer annealing	3	52 to 64 ° C	40 S
Extension	4	72 ° C	20 to 120 S
Repeat cycle	Go to step 2		30 cycles
Extension complete	5	72 ° C	10 min
PCR complete	6	4 ° C	

Gel purification of PCR product

Run PCR product on agarose and cut gel piece with the target band under a UV illuminator. Purification the gel piece with gel purification kit (Biotek) and elute the DNA with 20 μL of elution buffer. The eluted DNA will be used as primers for the second round PCR to incorporate the target gene into the aim vector.

Run second round PCR

The second round PCR are generally conduct at lower temperature regardless the

annealing temperature calculated based on target gene hybridization sequence. Lower the annealing temperature will increase the binding of the hybridization sequence at both ends of first round PCR product to the target vector, instead of self-binding. In the second round PCR, 2 μL of first round PCR product was used as primers for a 20 μL second round PCR reaction, and 2.5 minutes extension time is generally longer enough for the whole plasmid extension. The annealing temperature used was between 48 ℃ to 54 ℃.

DPNI digestion

DPNI is a methylation dependent restriction enzyme, which recognizes and cleaves the methylated adenine in GATC recognition sequence of DNA grow from *E.coli* dam^+ strain. However, DNA amplified by PCR is not methylated, so it cannot be cleaved. The 20 μL secondary PCR product were digested with 1μLDPN1 (Thermo Scientific) at 37 ℃ for 6 hour to remove template DNA and subsequently transformed into DH5α competent cell for positive colony screening.

Transformation

After digestion, 12 μL of PCR product were transformed into 200 μL of DH5α competent cell for single colonies and subsequently picked for sequencing. The super competence of the competent cell is critical for the successful transformation, as the efficiency of the PCR method is lower compared with ligation method.

Colony verification

PCR method is as easy to perform as ligation method, only without a concern that restriction enzyme sites in the target gene that conflict with the restriction enzyme sites in the MCS of target expression vector. The length of the target gene by PCR method should better less than 1500 base pairs, as longer than that will dramatically compromise the efficiency. Although it is rare to see, mutations do happen on the target gene or the express vector during the PCR, which might lead to no or wrong expression. Mutations by PCR was made on the wild type expression constructs with the similar procedures, except the common primers (like T7 promoter or T7 terminator in the pET series vector) was used as one of the primers for the first round PCR. In some circumstances, the second round PCR for constructs of single site mutation or multiple sites mutation can be done in just one PCR reaction, as the first round PCR product of different constructs can be mixed together and used as primers for the second round PCR. After DPNI digestion and transformation, single colonies can be picked and sent for sequencing to screen for constructs with right mutations.

For the p62 project, the ubiquitin binding associate (UBA) domain (residues 389-438) of mouse p62/SQSTM1 was cloned into a modified pET32M vector (Novagen) between restriction sites BamH1 and EcoR1 to make pET32M UBA^{WT}. Mutations S405E, W414F，K422，K422E, W414F&K422A, S405E&K414F&W422A were made based on the wild type pET32M UBA^{WT} by PCR method (not all constructs are

used in the thesis). The pET32M vector is thioredoxin fusion and His×6 tagged with a protease 3C cleavage site right before the target gene (Thioredoxin-His×6-3C cleavage site-target gene). The full length of human ubiquitin was cloned into modified pETM vector (Novagen) between restriction sites BamH1 and EcoR1. Mouse UVRAG and its mutants were cloned into a modified pcDNA 3.1 vector (Invitrogen) with an N-terminal Flag epitope tag.

2.4.2. Protein Expression and Purification

Expression of ubiquitin, p62 UBA WT and mutants (S405E, S409E, S405A, S409A, K422A and K422E) were induced in E.*coli* BL21 (DE3) cells by growing at 30 °C for 5-hour with 0.25 mM of isopropyl-β-D-thiogalactopyranoside (IPTG). Bacterial cells suspended in His-binding buffer (20 mM sodium phosphate, PH 7.4, 500mM NaCl, 40mM imidazole, 10% glycerol) were lysed by sonication and centrifuged for 2hr at 20,000 g at 4 °C. Supernatants were loaded onto the His-binding buffer equilibrated affinity column (His Trap HP, GE Healthcare) and washed with 15 column-volume of His-binding buffer. The Trx-His×6 tag in front of UBA and mutants or His×6 tag in front of Ubiquitin were removed by 3C protease cleavage and the untagged proteins were further purified by size-exclusion chromatography (Superdex 75, GE healthcare). The detailed background, methods and procedures for protein expression and purification are as follow.

2.4.2.1. Protein expression

Transformation for single colony

Expression constructs pET32M UBA^{WT}, pET32M UBA^{S405E}, pET32M UBA^{K422A} pET32M UBA^{K422E}, pET32M $UBA^{S405E\&W414F\&K422A}$, pET32M $UBA^{S405E\&W414F\&K422E}$ pETM Ubiquitin were transformed into *BL21* (DE3) (Novagen) and grown on LB agar plate with ampicillin for 12 to 16 hours at 37°C. The detailed protocol for the *BL21* (DE3) transformation is as follows. Mix 250 ng of plasmid with 50 uL of competent cells in an EP tube and place the tube on ice for 30 minutes. Heat shocks the mixture for 90 seconds at 42°C in a water bath or with a heat block, then immediately place the tube on ice for 2 minutes. After that, adding 600 uL of fresh LB medium without antibiotics and let the bacterial recover and express antibiotic resistance protein on a 150 rpm, 37°C shaker for 45 minutes. At the same time, pre-warm the 10 cm LB agar plate with ampicillin antibiotics at 37°C. Spread 100 uL of the transformation onto the plate and incubate with plate bottom up overnight at 37°C. Plate grow with single colony should be stored at cold room or 4°C refrigerator before pick for inoculation.

Inoculation for start culture

Single colony was picked and inoculated in a 100 mL glass flask with LB medium containing 100 μg/mL of ampicillin (100 mg/mL stock) on a 250 rpm, 37°C shaker overnight. Satellite colonies are tiny colony always grow around large colony. Those

satellite colonies grow because of the decreased antibiotic resistance around big colonies. Therefore, never pick satellite colonies for inoculation, as they do not have expression construct inside.

Dilution for enlarged cultivation

The overnight start culture are diluted into glass flask (2.8 liter) with 800 mL autoclaved LB medium at a volume ratio of 1:100 and grown on a shaker of 250 rpm at 37°C for 2.5 to 3 hours until OD_{600} reachs 0.6-0.8. Cell viabilities should remain high during cell growth and induction. 800 mL of culture in a 2.8-liter flask should provide sufficient air exchange to sustain cell growth. The start culture can be saved in 25% glycerol as stock at -80°C and be recovered for no more than two frozen-thaw cycles without significantly compromise of cell performance.

Induce protein expression

The culture in flask were moved to 30°C shaker and shaking for 5 minutes (cooling) before induced with 0.25 mM IPTG for 4 to 6 hours. Other than 30°C, which is the most commonly used induce temperature, 20°C or 16°C are also temperatures worth trying as lower temperature might slow down protein synthesis and help folding. Duration of induce time should be extended to 12-18 hours when inducing at lower temperature.

Centrifugation for cell pellet

Cells are pellet down in a pre-cooled centrifuge (Beckman) at 6000 rpm for 10 minutes. The cell pellet could be stored at -80°C before protein purification.

2.4.2.2. Protein purification

Sonication to release protein

Several methods are commonly used to lyse bacterial cells like French Press, homogenizer, freeze-thaw cycle or sonication. Among them, sonication is widely used for its easy of handle and high efficiency of cell wall disruption. This method delivers pulsed sound waves with high frequency through a vibrating probe that immersed in the cell suspension to agitate bacterial cells. Bacterial pellet from 800 mL culture was re-suspended in 30 mL His-binding buffer (20 mM sodium phosphate, PH 7.4, 500 mM NaCl, 40mM imidazole, 10% glycerol) with additives (1 mM of PMSF as serine and cysteine protease inhibitor, 0.7% of β-ME as antioxidant) in a plastic beaker and sonicated with directed a probe until cell lysate turn clear. Sodium phosphate buffer was always used as binding buffer as it supports better binding of His×6 tagged proteins to the column. Tris-NaCl buffer may increase the solubility of the protein after sonication, but it should be avoided for proteins with weak binding to the column since it may reduce the binding strength. The plastic beaker should be used instead of glass beaker because glass beaker is likely to break under strong sonication wave. The beaker used for sonication should be cooled in ice-water mixture to prevent overheating and denature of the protein. Perform the sonication with on and off cycle

(10 S/ 15 S) at an amplitude of 50% would efficiently reduce heat accumulation. If the protein solubility is good, protein can be easily released from the cell and cell lysate is in bright brown color after sonication.

Centrifugation and filtration for clarified lysate

The lysate are centrifuged in a pre-cooled high speed centrifuge (Beckman) for 2 hours at 20000 rpm to pellet the cell debris. The cell lysate supernatant is further filtered through 0.22 μm membrane to remove any remaining particles. Cell lysate and buffer need to be particles-free before applied into column and FPLC for purification.

Protein binding to column

Wash the His Trap column (GE) with 5 CV (column volume) of His-binding buffer to equilibrate the column. The clarified lysate were loaded onto the column by FPLC (GE Healthcare) at a flow rate of 1 mL/minute. 20 to 40 mM of imidazole can be added into the His-binding buffer to increase the selectivity of His-tagged proteins from cellular host proteins with exposed histidine. While 40 mM of imidazole is generally satisfactory to most proteins, the concentration gives highest protein purity and yield is protein dependent and has to be determined for each individual protein. Imidazole quality is essential, as pure imidazole gives no UV_{280} absorbance. His Trap column are pre-packed column with intensely cross-linked agarose beads and chelating group for nickel (Ni^{2+}) has been immobilized on the beads. Amino acid

histidine can easily form complex with metal ion nickel and this interaction increased dramatically with His×6 (His-His-His-His-His-His-), which is widely used as affinity tag in recombinant protein purification. His Trap column can be washed and stripped thoroughly and recharged with Ni^{2+} (2.5 mL of 1M $NiSO_4$ for 5 mL column) after 4 to 6 rounds of purification.

Washing off unspecific binding

The protein-loaded column was washed with His-binding buffer to remove unspecific binding. Usually 13 CV of His-binding buffer is needed to wash out most of the impurities. But for some proteins, 15-20 CV of wash is required to get satisfactory results.

Protein elution

The recombinant protein bind to column was eluted out with His-elution buffer (20 mM PBS, PH 7.4, 500 mM NaCl, 500 mM imidazole). 5 column volumes of His-elution buffer are commonly sufficient to elute out most of the bounded His-tagged protein.

Protein buffer change

The protein eluted out in elution buffer can be changed buffer and concentrated by Amicon (Merk Millipore) with appropriate cut-off size (the average pore size of

the membrane). Amicon is a centrifugal filter device that allows fast ultrafiltration of protein sample. Protein with molecule weight larger than the cut-off size of Amicon is trapped in the membrane vessel while buffer and molecules squeezed through. It is one of the most convenient and fastest way to change buffer and concentrate of protein sample. All the proteins are changed to Tris-NaCl buffer (50 mM Tris. HCl, PH 8.0, 150 mM NaCl) before proceed to the next step.

Tag and fusion protein cleavage

His×6 tag are removed by off-column digestion with protease 3C at 4°C for 18 to 24 hours. The digestion can also be done on-column if the protein is stable without fusion tag. For digestion of protein for the first time, off column digestion has to be performed prior on column digestion, as some proteins are unstable or aggregated without fusion tag during digestion, thus clot the column during on-column digestion.

Further purification by size exclusion chromatography

Size exclusion chromatography (SEC), also named as gel filtration, is a chromatographic method to separate molecules in solutions by their size or molecular weight as they pass through the SEC medium packed in a column. SEC medium, usually made of dextran, are small porous beads with high chemical and physical stability. Buffer compositions generally do not directly affect the separation of

molecules as they do not bind to the dextran medium, so buffer used can be varied to suit the sample or the application afterwards. What is more, due to the high stability of dextran medium, conditions like low temperature, metals, detergents, urea and other harsh condition can be all applied to the column. Protein of different sizes can be separated by SEC, thus increased the purity protein. By look into the peak site and retention volume, protein quality (whether homogenous without degradation) or oligomerization state (monomer, dimer, trimer, or protein aggregates) can also be assessed.

To perform SEC, 200 μL to 5 mL of concentrated protein sample were injected into the Hi Load Superdex 75 PG column (GE) pre-equilibrated with at least 120 mL of buffer. The flow rate is set to 1.0 mL/min and both column pressure and UV were monitored by FPLC system (GE). Peaks were collect and concentrated to 2 to 5 mM. Peak fractions are resolved on a SDS-PAGE and stained with commissure brilliant blue. Small sample volume and reduced flow rate would always give better resolution. At last, 1 μL of the protein sample was sent for mass spectroscopy to verify the identity of the protein.

Protein concentration assay

Protein concentration assay was done by the Bio-Rad DC protein assay (Bio-Rad) kit which is a colorimetric method similar to Lowry assay to determine protein

concentration following detergent solubilization (Lowry et al., 1951). The reaction begins between copper and protein in the alkaline solution, followed by the reduction of Folin reagent by copper-treated proteins. The color development is primarily due to the oxidation of aromatic residues tyrosine and tryptophan, and to a less extent of cysteine and histidine(Lowry et al., 1951; Peterson, 1979). The reduction of the Folin reagent develops a characteristic blue color with a maximum and minimum absorbance at 750 nm and 405 mm, respectively(Peterson, 1979), which can be read for absorbance at 750 nm directly with a spectrophotometer. If 750 nm is not available, absorbance between 650 to 750 nm can also be measured. The protein concentration can be read directly from the standard curve, which has to be freshly prepared together with the protein sample. This assay will take about 25 minutes to complete, including of 15 minutes incubation. Although tedious and time-consuming, proper handle with this method will always give satisfactory results. The detailed procedures can be refer to the manufacture's manual. Ubiquitin is a stable protein with very low UV absorbance. The overall compact structure of ubiquitin render it relatively stable in the concentration assay by Bio-Rad DC protein assay kit, resulting in lower concentration results. Boiling for 5 minutes to denature the protein before concentration assay would give accurate result.

The most accessible and simplest way to determine protein concentration in a well-defined buffer is to use ultraviolet-visible spectrophotometry together with the protein's extinction coefficient. The amino acids containing aromatic side chains, such

as tryptophan and tyrosine exhibit strong UV absorption. So the UV absorbance of protein is proportional to their aromatic residues content and protein concentration. The extinction coefficient of a protein can be calculated from the amino acid composition of the protein (Gill and Hippel, 1989). For most proteins with UV absorbance, measuring UV absorbance at 280 nm allows determination of protein concentration. Nevertheless, many factors have to be considered as they can greatly influence the accuracy of this method. First, the protein has to be highly pure, as a combination of proteins with different extinction coefficients is not suitable for this method. Second, the buffer should not containing any chemicals with UV absorbance or nucleic acids that interfere with this method. Lastly, the status of the protein also matters, as the oxidant state or other conditions that change the conformation of the protein may also interfere with this method.

Protein storage

After all the hard working to express and purify the recombinant proteins, the correct way to store the purified protein means everything. Purified proteins are often in a buffer condition that differs considerably from their native environments. So if buffer and storage conditions are not properly maintained, purified proteins may be degraded, aggregated or undergoes other modifications that compromise protein integrity and function. Several protein storage conditions are summarized as in the Table 2.6. The simplest way to store proteins is store them in autoclaved Eppendorf tube at 4°C for less than 24 hour as longer time are more likely to have bacterial growth

or protease degradation of the protein. For longer period storage of proteins such as protease 3C, store proteins in buffer with 25% glycerol at -20°C is a good option, as glycerol can be served as cryoprotectant and it is not interfere with the following usage of the protein. For proteins that need long term storage and prefer no additives to be added into the buffer, flash frozen the proteins in small aliquots with liquid nitrogen and store them in -80°C fridge or even liquid nitrogen would give a shelf life of several years. This storage condition is always used in the lab as the purified proteins are more often used beyond 24 hours after purification and the additives like glycerol is not desired or compatible with the *in vitro* functional studies and crystallization. The lyophilized methods can also be used if the protein can be dissolved in a volatile buffer, but some proteins should avoid this method, as they are not stable in freeze-drying process. Several points are key for all the different storage conditions. Firstly, all the buffers used in the protein purification should be autoclaved or filter sterilized, as microbial would digest and contaminate the protein. Secondly, all the tips used on pipette, the beaker for sonication, sample loop for lysate loading, glass tube for fraction collection, Amicon for buffer change and protein concentration and Eppendorf tubes for protein aliquot should be autoclaved or carefully washed for the aforementioned reason. Thirdly, concentrate the protein to a high concentration but do not form aggregates would protect the protein during storage. Last but not the least,

aliquot in small volume and avoid multiple freeze-thaw cycle.

Table 2.6 Purified protein storage

Storage condition	Shelf life
4° C in buffer	Less than 24 hours
20° C in buffer with 25% glycerol	1 year
Frozen in -80 ° C fridge or in liquid nitrogen	Several years
Lyophilized and frozen	Several years

2.4.3. Isothermal Titration Calorimetry (ITC)

ITC studies were performed at 25 ^{o}C with an iTC200 microcalorimeter (MicroCal Inc.). Protein samples were dialyzed with Tris buffer (50 mM Tris, PH 8.0, and 150 mM NaCl) and degassed prior to the experiment. For UBA-ubiquitin interaction, the injection syringe is loaded with ubiquitin and the cell is loaded with UBA, including WT, S405E, S409E, S405A, S409A, K422A and K422E. Typical titrations consisted of 36 injections until the heat generated is negligible. The equilibration time between injections is 200 seconds. Data were integrated and analyzed on Origin 7 provided by ITC manufacture. For each experiment, at least two independent titration experiments were performed.

2.4.4. Size exclusion chromatography (SEC)

Concentrated proteins for size-exclusion chromatography were centrifuged to remove any bubbles and particles. Size-exclusion column (Superdex 75, GE

Healthcare) equilibrated with at least one column-volume (120 mL) of Tris buffer was loaded with protein sample at the flow rate of 1.0 mL/min. The UV absorbance was plotted against retention volume by software Unicorn (GE Healthcare).

2.4.5. Static light scattering (SLS)

Static light scattering was performed on Wyatt Dawn 8+ (Wyatt Technology) and it is connected to an ÄKTA FPLC system (GE Healthcare). The ÄKTA system was equipped with a size exclusion column (Superdex 200 10/30 GL, GE Healthcare), and equilibrated with at least one column-volume of Tris buffer until the light scattering signal become stable. Concentrated proteins after size exclusion chromatography were centrifuged to remove any bubbles and particles before loaded onto the column at a flow rate of 0.5mL/min. Both UV signal and light scattering signal were plotted and analyzed by software ASTRA.

2.4.6. Differential Scanning Calorimetry (DSC)

Differential Scanning Calorimetry measurements were carried out using a MicroCal VP-DSC calorimeter (MicroCal Inc.) with 0.5ml cells. For the thermal stability data collection, all the protein samples were exchanged to buffer containing 20 mM HEPES, pH7.4, 115 mM NaCl, 1.2 mM $CaCl_2$, 1.2 mM $MgCl_2$ and 2.4 mM K_2HPO_4 by dialysis. Five rounds of buffer to buffer scans (10 to 90°C, 60°C /hr) were performed to acquire a high quality baseline and a consistent thermal history

prior to the protein data collection. The protein samples at a concentration of 200μM were degassed and warmed to 25°C before loaded into the sample cell. All the protein samples were injected in a temperature window between 15°C and 25°C. Data were analyzed by the software provided by the manufacturer (MicroCal Inc.), with steps including baseline subtraction, normalization and model fitting. For each experiment, at least three independent scans were performed.

2.4.7. NMR (HSQC)

^{1}H-^{15}N HSQC spectra of p62 UBA WT and S409E were collected at a concentration of 100 μM in 20 mM sodium phosphate buffer, pH 6.8, 5 mM potassium chloride, 1 mM EDTA and 10% D_2O. For ubiquitin titration, 6-equimolar of ubiquitin was mixed with the ^{15}N labeled UBA sample for the data collection. The spectra were acquired with a Bruker Avance 700 MHz spectrometer at 20°C and data were processed by the software provided by the manufacturer (Bruker Corporation).

2.4.8. Ub binding assay

For cell-based poly-Ub binding assay, p62 knockout MEFs transiently transfected with FLAG-p62 WT, S409A, S409E, K422A, S409E/K422A or empty vector were lysed with RIPA buffer. To generate poly-Ub proteins, normal p62 knockout MEFs were treated with MG132 and then lysed with RIPA buffer. Same amount of protein lysates from each pool were mixed and incubated with M2 FLAG

affinity gel beads for overnight at 4°C. Beads were extensively washed with RIPA buffer five times and then subjected to immunoblot assay.

2.4.9. Crystallization and structure determination

The crystals of both S405E and S409E were grown at 16^{o}C by the hanging drop vapor diffusion method. 1μL of protein (2.5 mM) in Tris buffer (150 mM NaCl, 150 mM Tris, PH 8.0) was mixed with 1μL of reservoir buffer. S405E crystal was grown in buffer 0.05 M potassium phosphate monobasic, 20% w/v polyethylene glycol 8,000 after five days of incubation at 16^{o}C. S409E was grown in buffer 100mM citric acid, pH3.5, 25% PEG3350 after seven days of incubation at 16^{o}C.
Both crystals were cryoprotected in reservoir solution plus 20% glycerol for 10 seconds before mounted to the in-house Rigaku MicroMaxTM-007HF X-ray machine for data collection. Diffraction data were collected at 100K, integrated by Mosflm (Leslie, 2006) and scaled by the SCALA module (Evans, 2006) in CCP4. All the structures were solved by molecular replacement using the PHASER module in the CCP4i suite of programs with mouse UBA wild-type structure (PDB ID: 3B0F) as search model (McCoy, 2007). The subsequent structural refinement was conducted using REFMAC module in CCP4 (Murshudov et al., 1997). Manual structure rebuilding was done using WINCOOT (Emsley and Cowtan, 2004). Data collection and refinement statistics are summarized in table 2.1. The coordinates of S405E and S409E have been deposited to Protein Data Bank with the respective

PDB ID5HH2 and 5HGY. The structure figures were prepared using the CCP4mg package (Potterton et al., 2004) in CCP4.

Chapter 3. Potent Beclin1-UVRAG interaction via coiled coil region is critical to promote Vps34-dependent endocytic trafficking and can be targeted for modulation

3.1. Introduction

3.1.1. Atg14L and UVRAG are mutually exclusive binding partners of Beclin1 mediated by their respective coiled coil domains

The mammalian Class III phosphatidylinositol 3-kinase (PI3KC3) complex, also termed the Beclin1-Vps34 complex, is a dynamic multi-protein assembly that plays critical roles in membrane-mediated intracellular transportation processes such as autophagy, endocytic trafficking and phagocytosis (Funderburk et al., 2010). Core members of this complex include the lipid kinase Vps34 that serves as the major producer of phosphatidylinositol 3-phosphate (PI3P) lipids; a serine/threonine kinase Vps15 stably associated with Vps34, the scaffolding molecule Beclin1 and either Atg14L or UVRAG as the Beclin1-binding partner (Itakura and Mizushima, 2009a). The binding of UVRAG and ATG14L to Beclin1 coiled coil domain is mutually exclusive through their respective coiled coil domain (Itakura et al., 2008; Itakura and Mizushima, 2009a). The Atg14L-containing form is termed Complex I and is mainly involved in early-stage autophagy induction. Atg14L is responsible for directing Complex I to ER sites to promote autophagosome biogenesis (Matsunaga et al., 2009a; Zhong et al., 2009). The UVRAG-containing form, on the other hand, is termed Complex II and play critical roles in late-stage autophagy execution and degradative

endocytic trafficking (Liang et al., 2006b; Liang et al., 2008b).

3.1.2. Beclin1 coiled coil domain is a metastable homodimer with an imperfect interface

The Beclin1 coiled coil domain forms an antiparallel homodimer, with each peptide chain consisting of 13 heptad repeats (Li et al., 2012c). For antiparallel coiled coils, hydrophobic residues at position *a* on one peptide chain are generally packed against the corresponding hydrophobic residues at position *d'* of another peptide chain to form *a-d'* packings. Those *a-d'* packings help to stabilize the coiled coil structure. Close look into the dimer interface of Beclin1 coiled coils revealed that, out of 13 unique *a-d'* pairs formed between heptad repeats, only 7 pairings exert favorable Van del Waals interactions to stabilize the antiparallel dimer. The remaining 6 *a-d'* pairings are either contain charged residues or residues with bulky polar side chains that significantly weaken dimer stability (Li et al., 2012c). In addition, all Beclin1 residues involved in *a-d'* pairings are highly conserved among different organisms. Those observations suggest that the antiparallel Beclin1 coiled coils is unstable and the metastable feature is conserved. The biochemical studies confirmed the metastable nature of Beclin1 coiled coils. The CD spectrum of Beclin1 coiled coil domain show that the dimeric structure is unstable at physiological temperature. The exchange assay further show that the metastable Beclin1 coiled coil domain readily undergoes dynamic exchange between dimer and monomer (Li et al., 2012c). Beclin1 coiled coil

domain is a metastable homodimer with an imperfect interface that with function significance.

3.1.3. Beclin1 coiled coil domain undergoes dimer-to-monomer transition upon interaction with Atg14L and UVRAG to form heterodimeric coiled coil assembly

Beclin1 coiled coil domain interacts with coiled coil domain of Atg14L and UVRAG exclusively to form two distinct Beclin1-Vps34 complex I and II (Itakura et al., 2008). Both coiled coil domain of Atg14L and UVRAG are in monomeric state. The metastable Beclin1 coiled coil domain readily undergoes dimer-to-monomer transition upon interaction with Atg14L and UVRAG to form heterodimeric coiled coil assembly. Coiled coil domain of Beclin1 binds to coiled coil region of Atg14L and UVRAG with high affinity (K_d ~3.22 and 0.24 μM, respectively), compared with the relatively weak association of Beclin1 coiled coil domain homodimer (K_d ~89 μM,) (Li et al., 2012c). The coiled coil interaction of Beclin1-UVRAG is stronger than Beclin1-Atg14L, as suggest by the smaller dissociation constant (K_d 0.24 *versus* 3.22 μM). Moreover, Beclin1-UVRAG interaction is more resistant to high salt environment than Beclin1-Atg14L interaction, indicating that Beclin1-UVRAG interaction is stronger and more hydrophobic in nature.

3.1.4. The Beclin1-UVRAG interaction is critical for autophagy and endocytic trafficking

The ultraviolet (UV) radiation resistance-associated gene (UVRAG) is isolated and named for its ability to partially complement the ultraviolet sensitivity in xeroderma pagmentosum cell line (Perelman et al., 1997). The human *UVRAG* gene is localized at the chromosome locus 11q13 and locus 11q13 is implicated in a variety of tumors (Bekri et al., 1997; Perelman et al., 1997). Studies revealed that *UVRAG* is highly conserved and functions as a tumor suppressor (Liang et al., 2006a). UVRAG has also been reported as a regulator in autophagy and endosomal trafficking (Liang et al., 2006a; Liang et al., 2008a). *UVRAG* is reported to be mono-allelically mutated in various human tumors (Ionov et al., 2004). The tumor-suppressing activity of UVRAG has so for been largely attributed to its autophagy-promoting ability. UVRAG is firstly described by Liang as a novel autophagic protein that binds to Beclin1 and functions as a tumor suppressor (Liang et al., 2006a). HCT116 human colon cancer cells with very low level expression of UVRAG are defective in autophagy. UVRAG reconstitution greatly restored autophagy and suppressed cancer cell proliferation (Liang et al., 2006a). In addition, knock down of *UVRAG* suppressed autophagy (Liang et al., 2006a). Recent studies show that truncation of *UVRAG* gene promotes tumorigenesis in colorectal cancers (He et al., 2015). MicroRNA 183 (miR-183) has been reported to target *UVRAG* for autophagy regulation and inhibition of endogenous miR-183 enhanced autophagy activity (Huangfu et al., 2015). Although UVRAG has been largely reported as a putative tumor suppressor and positively

regulates autophagy, its role in autophagy is with controversy. For example, UVRAG mutations in microsatellite unstable cancer does not affect autophagy (Knævelsrud et al., 2010).

Vps34 is a Class III phosphatidylinositol 3-kinase (PI3KC3) that forms a core complex with Beclin 1 and Vps15, and functions in various trafficking pathways including endocytosis, multi-vesicular body formation and autophagy (Itakura and Mizushima, 2009b). In yeast, there are two functional distinct PI3K complexes. Vps34, Vps15, Vps30/Atg6 and Atg14L form complex I that is essential for autophagy. In contrast, Vps34, Vps30/Atg6 and Vps38 form complex II and mainly functions in vacuolar protein sorting pathway (Itakura et al., 2008). UVRAG is a putative mammalian orthologue of yeast Vps38 (Itakura and Mizushima, 2009b). UVRAG binds to Beclin 1 and up-regulates Vps34 activity, which leads to increased PI3P production and enhanced autophagosome formation (Liang et al., 2006a). It has also been reported that UVRAG interacts with Vps34 core complex to promote autophagosome and endosome maturation (Matsunaga et al., 2009b). The Vps16-binding ability of UVRAG C2 domain and CEP63-binding domain have been reported to recruit membrane for fusion machinery, which promotes autophagosome maturation and later step of endocytosis. Endosome is a membrane-bound compartment inside eukaryotic cells that transports extracellular molecules, plasma membrane receptor proteins or ligands internalized for lysosomal degradation. UVRAG functions not exclusively in autophagy regulation, instead a large portion of

UVRAG present at the endosomal compartments to execute endosome-associated functions (Liang et al., 2008a). UVRAG was reported to promote EGF receptor (EGFR) degradation through endocytic trafficking and depletion of UVRAG leads to sustained EGFR signaling (Liang et al., 2008c). BSA (bovine serum albumin) is a well-studied cargo endocytosed and designated for lysosomal degradation. In a DQ-BSA endocytic processing assay performed with macrophage RAW264.7, UVRAG over expression accelerated the DQ-BSA degradation without effecting the total amount of internalized BSA (Liang et al., 2008a). UVRAG was also found to promote lysosomal protein cathepsin D degradation through enhanced intracellular protein sorting from the TGN to lysosomes. As expected, restore of UVRAG expression in UVRAG-deficient HCT116 cells promotes cathepsin D maturation (Itakura et al., 2008; Liang et al., 2008c). These findings suggest that UVRAG accelerates endocytic trafficking of cargo to late endosome/lysosome for degradation.

There are also evidences that UVRAG interacts with C-Vps to stimulate endosome fusion, which promotes endocytic trafficking and degradation of cargo. The function of UVRAG-C-Vps interaction is different from the function mediated by UVRAG-Beclin1 interaction. This notion is supported by several reports. First, UVRAG C2 domain and CEP63 domain that responsible for Atg16 binding are not required for Beclin 1 binding. Second, while Beclin1-Class III PI(3)K mainly localized at the trans-Golgi network (Kihara et al., 2001), C-Vps are largely endosome-associated (Kim et al., 2001; Kim et al., 2003; Richardson et al., 2004).

Third, C-Vps proteins recruits to autophagosomes does not regulate autophagy, which is mainly mediated through UVRAG-Beclin 1 interaction (Liang et al., 2006a). What is more, UVRAG defective in Beclin1 binding but retain C-Vps binding is able to mediate $LC3^{+}$ and $LAMP1^{+}$ structures formation. In contrast, UVRAG defective in C-Vps interaction but retain Beclin1 binding is able to promote autophagy (Liang et al., 2008a). These results indicated that UVRAG might function as a trafficking effector in Beclin1-Class III PI(3)P and C-Vps complexes to contribute in autophagy and endocytic trafficking pathways.

3.1.5. UVRAG impacts endocytic trafficking via interaction with the HOPS complex

Initial recognition of Rab GTPase on transport vesicles by multi-subunit tethering complexes and subsequent coupling to SNARE-mediated fusion are two events required for membrane fusion within the eukaryotic endomembrane system (Bröcker et al., 2012). The conserved vacuolar/lysosomal homotypic fusion and vacuole protein sorting (HOPS) tethering complex, which is the core complex of class C vacuolar protein sorting (C-Vps), is thought to couple Rab activation and SNAREs assembly during membrane fusion (Nakamura et al., 1997; Peplowska et al.). UVRAG was reported to interact with HOPS, so as to stimulate autophagosome maturation and endosomal fusion, thereby enhancing both the autophagic and endocytic protein degradation (Liang et al., 2008a). However, the role of UVRAG in

autophagosome formation and autophagosome-lysosome fusion is controversial (Farr et al., 2010; Itakura et al., 2008).

3.1.6. Functional roles of UVRAG beyond autophagy

UVRAG is reported to help in preservation of genomic stability and centrosome integrity, which is mainly mediated by association of CEP63 with UVRAG CEP63-binding domain and independent of its autophagy related functions (Zhao et al., 2012). At the same time, UVRAG DNAPK-binding domain activates DNAPK to promote DNA double-strand-break (DSB) repair. UVRAG knock down increased radiation-induced DSBs (Myung Park et al., 2014). Those functions may confer tumor suppressor role of UVRAG that independent of autophagy (Zhao et al., 2012). In addition, UVRAG C2 domain interacts with BCL2-associated X (Bax) protein to regulate apoptosis (Yin et al., 2011). By binding to Bax, UVRAG blocks Bax translocation to mitochondrial membrane, which disrupts mitochondrial membrane potential, releases of cytochrome C and subsequent activation of caspase-9 and caspase-3, so as to induce apoptosis (Zhu and He, 2014). UVRAG has also been reported to play a role in control of Drosophila organ rotation, which is important for development of left-right body asymmetry (Lee et al., 2011a). *UVRAG* gene in human patient with left-right axis malformation has also been identified as disrupted (A et al., 2000).

3.2. Results

3.2.1. The Beclin1-UVRAG complex structure reveals a parallel coiled coil assembly

Beclin1 coiled coil domain displayed the prominent motif of heptad repeat *abcdefg* over a long stretch of amino acid sequence (174-266, ~90 residues). In contrast, the coil coiled domain of UVRAG only shows short stretches of such repeats (228-275, ~50 residues) interspersed by Gly-rich flexible segments. In order to identify the most critical region of Beclin1 coiled coil domain for UVRAG binding, a series of Beclin1 constructs scan through the entire Beclin1 coiled coil domain (residues 174-266) from N- to C-terminal were generated. Isothermal Titration Calorimetry (ITC) measurements reveal that the N terminal part (residues 174-223) of the Beclin1 coiled coil domain binds to UVRAG with high binding affinity (K_d ~0.30 μM) comparable to that for the entire Beclin1 coiled coil domain (K_d ~0.24 μM). So Beclin1 with residues from 174 to 223 was linked to UVRAG (residues 228-275) with a 10 residues GS*5 linker (GSGSGSGSGS) (Figure 3.1 a). Previous work done in the lab by Dr. He Yunjiao solved the crystal structure of this linked Beclin1-UVRAG heterodimeric coiled coil domain complex. The structure was determined by data collected at synchrotron that diffract to 1.8 Å resolution. The structure shows that, UVRAG and Beclin1 form a canonical parallel coiled coil heterodimer (Figure 3.1 b), which is distinct from the anti-paralleled homodimer of Beclin1 coiled coil domain (Li et al., 2012c). The $(GS)_5$ linker is not visible in the structure due to high flexibility

of the linker.

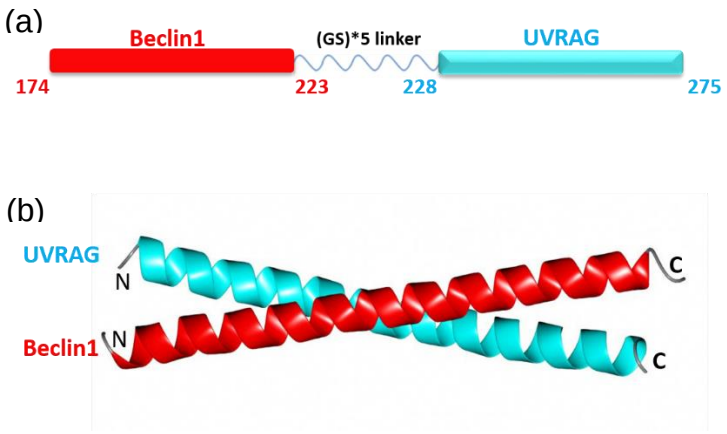

Figure 3.1 Crystal structure of Beclin1-UVRAG coiled coil complex

(a) The schematic diagram of Beclin1 and UVRAG linked with a (GS)*5 linker.
(b) The parallel heterodimeric crystal structure of Beclin1-UVRAG complex.

3.2.2. The Beclin1-UVRAG interface is significantly stabilized by hydrophobic pairings and electrostatically complementary interactions

Hydrophobic interaction, hydrogen bond and electrostatic interaction are major forces contribute to protein interaction. A signature feature of coiled coil dimer is the "leucine zippers" that consist of highly hydrophobic amino acid side chains. Those "leucine zippers" at the dimer interface "zip" and stabilize the coiled coil assembly. Close analysis of the interface of Beclin1-UVRAG coiled coil complex yields information on the molecular determinants that render the Beclin1-UVRAG heterodimer stable. First of all, Beclin1-UVRAG complex contains five pairs of perfect "leucine zippers" (L178*a*-L232*a'*, L185*a*-L239*a'*, L192*a*-L246*a'*, L196*d*-L250*d'* and L210*d*-L264*d'*, Beclin1 residues underlined) at the heterodimer interface

to stabilize the parallel coiled coil assembly. (Figure 3.2a). In addition to those hydrophobic “leucine zipper” pairs, negatively charged side chain E260 and polar side chain Q252 at the dimer interface in UVRAG form electrostatic interaction and hydrogen bond with positively charged side chain R203 in Beclin1. Moreover, interaction between UVRAG hydrophobic residue L271 and Beclin1 nonpolar residue A217 also contributes to stability of Beclin1-UVRAG dimer structure. In summary, all the hydrophobic pairings and additional stabilizing interactions render Beclin1-UVRAG complex notably stable.

In order to confirm our structural findings and further delineate the molecular determinants that facilitate stable Beclin1-UVRAG interaction, a series of UVRAG mutants were generated based on the complex structure, in which one, two, five and all six of hydrophobic leucine (L) residues involved in leucine zipper formation were replaced with polar and negatively charged glutamic acid (E), in the hope of disrupting the hydrophobic interactions that “zip” Beclin1 and UVRAG together (Figure 3.2 b). UVRAG with different number of L to E mutations (single-point, double-point, penta-point and hexa-point) were cloned into pETM vector or pET32M vector for protein expression.

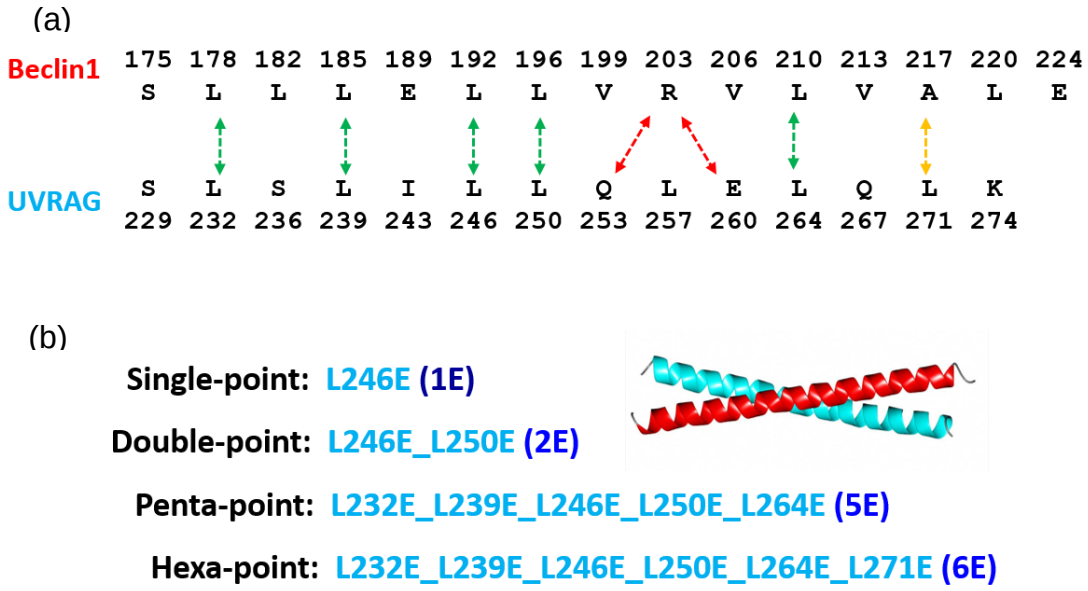

Figure 3.2 Key residues for Beclin1-UVRAG interaction

(a) The coiled coil interface of Beclin1-UVRAG heterodimer. Green arrows mark five pairs of "leucine zippers"; Red arrows denote the electrostatic interactions while yellow arrow indicates moderate hydrophobic interaction.
(b) Design of UVRAG Leu-to-Glu mutants.

Dr. He Yunjiao purified protein of Beclin1 and UVRAG mutants from *E.coli* and performed Isothermal Titration Calorimetry (ITC). ITC results show that the single Leu-to-Glu mutation (termed 1E) already significantly weakens its binding to Beclin1 coiled coil domain (K_d ~180 μM) while additional Leu-to-Glu mutations to replace two or more of the leucine residues (termed 2E, 5E and 6E) completely abolish such binding. (Figure 3.3 a and b). These data suggest that hydrophobic leucine residues on UVRAG collectively contribute to the strong Beclin1-UVRAG interaction.

(a)

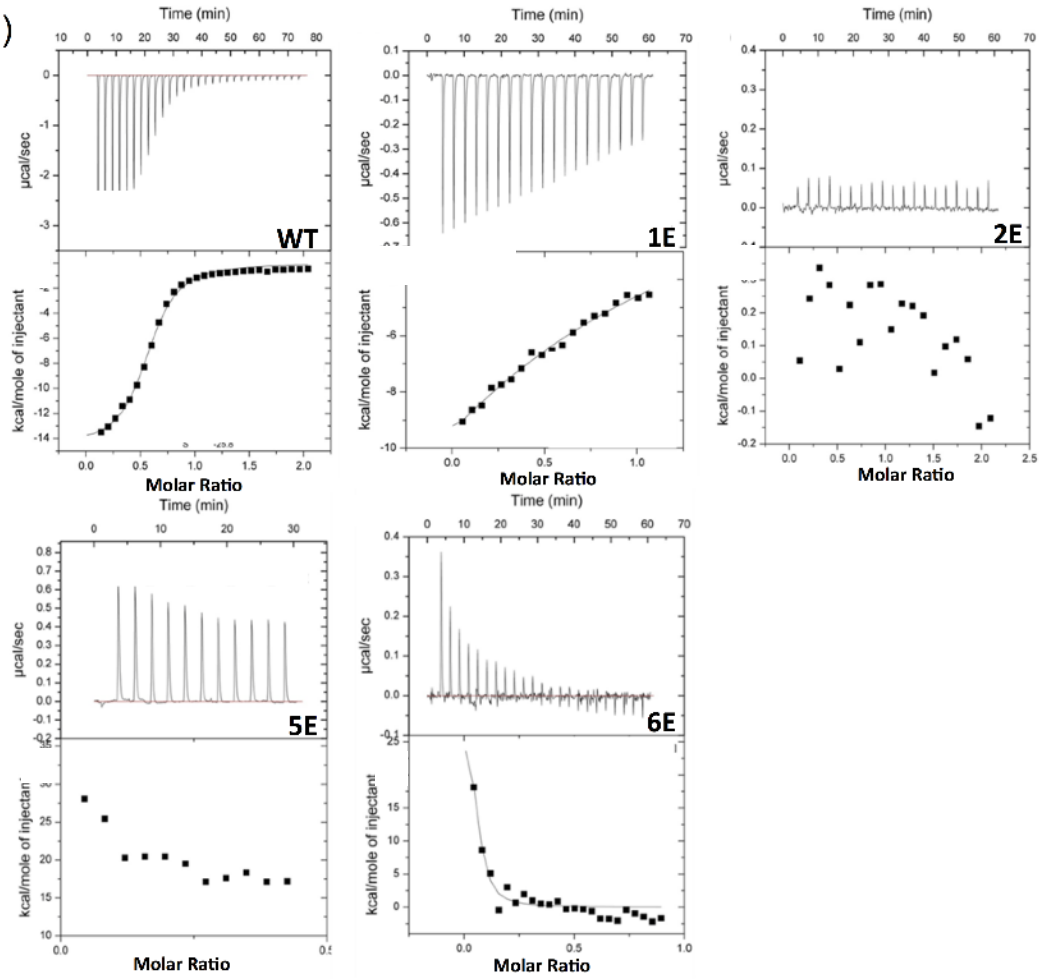

(b)

UVRAG	Mutations	Kd
WT	None	0.3 µM
1E	L246E	180 µM
2E	L246E_L250E	Not detectable
5E	L232E_L239E_L246E_L250E_L264E	Not detectable
6E	L232E_L239E_L246E_L250E_L264E_L271E	Not detectable

Figure 3.3 UVRAG mutations with reduced Beclin1 affinity

(a) ITC titration of UVRAG WT and mutants with Beclin1. UVRAG in syringe were titrated into cell with Beclin1. Top parts are ITC thermograms of Beclin1 titrated to UVRAG WT and mutants (1E, 2E, 5E and 6E). Bottom parts are plots of corresponding integrated heat values.
(b) Data from (a) were fitted with single site model with K_d summarized.

ITC studies confirmed a group of leucine residues in UVRAG that are critical for

Beclin1-UVRAG interaction. Next we tested those UVRAG mutants in mammalian cell for their interaction with endogenous Beclin1 by co-immunoprecipitation (Co-IP). FLAG-tagged full length UVRAG WT and mutants (1E, 2E, 5E and 6E) were transiently transfected into HEK293T cell and their interaction with endogenous Beclin1 was assessed. Our data (Figure 3.4) show that all UVRAG mutants can pull down similar amount of endogenous Beclin1, under both normal feed and nutrient deprived conditions.

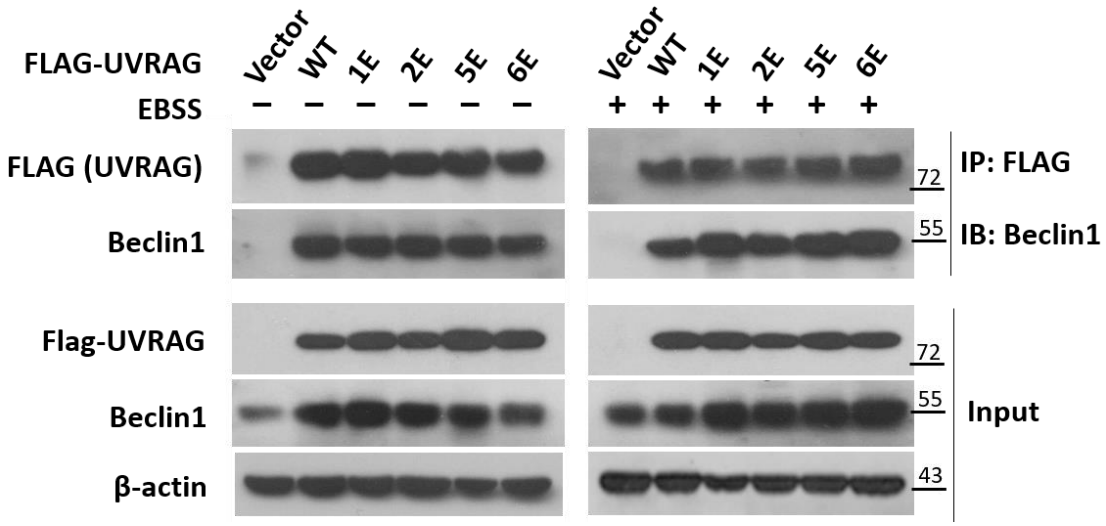

Figure 3.4 Co-immunoprecipitation results to characterize the association between Beclin1 and UVRAG Leu-to-Glu mutants *in vivo*

pCDNA3.1 Flag vector, full length UVRAG WT and UVRAG mutants (1E, 2E, 5E and 6E) were transiently transfected into HEK293T cell for 24 hours. Cells were treated with or without EBSS buffer for 2 hour before cell collection and lysis for immunoprecipitation by magnetic anti-Flag beads. The resulting immuno-complexes were resolved on a SDS-PAGE, followed by blotting and the subsequent detection of Beclin1.

These data does not agree with the *in vitro* ITC data. Several factors could lead to this discrepancy. First of all, while only coiled coil domain of UVRAG (229-274)

and Beclin1 (175-224) were used in ITC experiments, co-immunoprecipitation experiments used full-length proteins. So there is a possibility that other regions of UVRAG or Beclin1 might be involved in the interaction as well. Secondly, the sensitivity of the two methods is different. While ITC provides quantitative measurement of direct physical interaction, Co-immunoprecitation assay is more sensitive to detect overall co-precipitation of proteins but does not discriminate direct and indirect protein-protein interaction.

To further investigate the impact of these Leu-to-Glu mutations on the potency of the Beclin1-UVRAG interaction, we co-transfected those UVRAG mutants and Atg14L into HEK293T cells and probed their respective interaction with endogenous Beclin1 by co-immunoprecipitation experiments. This setup is intended to compare the binding affinity of Atg14L and UVRAG mutants to endogenous Beclin1 as they are mutually exclusive and essentially competitive binding partners of Beclin1. Our co-immunoprecipitation results show that in the presence of transiently over-expressed Atg14L, both 1E and 2E UVRAG constructs can pull down similar amount of endogenous Beclin1 as compared to UVRAG wild type. However, 5E and 6E constructs didn't pull down detectable amount of Beclin1, suggesting the Beclin1-binding potency of these mutants have been weakened and thus cannot compete with Atg14L (Figure 3.5). In summary these competitive co-immunoprecipitation experiments confirm that mutational perturbation of the key hydrophobic residues identified from our Beclin1-UVRAG complex structure leads to significantly

weakened interaction between these two molecules with the magnitude of such

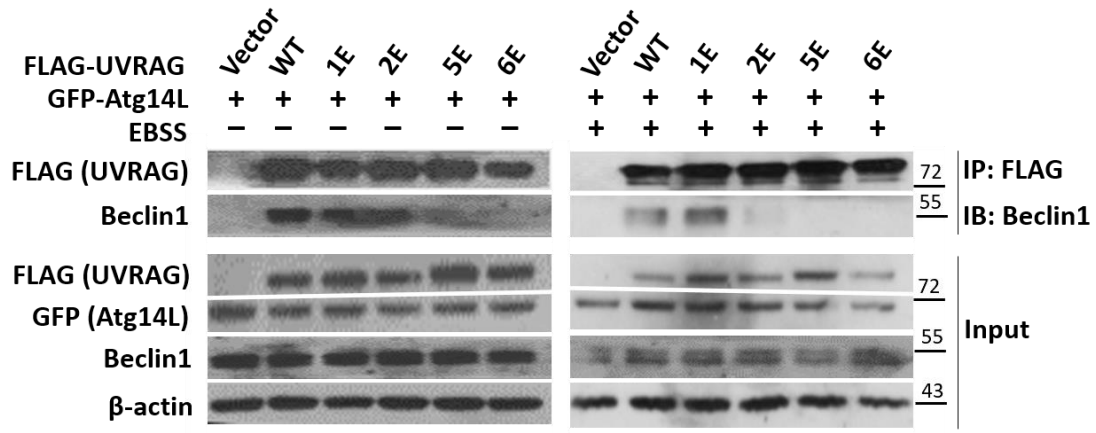

weakening tied to the number of mutations incorporated.

Figure 3.5 Competitive co-immunoprecipitation experiments to compare the *in vivo* potency of Beclin1 association between UVRAG mutants and Atg14L

pCDNA3.1 full length UVRAG WT or UVRAG mutants (1E, 2E, 5E and 6E) were transiently co-transfected with pEGFP N3 ATG14L into HEK293T cell for 24 hours. Cells were treated with or without EBSS buffer for 2 hour before cell collection and lysis for immunoprecipitation by magnetic anti-Flag beads. The resulting immuno-complexes were resolved on a SDS-PAGE, followed by blotting and the subsequent detection of Beclin 1.

These data not only prove that the "leucine zippers" stabilized UVRAG-Beclin 1 heterodimer, but also imply the essential role of this interaction in the homeostasis of Beclin1-UVRAG and Belin1-ATG14L complexes.

3.2.3. Potent Beclin1-UVRAG interaction via coiled coil domains is required to promote lysosomal degradation of EGFR but not critical for autophagy

After our structural and biochemical studies confirm a highly stable Beclin1-UVRAG coiled coil complex underpinned by a predominantly hydrophobic interface,

we set out to understand the functional significance of this potent interaction on Vps34-dependent autophagy and endosomal trafficking. This investigation is particularly relevant considering that the Beclin1 coiled coil domain forms only metastable homodimer due to a series of “imperfect” pairings at its otherwise hydrophobic interface(Li et al., 2012b). It is intriguing whether the potent Beclin1-UVRAG interaction is required for activities mediated by the UVRAG-containing Beclin1-Vps34 complex.

We transfected UVRAG mutants (1E to 6E) into HeLa cells stably expressing GFP-LC3 to assess the impact of Beclin1-UVRAG interaction on autophagy activity. Our results show that over-expression of wild-type UVRAG, as well as its mutants, caused no detectable difference in terms of LC3 puncta formation (Figure 3.6a). Furthermore, the impact by these UVRAG constructs on autophagy marker, such as p62 or LC3 is also negligible, whether in the presence or absence of lysosomal inhibitor chloroquine (CQ) (Figure 3.6b). Similar results were observed in HEK293T cells, as over-expression of either wild-type UVRAG or 6E mutant caused no change in the total amount of p62 or the relative ratio of LC3-I and II (Figure 3.6c). These results suggest that potent Beclin1-UVRAG interaction is not required for the execution of autophagy.

(a)

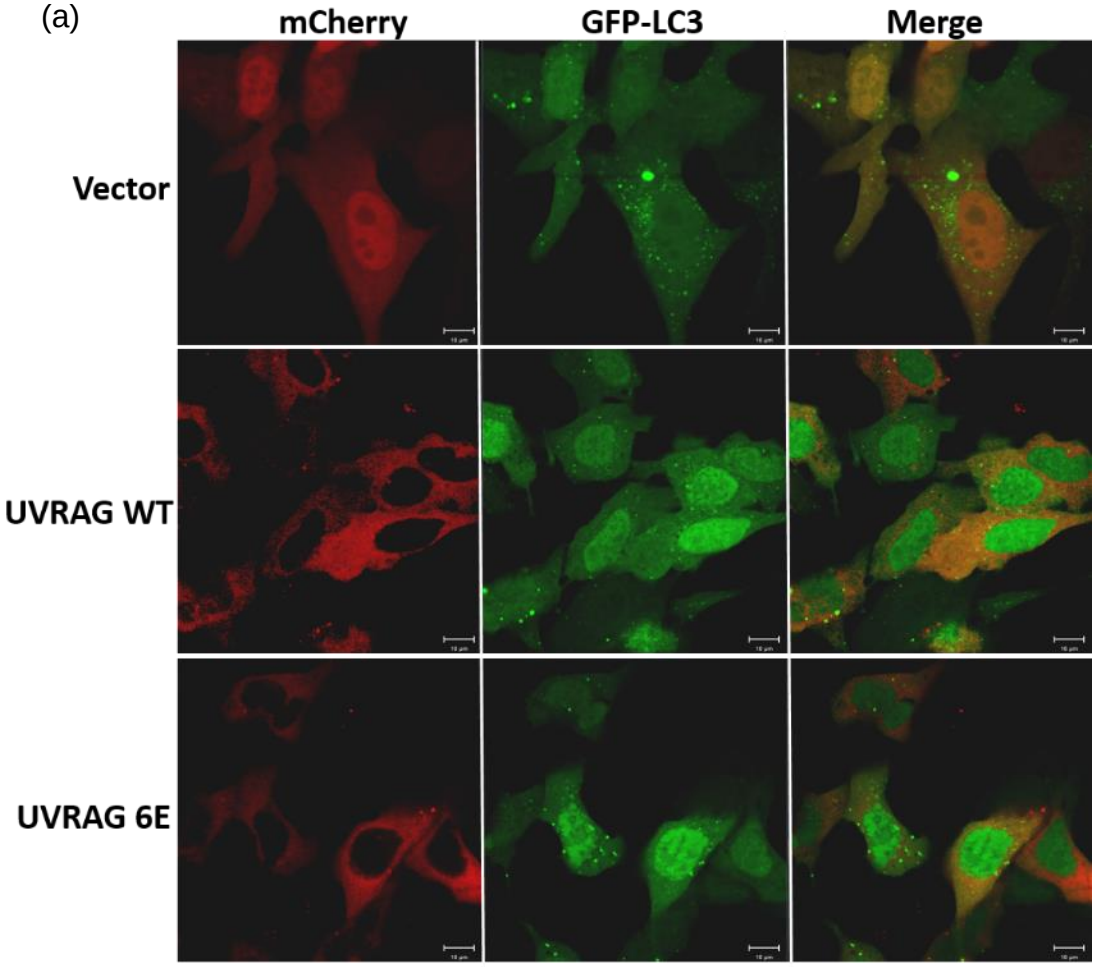
mCherry
GFP-LC3
Merge
Vector
UVRAG WT
UVRAG 6E

(b)

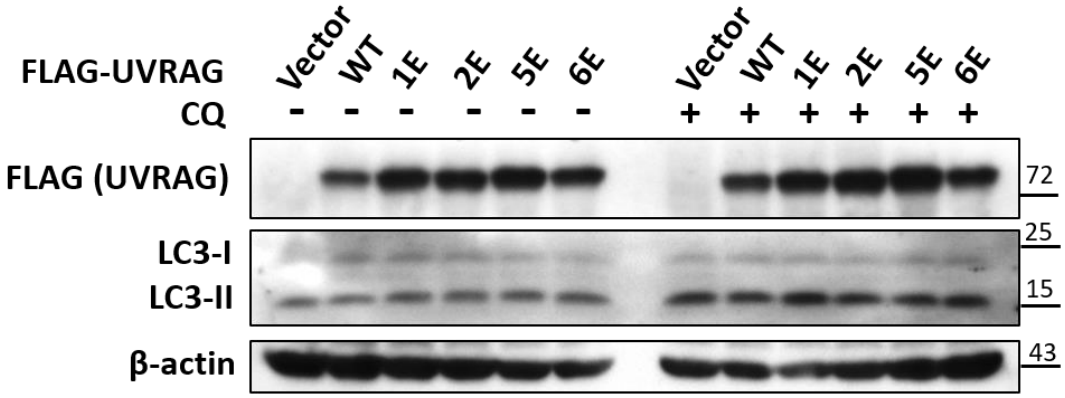
FLAG-UVRAG
Vector
WT
1E
2E
5E
6E
Vector
WT
1E
2E
5E
6E
CQ
- - - - - - + + + + + +
FLAG (UVRAG)
72
LC3-I
LC3-II
25
15
β-actin
43

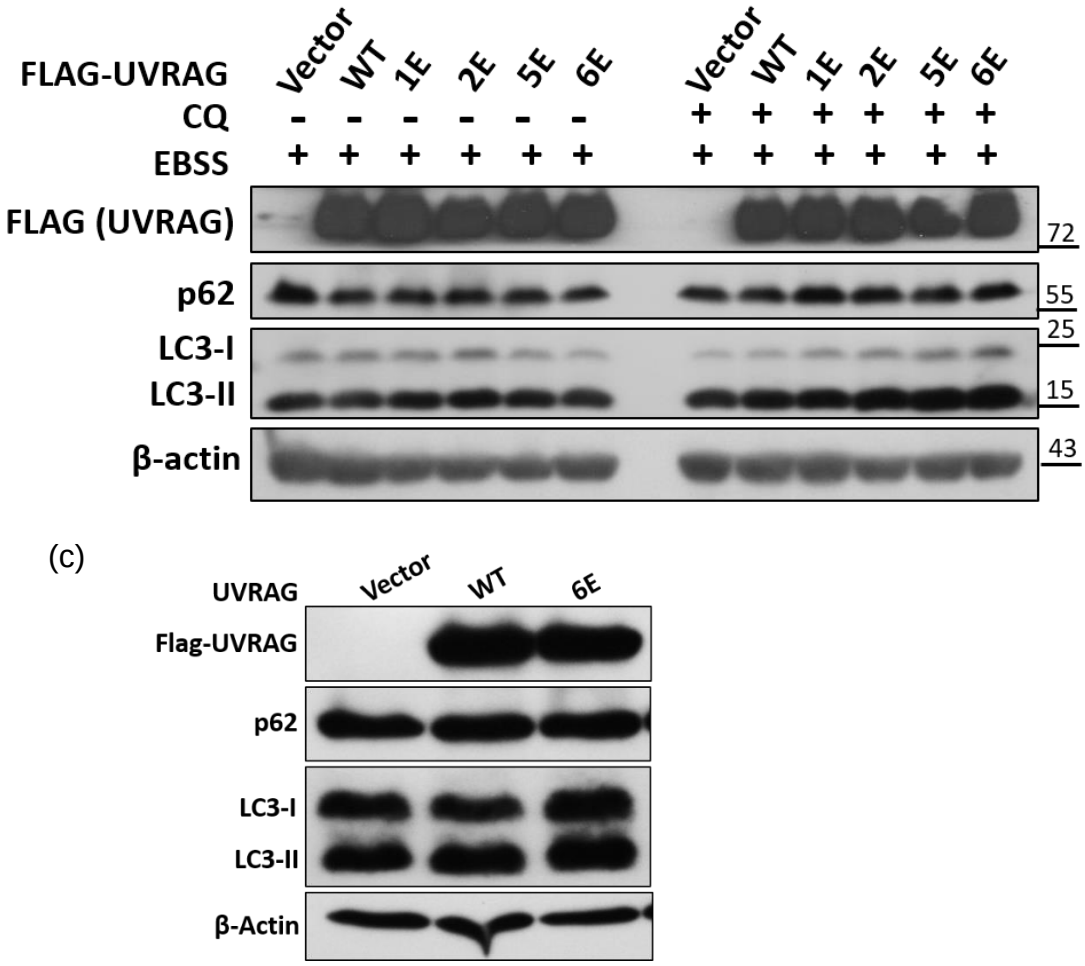

Figure 3.6 The potent Beclin1-UVRAG interaction is not essential for autophagy

(a) Representative confocal fluorescent images of HeLa cells stably expressing GFP-LC3 after transfection of mCherry-tagged UVRAG wild-type (WT) and 6E mutant construct. The pattern of LC3 puncta formation is little affected by over-expression of either WT or 6E. Scale bar represents 10 μm.
(b) Western blots of autophagy marker LC3 in HeLa cells stably expressing GFP-LC3 after co-transfection with FLAG-tagged UVRAG constructs either in the absence (-) or presence (+) of chloroquine (25μM, 3hr).
(c) Western blots of autophagy marker LC3 in HeLa cells stably expressing GFP-LC3 after co-transfection with FLAG-tagged UVRAG constructs either in the absence (-) or presence (+) of chloroquine (25μM, 3hr)

To assess the importance of potent Beclin1-UVRAG interaction in facilitating lysosomal degradation of EGFR, we transfected FLAG-tagged UVRAG constructs into HEK293T cells and tracked the EGFR degradation process after overnight

nutrient starvation followed by EGF stimulation. Over-expression of UVRAG wild-type, 1E and 2E constructs all led to significantly enhanced EGFR degradation while 5E and 6E failed to show similar effects (Figure 3.7). To further confirm these findings, we conducted similar experiments using A549 non-small cell lung cancer (NSCLC) cells. The EGFR degradation profile in these cells is significantly prolonged as compared to that in HEK293T (half-life ~ 3 hours with ~ 20% remaining after 5 hours in A549), probably to sustain excessive proliferation. Nonetheless, over-expression of wild-type UVRAG and 1E construct in A549 significantly enhanced the degradation profile of EGFR, shortening the half-life to ~ 2 hours with less than 10% remaining after 5 hours (Figure 3.8 a and b). 2E construct showed a weaker effect, with half-life comparable to that for control, but the overall degradation after 5 hours was improved (~ 5% remaining vs. 20% for control). However, 5E and 6E constructs didn't induce promotional effect at all. Their EGFR degradation profile is largely identical to that for control (Figure 3.8 a, b and c). These data suggest that the promotional effect of UVRAG on EGFR degradation is modulated by the potency of the Beclin1-UVRAG interaction. Only strong interactions afforded by wild type or 1E construct lead to significant enhancement to EGFR degradation. Weaker constructs like 2E can only induce subdued effects while constructs like 5E and 6E that are severely weakened and fail to compete with Atg14L cannot induce any promotion.

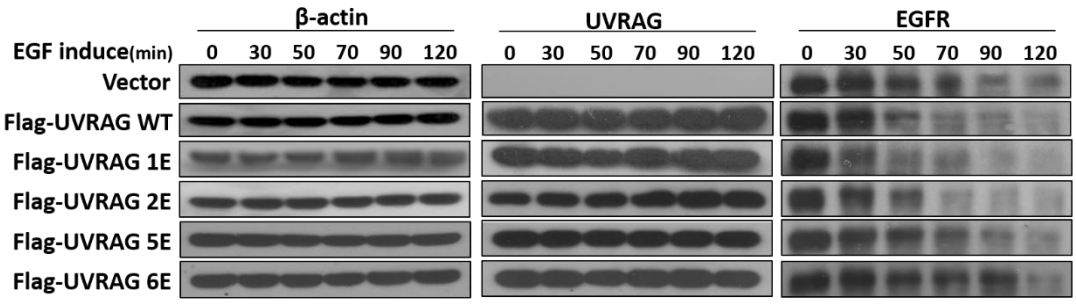

Figure 3.7 The potent Beclin1-UVRAG interaction is important for EGFR degradation in HEK293T cells

After transfection with UVRAG constructs, HEK293T cells were starved overnight and stimulated with EGF. EGFR level in cell lysate was analyzed by western blots at specific time points over the period of 120 minutes. Over-expression of wild-type, 1E and 2E UVRAG constructs lead to enhanced EGFR degradation while 5E and 6E fail to do so.

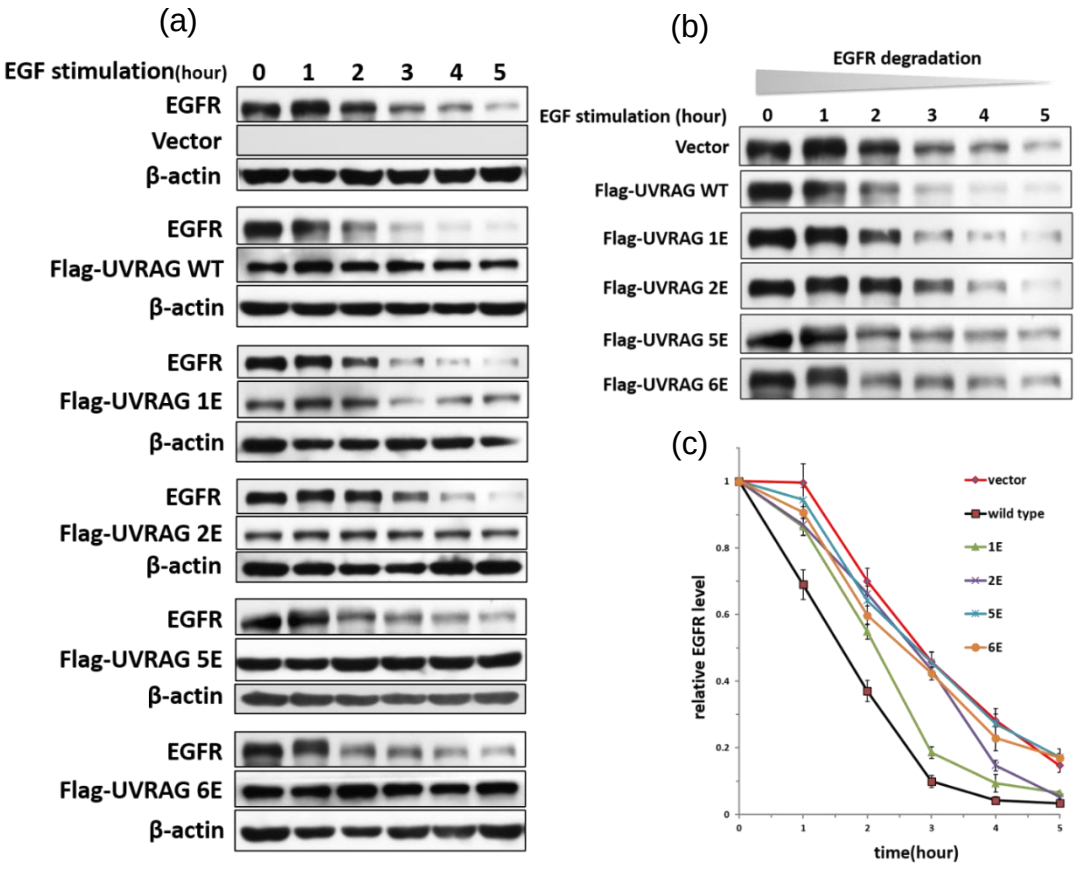

Figure 3.8 The potent Beclin1-UVRAG interaction is important for EGFR degradation in A549 non-small cell lung cancer cells

The time course for EGFR degradation in A549 cells is prolonged (~ 5 hours) as

compared to that in HEK293T (~ 2 hours). Nonetheless similar results were obtained. Over-expression of wild-type, 1E and 2E constructs lead to enhanced EGFR degradation while 5E and 6E fail to do so. Experiments were repeated 3 times and the statistical plot is shown on the right.

These data proved an essential role of UVRAG in EGFR degradation through endocytosis pathway and suggest that Beclin1-UVRAG interaction is important for EGFR degradation. To sum up, Beclin1-UVRAG interaction plays an essential role in endocytic degradation of EGFR but le ss essential for autophagy.

3.2.4. Structure-based rational design of Beclin1-targeting stapled peptides

Given the importance of the Beclin1-UVRAG interaction in facilitating lysosomal degradation of EGFR, we proceeded to structure-based rational design of Beclin1-targeting stapled peptide with the aim to promote Beclin1-UVRAG interaction and enhance EGFR degradation. These compounds, if successful, may have the translational potential to serve as novel approach to suppress EGFR-driven proliferation in cancer cells. Specifically, our plan is to develop small-molecule compounds in the form of stapled peptides that can bind to the C-terminal region of Beclin1 coiled coil domain, away from the UVRAG binding site (Fig 3.9). We expect these stapled peptides to disrupt the metastable dimer interface of Beclin1 coiled coil domain, facilitate the binding of monomeric Beclin1 to Atg14L and UVRAG, thus promote autophagy and enhance lysosomal degradation of EGFR.

Figure 3.9 The design principle of Beclin1-specific α-helical stapled peptides

The coiled coil (CC) domains of Beclin1 and UVRAG are drawn in relative scale to demonstrate the hydrophobic interface formed between the N-terminal half of Beclin1 CC domain and UVRAG. The stapled peptide is shown as a short ribbon. The spheres on the ribbon represent the chemically engineered staples to stabilize the α-helical structure. The two Ys mark Beclin1 residue Y227 and Y231, which correspond to the EGFR-phosphorylated Y229 and Y233 in human Beclin1. The stapled peptide is designed to bind to the C-terminal half of Beclin1 CC region starting from around Y227 and Y231.

As the first step of our design effort toward Beclin1-specific autophagy modulators, we need to prove that the C-terminal region of Beclin1 (residues 231-245) is not required for UVRAG binding and mutational perturbation at this region to prevent the formation of Beclin1 homodimer would be beneficial for its interaction with UVRAG. We generated a Beclin1 mutant L241E/L245E (mBeclin1) to weaken the hydrophobic leucine zipper pairs at the homodimer interface of Beclin1 coiled coil domain. These mutations are predicted to weaken the Beclin1 homodimer but should not interfere with the Beclin1-UVRAG interaction as they are outside of the Beclin1 construct (residues 174-223) used in Beclin1-UVRAG structure. ITC profile show that indeed the binding affinity of mBeclin1 to UVRAG is ~ 20 times stronger than that of Beclin1 wild-type (Figure 3.10).

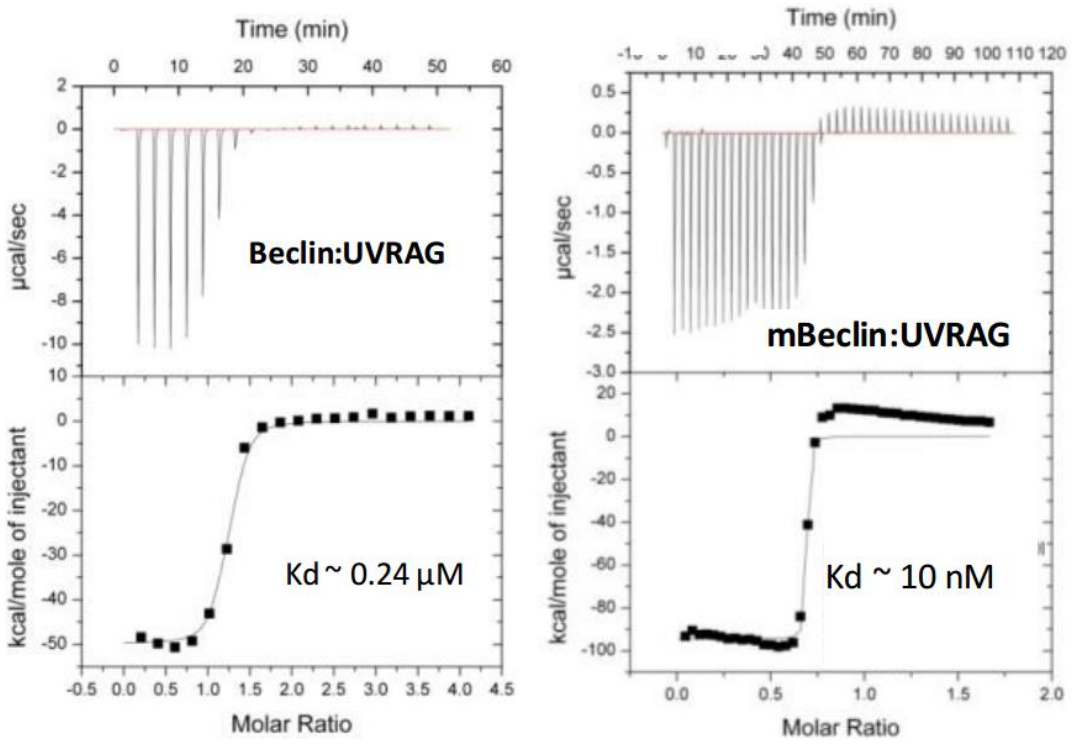

Figure 3.10 ITC profile show that Beclin1 with mutation in the C-terminal region of its CC domain (mBeclin) binds to UVRAG stronger than wild-type

Guided by experimental findings, we decided to generate stapled peptides that specifically bind to Beclin1 coiled coil region 231-245. While our ITC confirmed the importance of targeting L241 and L245 in our design process, we set the N-terminal starting point at Y231 as this residue corresponds to a site phosphorylated by EGFR in human Beclin1 to blunt its degradation(Wei et al., 2013). The next residue S232 is also a phosphorylation site targeted by Akt that functions to inhibit autophagy and facilitates Akt-driven tumorigenesis (Wang et al., 2012). Protecting this region with stapled peptides would potentially lead to more effective attenuation of EGFR signaling and inhibition of cancer cell proliferation. By integrating our structural findings as well as previous studies we believe region 231-245 of Beclin1 is the most effective target.

Beclin1-specific stapled peptide can be computationally built by simply taking the α-helical segment that interacts with the target region within the Beclin1 homodimer structure. In our case, the stapled peptide SP1 should have the sequence corresponding to residue 192-206 (Figure 3.11 a). A two-turn hydrocarbon staple is introduced *in silico* to link a pair of residues located at *i* and *i+7* positions at the non-binding surface of the peptide to help stabilize the α-helical structure but not to interfere with Beclin1 binding (Figure 3.11 a and b).

Small peptides like simple alpha helices often do not exhibit enough helicity in solution, thus lead to weak or even loss of binding to target protein. Also, random chain of the peptide in solution is prone to proteolytic degradation. To lock the short peptide in a preferred and confined conformation, synthetic braces like hydrocarbon are introduced into the peptide. Un-natural amino acids introduced hydrocarbon ring into the peptide through ring-closing reaction of the olefin terminals (Figure 3.11 c). The resulting ring formed in the peptide servers as brace to render short peptide stable with increased target binding and cell penetration ability, while resistant to proteolytic degradation. For stapled peptides used in this project, non-natural amino acids R8 and S5 with olefin terminal were introduced by rule of "i, i+7" (Figure 3.11 c and d). Figure 3.11 d shows the sequence of stapled peptide SP4 and how it is been stapled by non-natural amino acids R8 and S5.

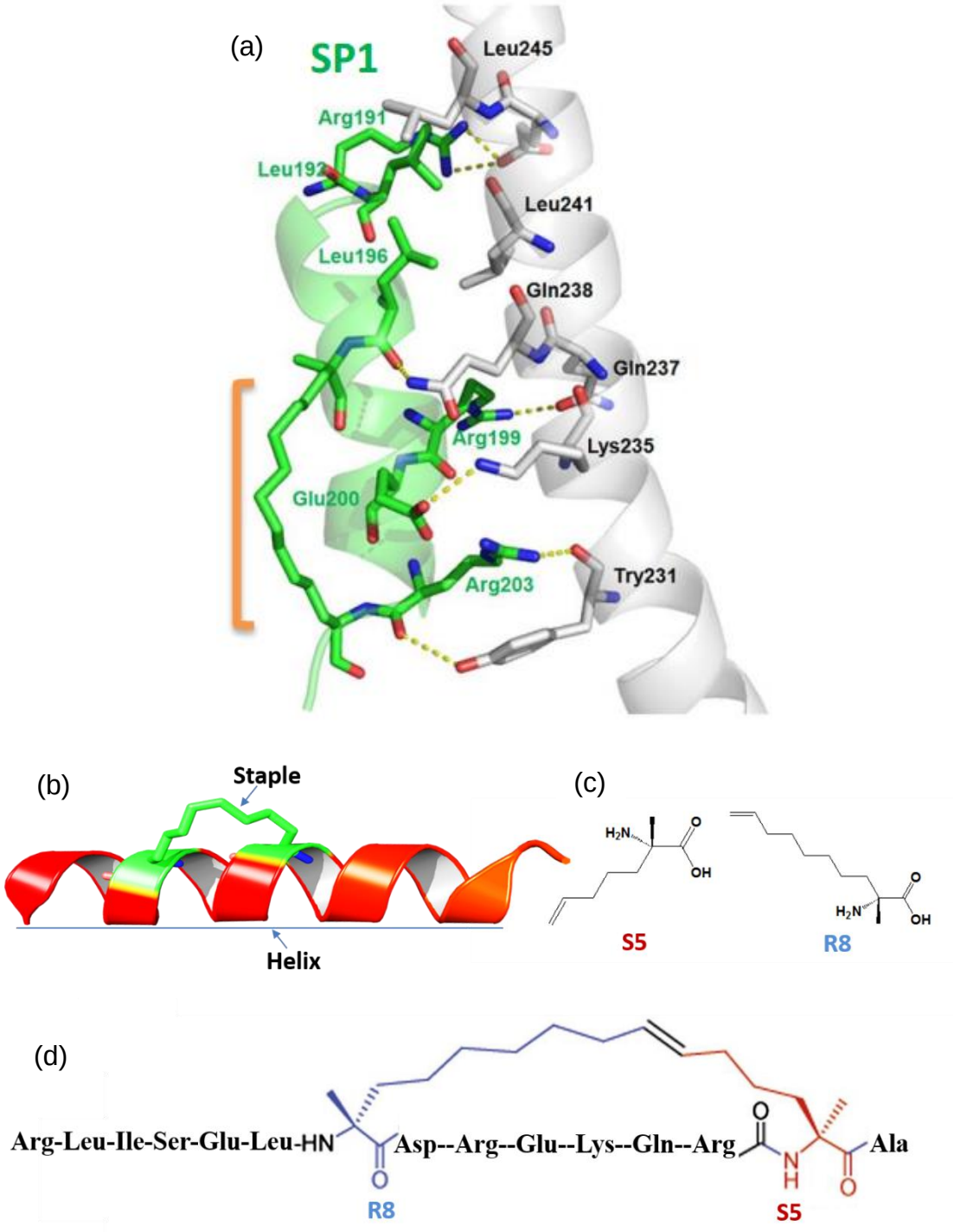

Figure 3.11 Structure-based rational design of stapled peptides to target the Beclin1 coiled coil domain

(a) Model of a computationally designed stapled peptide SP1 binding to the C-terminal region of Beclin1 CC domain. The orange bracket highlights the hydrocarbon staple. The residues are numbered according to Beclin1 sequence.
(b) Carton description of the stapled peptide. The red color depicts the peptide in helix, and the green color denotes the un-natural residues that lock the peptide conformation.
(c) Non-natural amino acids R8 and S5 with olefin terminal were used as building

blocks in stapled peptide.
(d) Non-natural amino acids R8 and S5 in stapled peptide SP4.

Computational optimization to enhance the binding affinity of SP1 toward the target region has been carried out. A library of stapled peptides was generated in which residues deemed critical for target site binding were unchanged while other amino acid residues were computationally varied (Table 3.1). The binding modes of these stapled peptides to the Beclin1 molecule were characterized by molecular dynamics (MD) simulation and their binding energies were computational calculated using the force field-based MM-GB/SA method. Certain sequence changes, such as replacing Val with Ala and Gln with Ser in SP4, led to significantly improved binding energy (Table 3.1).

12 stapled peptides were designed as the top candidates based on their computational interaction energy (binding ability) to Beclin 1 CCD (Table 3.1). Peptides SP4, SP9 and SP12 with high interaction energy were synthesized (Synpeptide, Shanghai) and screened for Beclin CCD binding.

Table 3.1 Computational modeling optimized stapled peptides

Number	Sequence	Interaction energy (kcal/mol)
SP1	Ac-RLIQEL(R8)DREAQR(S5)V-NH_2	-29.75±6.62
SP2	Ac-TLIQEL(R8)DREAQR(S5)S-NH_2	-43.69±5.21
SP3	Ac-RLISEL(R8)DREKQR(S5)V-NH_2	-47.51±3.96
SP4	Ac-RLISEL(R8)DREKQR(S5)A-NH_2	-56.05±6.87
SP5	Ac-RLIQEL(R8)DREKQR(S5)S-NH_2	-40.75±5.59
SP6	Ac-RLISEL(R8)DREKQR(S5)S-NH_2	-47.40±6.90
SP7	Ac-RLIQEL(R8)DREKQR(S5)R-NH_2	-45.77±5.13
SP8	Ac-RLIQEL(R8)DREKER(S5)A-NH_2	-49.78±6.34
SP9	Ac-LLISEL(R8)DREKQR(S5)A-NH_2	-74.52 ±4.31
SP10	Ac-RLLSEL(R8)DREKQR(S5)A-NH_2	-55.69 ±5.15
SP11	Ac-LLLSRL(R8)DREKQR(S5)A-NH_2	-50.47 ±5.23
SP12	Ac-LLISQL (R8)DREKQR(S5)A-NH_2	-56.05±4.35

The computationally optimized derivative SP4 was chemically synthesized following the method pioneered by Verdine, et. al. (Kim et al., 2011c). The importance of the hydrocarbon staple in maintaining the α-helical structure of the designed peptides is confirmed by circular dichroism (CD) measurements. The CD spectrum of peptide P4, which is the same as SP4 but without the hydrocarbon staple, shows largely loop-like profile (Figure 3.12 a). The CD spectrum of SP4, however, reveals high α-helical content. ITC profile showed direct interaction between SP4 and Beclin1 coiled coil domain with K_d ~ 2 μM, suggesting that this molecule can specifically bind to Beclin1 coiled coil domain and most likely at the intended target region of 231-245 (Figure 3.12 b). Furthermore, SP4 induced dimer-

to-monomer transition in Beclin1 coiled coil domain. The Light Scattering (LS) profile of Beclin1 coiled coil domain in absence of SP4 indicates a homodimer with predicted molecular weight of 24.8 kDa. However, the presence of SP4 would cause Beclin1 coiled coil domain to adopt a monomeric form as the predicted molecular weight is 15.8 kDa (Figure 3.12 c).

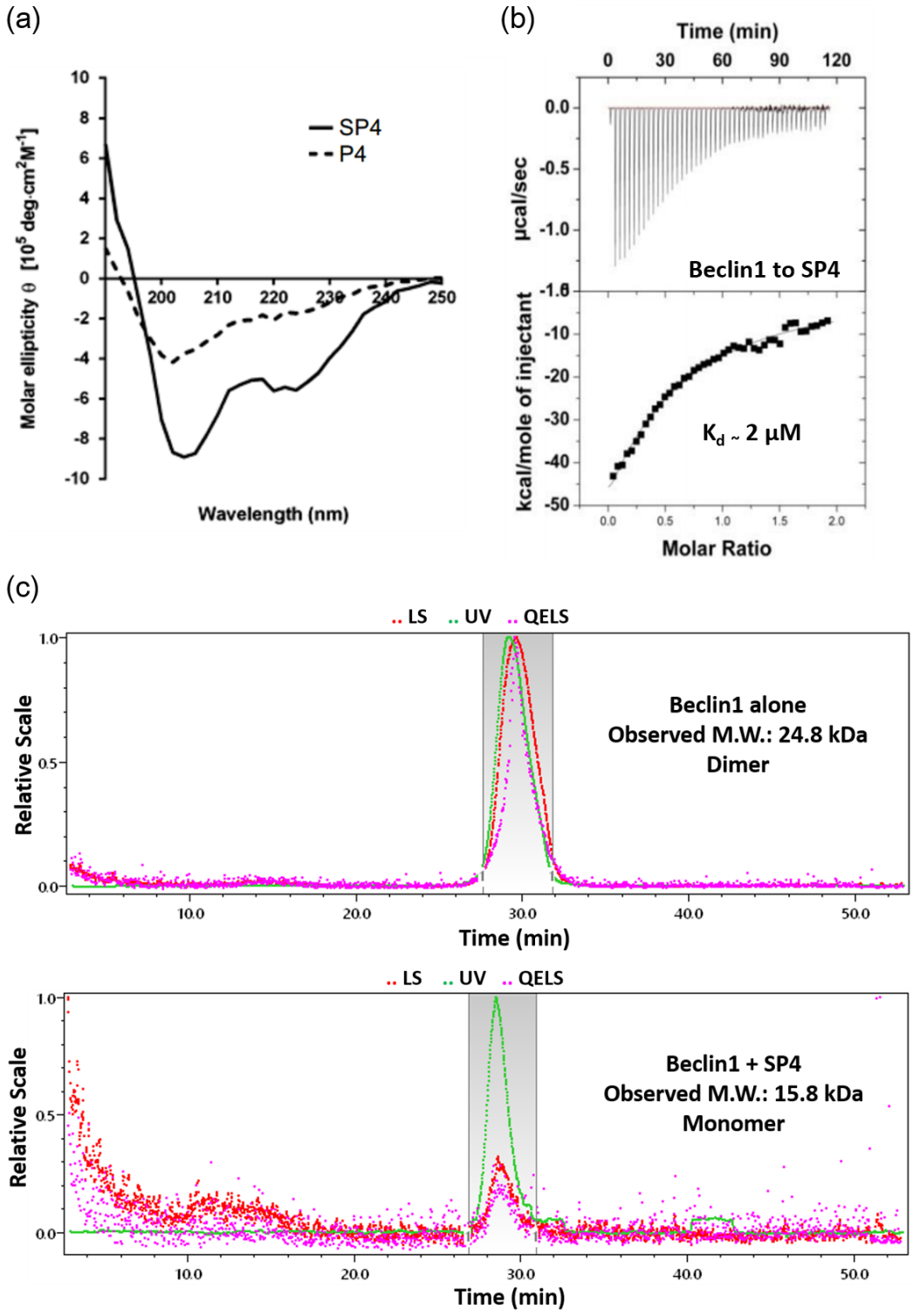

Figure 3.12 Stapled peptides bind to Beclin1 and make Beclin1 monomeric

(a) Circular dichroism spectra of stapled peptide SP4 and its unstapled version P4.
(b) SP4 binds to Beclin1 CC domain as confirmed by ITC measurements.
(c) SP4 induces dimer-to-monomer transition as shown by dynamic light scattering measurements. Beclin1 CC domain mixed with SP4 is passed through size exclusion chromatography and its time-dependent profile for dynamic light scattering (purple)

and UV absorbance (green) are plotted. The oligomeric state of the Beclin1 molecule is inferred from the molecular weight estimated from the light scattering profile.

In summary, structure-based rational design targeting the Beclin1 coiled coil domain at region 231-245 has yielded stapled peptides that specifically bind to Beclin1 coiled coil domain and render it monomeric to promote Beclin1-UVRAG interaction.

3.2.5. Rationally designed stapled peptides promote autophagy and enhance EGFR degradation

Trans-activator of transcription (Tat) is a protein encoded by Tat gene in human immunodeficiency virus 1 (HIV-1). The protein transduction domain of Tat contains a cell-penetrating peptide that is characterized to penetrate through cell membrane. Tat is appended in front of the SP4 to help it get into the cell (Table 3.2). Peptide with sequence shuffled randomly (Scrambled peptide) from SP4 was served as peptide control. To stabilize the peptide, N- and C terminals of the peptide were modified with acetyl group (Ac-) and an amine group (-NH2), respectively (Table 3.2). Both Tat tagged peptides were dissolved in H_2O with good solubility to high concentration (25mM). SP4 will be used for the following studies.

Table 3.2 Peptide components and stapled peptide

Peptide	Sequence
Stapled peptide	Ac-RLISEL(R8)DREKQR(S5)A-NH_2
Scrambled peptide	Ac-RALRIQSKEELRD-NH_2
Tat tag	YGRKKRRQRRR
Tat-Stapled peptide	Ac-YGRKKRRQRRR-RLISEL(R8)DREKQR(S5)A-NH_2
Tat-Scrambled peptide	Ac-YGRKKRRQRRR-RALRIQSKEELRD-NH_2

3.2.5.1. Cell viability test

Firstly, cell viability assay was performed by MTT methods. HEK293T and A549 cells seeded in 96-well plate were treated with 12.5 μM and 25 μM of Tat-Scrambled peptide or Tat-Stapled peptide. After treatment, cells were proceed to MTT assay. HEK293T cell treated with peptides (Tat-Scrambled and Tat-Stapled) for 24 hours show similar cell viability compared with cell without peptide treatment (Control) (Figure 3.13 a**)**, which suggests very low cell toxicity of peptides to HEK293T cell. At the same time, A549 cell treated with peptides for 5 hours maintained more than 98% of cell viability compared with control, which suggest low toxicity of both peptides under the given concentration and time course (Figure 3.13 b). However, prolonged peptide treatment to 24 hour reduced A549 cell viability (Figure 3.13 b). Peptide treatment for 5 hours with concentration less than 25 μM is considered as safe for A549 cell and all the assays with peptide treatment will be no more than 5 hours.

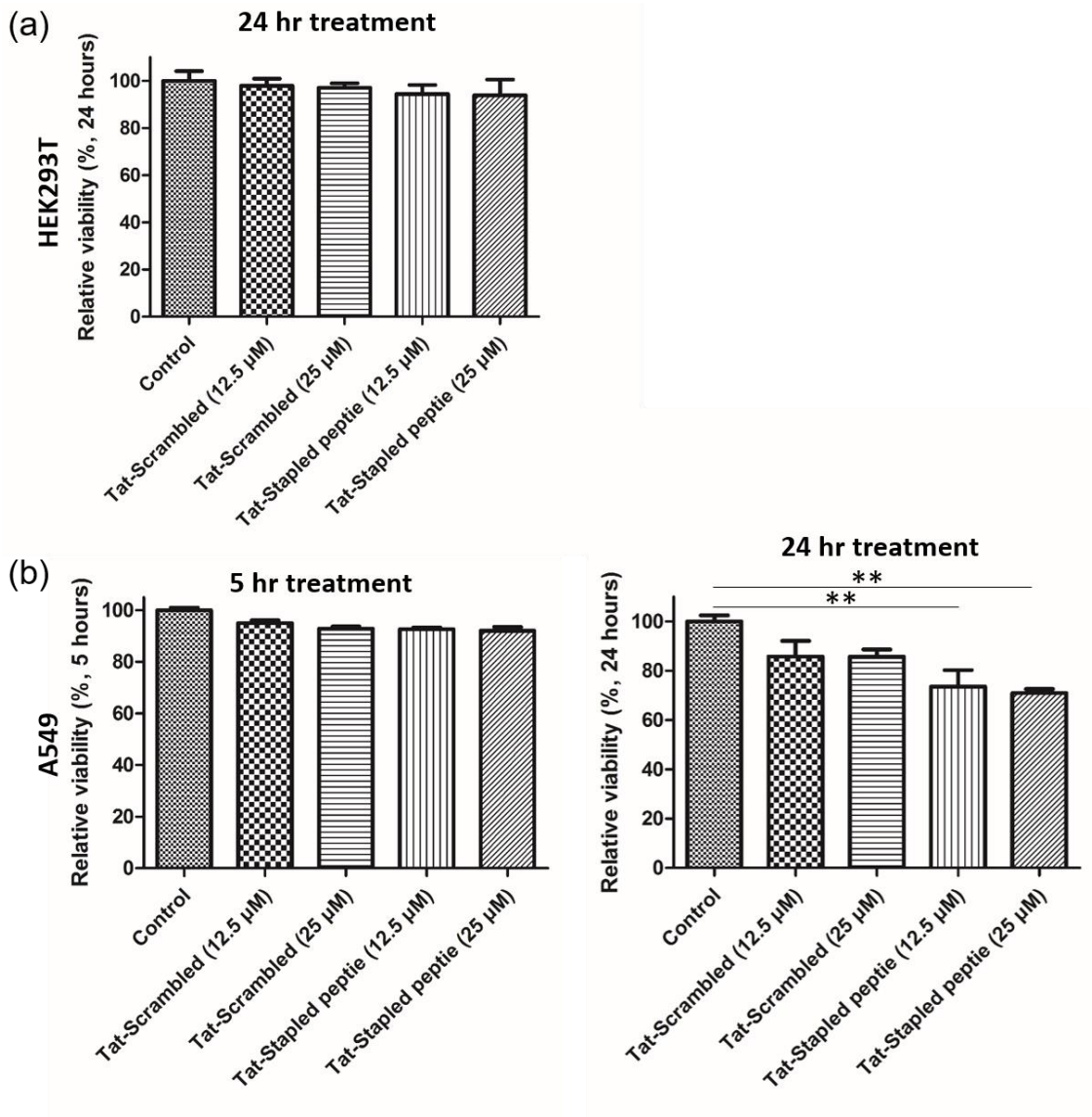

Figure 3.13 Peptides on viability of HEK293T and A549

HEK293T (a) and A549 (b) cells seeded in 96-well plate were treated with Tat-Scrambled peptide (12.5 and 25 μM) and Tat-Stapled peptide (12.5 and 25 μM) for 5-hour and 24-hour. Cell viability assay was conducted by MTT method. No significant cell viability loss in peptide treated HEK293T cell (24 hours) and A549 cell (5 hour). Prolonged treatment (24 hours) decreased cell viability in A549 cell. Similar results were observed in three independent experiments. ***P*, 0.01; t-test.

3.2.5.2. Stapled peptide co-localizes with Beclin1

To further confirm the stapled peptide and Beclin 1 interaction *in vivo*, GFP tagged Beclin1 or GFP tag alone were transiently over expressed in A549 cell and

treated with 25uM of Rhodamine-labeled stapled peptide (Rhodamine-Stapled peptide) for 3 hours. Cells washed 3 times with PBS were changed to complete medium for live cell imaging on Leica SP8 confocal microscope. The signal of GFP (488nm) and Rhodamine (552nm) were captured in a sequential manner to exclude interference. As show in Figure 3.14, Beclin1 is mainly distributed in cell cytosol. In contrast, GFP tag alone is distributed evenly across the whole cell, including nucleus (Figure 3.14). Peptide treatment did not change the distribution pattern of GFP tag in the cell. However, peptide treatment induced formation of GFP-Beclin1 punctas that is largely co-localized with the Rhodamine-labeled stapled peptide. Those co-localizations suggest binding of stapled peptide with Beclin1 in A549 cell.

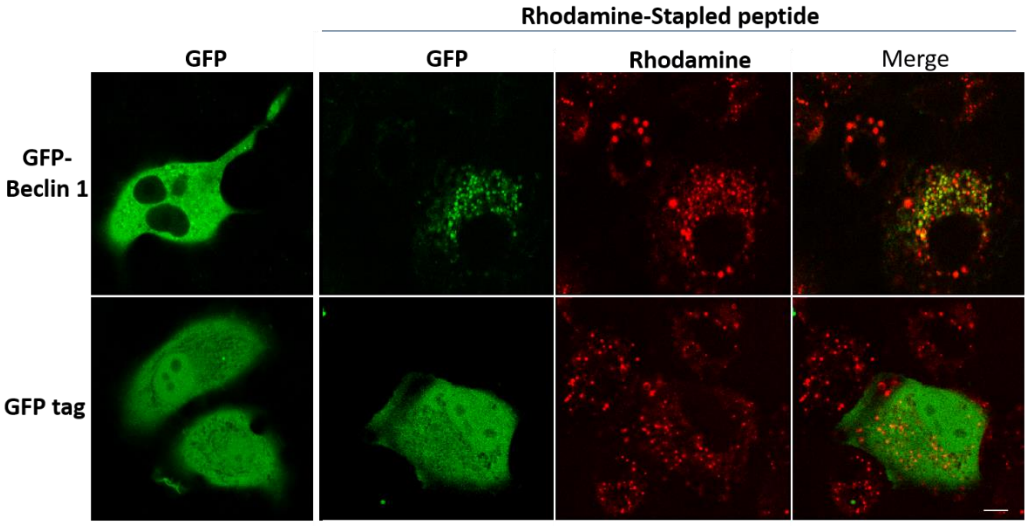

Figure 3.14 Stapled peptide co-localizes with Beclin1

A549 cells were transiently overexpressed with GFP-Beclin1 or GFP tag alone and treated with Rhodamine-labeled stapled peptide. Live cell imaging were recorded for GFP (488nm) and Rhodamine (552 nm). The yellow dots indicate the co-localization of stapled peptide with Beclin1. Representative confocal fluorescence images were shown. Scale bar represents 10 μm.

3.2.5.3. Stapled peptide co-localizes with LC3

In HeLa cells stably expressing GFP-LC3, Rhodamine-stapled peptide treatment induced formation of GFP-LC3 punctas that were partially co-localized with stapled peptide (Figure 3.15). As the peptide was designed and proved to bind Beclin1, the partial co-localization of peptide and LC3 might be indirect. Although this partially co-localization does not necessarily prove direct interaction of peptide and LC3, it dose suggests the involvement of the stapled peptide in autophagy machinery.

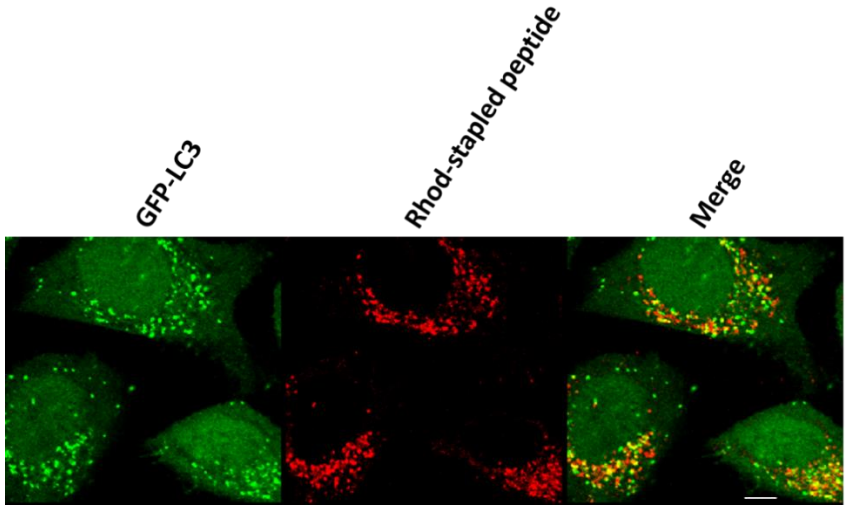

Figure 3.15 Partial co-localization of peptide with LC3

HeLa cells stably expressing GFP-LC3 were treated with Rhodamine-stapled peptide for 3 hour in complete medium with 25uM of Chloroquine. Live cell imaging were recorded for GFP (488nm) and Rhodamine (552nm). Representative confocal fluorescence images were shown. Scale bar represents 10 μm.

3.2.5.4. Stapled peptide promotes autophagy

The biological efficacy of the designed stapled peptide in modulating autophagy and EGFR degradation was characterized using cell-based assays. Our results shown that basal autophagy is low as indicated by very few GFP-LC3 punctas in HeLa GFP-

LC3 cell. Tat-stapled peptide treatment greatly increased the number of GFP-LC3 punctas compared with both Control (vehicle) and Tat-scrambled peptide group (Figure 3.16 a and b), which suggests that Tat-stapled peptide induced autophagy.

There is a possibility that increased GFP-LC3 puncta maybe due to the inhibition of fusion between autophagosome (where LC3 punctas stays) and lysosome, which result in blockage of GFP-LC3 degradation and more GFP-LC3 punctas. In order to test this possibility, autolysosome neutralizer Chloroquine (CQ) was added in HeLa GFP-LC3 cell. CQ is an old anti-malarial drug that accumulates in acidic lysosome and raises its PH. It neutralizes lysosome and inhibits autophagosome-lysosome fusion and lysosomal degradation. As shown in Figure 3.16 a, increased number of GFP-LC3 punctas formed after CQ treatment compared with Control group suggests blockage of lysosome degradation. Both Control group and Tat-scrambled group shown increased but similar number of punctas upon CQ treatment. In contrast, Tat-stapled peptide treatment in combination with CQ greatly increased the number of GFP-LC3 punctas, which suggests autophagy flux. Together, increased number of punctas in conditions with or without CQ proved the autophagy induction ability of Tat-stapled peptide. The number of GFP-LC3 punctas was quantified in Figure 3.16 b.

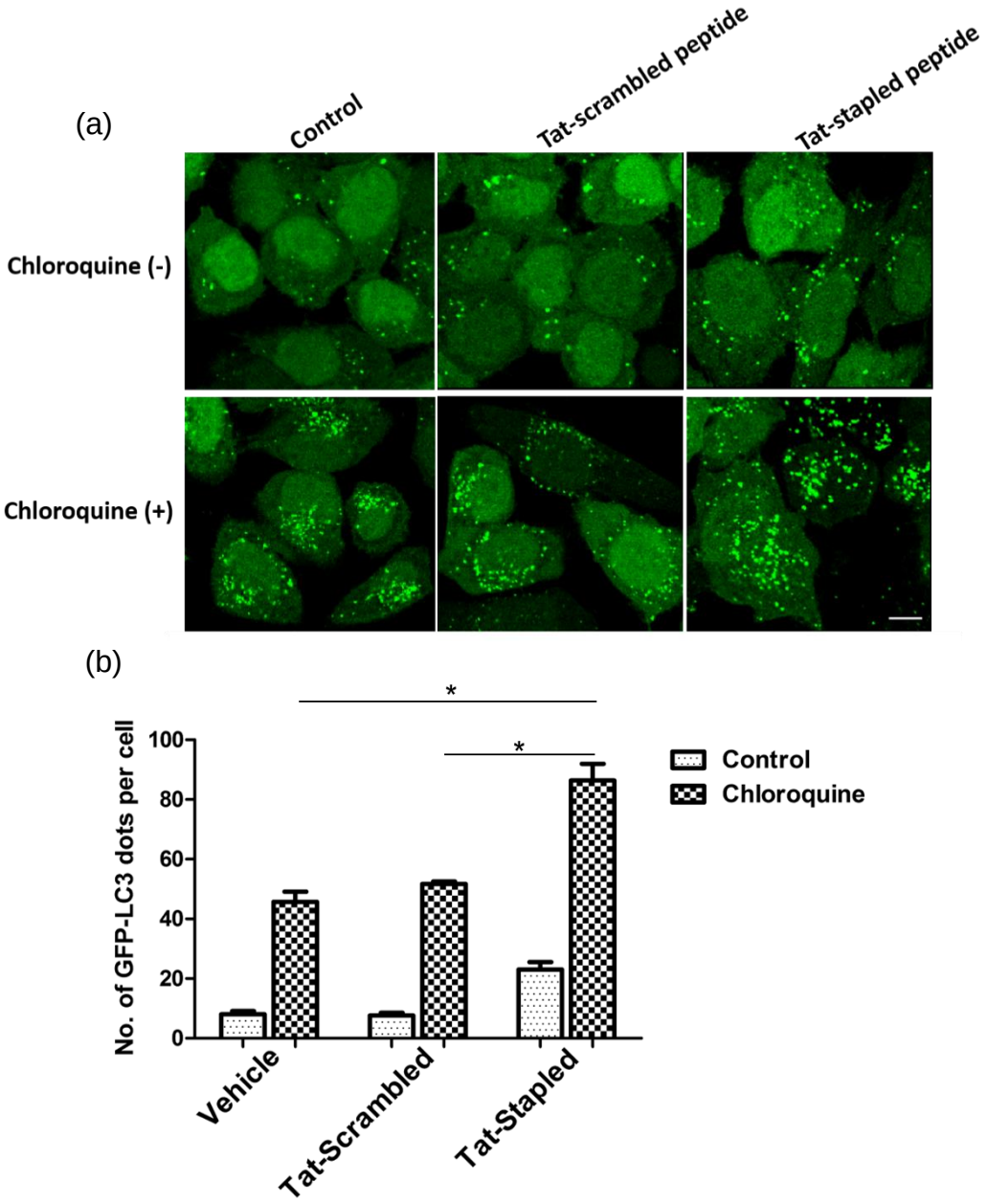

Figure 3.16 Tat-stapled peptide induced GFP-LC3 puncta formation

(a) Representative confocal fluorescence images of HeLa cells stably expressing GFP-LC3 after treatment with vesicle water (control), Tat-scrambled peptide (Tat-scrambled) and Tat-SP4 stapled peptide (Tat-stapled). HeLa cell stably expressing GFP-LC3 was treated with 25 μM of peptide alone or in combination with CQ (30 μM,) for 3 hours. After treatment, the cells were fixed by 4% PFA, washed with PBS and observed for GFP-LC3 at 488nm under a confocal microscope. Representative confocal fluorescence images were shown. Scale bar represents 10 μm.
(b) Histogram to show quantification of the results from (a). Error bars represent ±s.e.m of triplicate samples. **P,* 0.05. t-test.

The effect of stapled peptide on autophagy was further tested on different cell lines (H1975, A549, HeLa) for LC3 lipidation by western blot. H1975 is a NSCLC cell line with TKI insensitive mutation T790M on EGFR. Our results show that Tat-stapled peptide treatment (12.5 μM and 25 μM) induced LC3 lipidation in H1975 cell (Figure 3.17 a). In addition, Tat-stapled peptide treatment on A549 with different time courses (3 hours and 5hours) also induced LC3 lipidation (Figure 3.17 b). Moreover, HeLa cell treated with stapled peptide and CQ induced LC3 lipidation (Figure 3.17 c), which suggest autophagy flux.

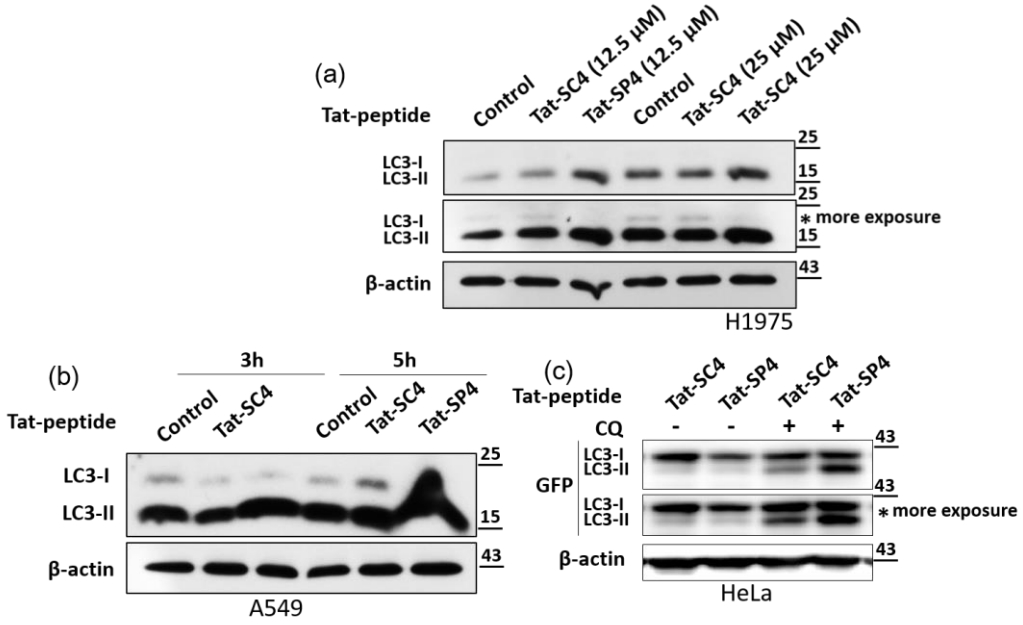

Figure 3.17 Stapled peptide induced LC3 lipidation

(**a**) H1975 cells treated with different concentrations of peptide for 3 hours in normal medium were immunoblotted for LC3.
(**b**) A549 cells treated with 25 μM of peptide in normal medium for 3 and 5 hours were immunoblotted for LC3.
(**c**) HeLa cells stably expressing GFP-LC3 were treated with peptide (25 μM) in the presence of absence of CQ (30 μM) for 3 hours and immunoblotted for GFP-LC3.
"*" in (a) and (c) means more exposure.

3.2.5.5. Stapled peptide promotes EGFR degradation

Our peptide data so far suggested autophagy enhancing ability of the Tat-stabled peptide. To our surprise, Tat-stapled peptide also enhanced the EGF induced degradation of EGFR in HEK293T cell. As shown in Figure 3.18 a and b, there is noticeable less amount of EGFR in Tat-stapled peptide treated HEK293T cells compared with Tat-scrambled peptide treated cells after 30 minutes of EGF stimulation. This difference is more obvious at time point 90 minutes post EGF stimulation, as EGFR was almost gone in Tat-stapled peptide treated group while in both Control and Tat-scrambled peptide treated groups, EGFR level is remain noticeable, albeit much degraded.

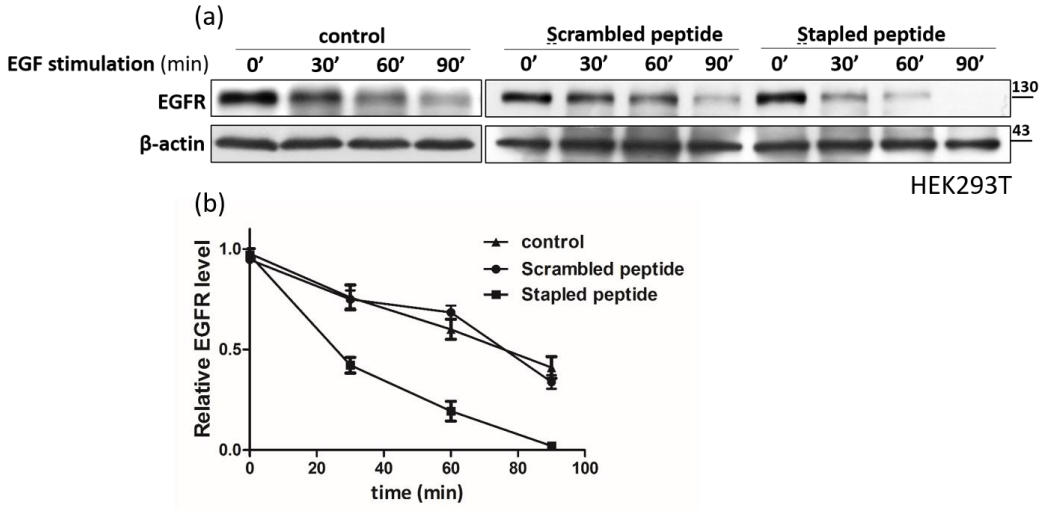

Figure 3.18 Stapled peptide induced EGFR degradation in HEK293T cell

HEK293T cells were FBS starved overnight, then stimulated with 200ng/mL of EGF for different time course together with 25 μM of stapled peptide or scrambled peptide.
(a) Cells were collected and detected the EGFR level by western blot.
(**b**) EGFR level was quantified from three independent experiments.

Collectively, our data confirm that rationally designed stapled peptide SP4 can

promote autophagy activity and enhance EGFR degradation in a Beclin1-dependent manner.

3.3. Discussion

Beclin1 is an essential scaffolding protein within the Beclin1-Vps34 complex. Many autophagy modulators exert their regulatory effect on Vps34 activity by directly interacting with Beclin1. Atg14L and UVRAG, the two key Vps34 regulators, associate with Beclin1 constitutively and form mutually exclusive Atg14L- or UVRAG-containing Beclin1-Vps34 complexes with significantly enhanced Vps34 activity and distinct functional profiles (Liang et al., 2007; Liang et al., 2008d). Other regulators, such as Bcl2, NRBF2, Rubicon, Bif-2 further impinge onto the Atg14L/UVRAG-containing Beclin1-Vps34 complexes via dynamic or transient interactions with Beclin1, Atg14L or UVRAG to modulate Vps34 activity. Those factors collectively target the Beclin1-Vps34 complex to exert temporal and spatial regulation on Vps34-dependent membrane trafficking processes in response to diverse cellular context ranging from nutrient starvation and hypoxia to proteotoxicity and immunity.

The Beclin1 coiled coil region is critical for its interaction with Atg14L and UVRAG. Interestingly both Atg14L and UVRAG contain coiled coil domain. While Beclin1 coiled coil domain forms homodimer, the Beclin1-Atg14L/UVRAG coiled coil assembly is heterodimeric. It is not clear how such different and distinct coiled

coil assemblies are coordinated, especially during the execution of autophagy process. Furthermore, our previous study on the homodimeric structure of the Beclin1 coiled coil domain suggest that the "imperfect" features of this region, i.e. the charged and polar residues at the otherwise hydrophobic interface, may be beneficial for the Beclin1-Atg14L/UVRAG interaction, as replacing them with canonical hydrophobic residues lead to stabilization of Beclin1 homodimer and impede the Beclin1-Atg14L/UVRAG interaction(Li et al., 2012c).

In our study, crystal structure of Beclin1-UVRAG complex revealed five pairs of "leucine zippers" and one extra pair of hydrophobic interaction in the heterodimer interface. Mutations of leucine (L) to glutamic acid (E) on interface of UVRAG disrupt those hydrophobic interactions. Loss of "leucine zippers" on multiple sites of UVRAG weakened or abolished Beclin1-UVRAG interaction.

To investigate the functional significance of the potent Beclin1-UVRAG interaction, we generated UVRAG mutants by replacing one, two, five or six of the leucine residues at the coiled coil interface with glutamate to gradually weaken the complex. In contrast to loss of interaction *in vitro* (by ITC), these Leu-to Glu mutations retain interaction with Beclin1 *in vivo* (by co-immunoprecipitation). Co-transfection of these UVRAG mutants with Atg14L weakened or abolished Beclin1-UVRAG complex in an extent that is proportional to the number of Leu-to Glu mutations. These results proved once again the competitive nature of UVRAG and Atg14Lfor Beclin1

binding. These mutants enable us to investigate precisely the role of Beclin1-UVRAG interaction in mediating Vps34-depndent autophagy and endocytic trafficking.

Similar to previous findings, we find the Beclin1-UVRAG interaction to be non-essential for autophagy execution (Kim et al., 2015). Over-expression of wild-type UVRAG and Leu-to-Glu mutants with weakened binding show no promotional effect on autophagy as measured by LC3 puncta, p62 turnover or LC3 lipidation. However, potent Beclin1-UVRAG is required in endocytic trafficking because over-expression of wild-type UVRAG promotes lysosomal degradation of EGFR while UVRAG mutants with weakened Beclin1 binding fail to do so. These results provide new information for us to delineate the distinct roles of UVRAG in multiple processes including endocytic trafficking. Previous study by Liang et. al. reported that UVRAG is a Beclin1-binding protein known to coordinate autophagosome formation/maturation and endocytic trafficking (Liang et al., 2008a). It interacts with Class C Vps complex to enhance lysosomal fusion of autophagosomes and endosomes by stimulating Rab7 GTPase activity (Liang et al., 2008b). Furthermore, the Class C Vps-UVRAG interaction is genetically separable from the Beclin1-UVRAG interaction and appears to promote lysosomal degradation of EGFR in a parallel manner (Liang et al., 2008b). However, our mutational studies seem to argue that the Beclin1-UVRAG interaction plays a dominant role in lysosomal degradative trafficking because Leu-to-Glu mutants with weakened binding to Beclin1 but expected to retain interaction with Class C Vps, fail to promote EGFR degradation.

Lastly, there is intense interest to target the autophagy process for disease-modifying therapies with multiple clinical trials ongoing using autophagy inhibitor chloroquine (CQ) for cancer therapy (Barnard et al., 2014). However, potent and specific modulators are lacking because ligands like CQ and rapamycin are not specific to autophagy and may have off-target effect. A previous study reported a Beclin1 peptide derived from its membrane-binding region that can induce autophagy via a negative regulator GAPR-1 and decrease the replication of pathogens in cell- and animal-based models (Shoji-Kawata et al., 2013). Here we present a new strategy of generating Beclin1 peptides for autophagy modulation. By specifically targeting the Beclin1 coiled coil domain right outside of the UVRAG binding site, rational designed Beclin1 peptides with hydrocarbon staples to stabilize their α-helical structure can bind to Beclin1, promote its dimer-to-monomer transition and might assist Atg14L/UVRAG binding. As a result, both autophagy and endocytic trafficking can be enhanced while EGFR signaling can be attenuated by the peptide. Our approach presents a new Beclin1-specific strategy to target the Beclin1-Vps34 complex for anti-cancer treatment.

3.4. Materials and Methods

3.4.1. Cell Lines and Cell Culture

Human embryonic kidney cell (HEK293T), A549 and HeLa cell lines were cultured with Dulbecco's Modified Eagle's Medium (DMEM) (Sigma-Aldrich, D7777) supplemented with 10% FBS (Gibco™, 26140079) and 1% penicillin-streptomycin (PS) (Gibco™, 15140122) in a 5% CO2, 37°C incubator. HeLa cell with stable expression of GFP-LC3 was a kindly gift from Dr. Han-Ming Shen's lab (The National University of Singapore), which is also cultured in the DMEM. Cell lines were recovered from liquid nitrogen in T25 cell culture flask (Corning, 430639), and then transferred into 10 cm petri dish (Corning, 70165-100) for culture. All the cell lines were cultured for at least 2 passages before used in formal experiments. The transfection experiments were done in 6-well plate (Corning, 430639). For HEK293T cell transfection, the culture plate bottom surface was pre-coated with poly-L-lysine (Sigma-Aldrich, P9155) to facilitate cell attachment. All the cell lines used in the experiment were mycoplasma detected negative by MycoAlert™ PLUS Mycoplasma Detection Kit (Lonza). This test exploits the activity of mycoplasmal enzymes that exist in all the six mycoplasmas that mostly common found in contaminated cells and other vast majority of 180 mycoplasmas species. This test does not react with enzymes presents in eukaryotic cells. Viable mycoplasmas in the test medium are lysed and the released enzymes react with the MycoAlert™ PLUS substrate, which converts ADP to ATP. The resulting ATP is then transferred to a luciferase enzyme in the

MycoAlert™ PLUS reagent, which gives out luminescence signal that can be read by a luminometer. To perform the test, fresh culture medium were centrifuged in a Eppendorf tube at 200g for 5 minutes and the supernatant are used as sample in the text. Bring all reagents and sample up to room temperature. Transfer 100 μL of sample into an Eppendorf tube and add 100 μL of MycoAlert™ PLUS reagent. Mix well and wait for 5 minutes before read with a luminometer (Reading A). Add 100 μL MycoAlert™ PLUS substrate in the 200 μL reactant used for Reading A. Mix well and wait for 10 minutes before read with a luminometer (Reading B). Calculate the ratio of Reading B/Reading A. The ratio < 1 indicates negative for mycoplasma while ratio > 1.2 suggests mycoplasma contamination. Alternatively, repeat the text 24-48 hours later if the ratio is between 1 and 1.2. All the cell lines used in the experiment were regularly tested for mycoplasma. Only cell lines negative in mycoplasma test were used for experiment.

3.4.2. Reagents and Antibodies

The reagents used for cell treatments were Chloroquine (CQ) (Sigma-Aldrich, C6628), Rapamycin (Sigma-Aldrich, R8781), Earle's Balanced Salt Solution (EBSS) (Gibco™, 14155063), Epidermal Growth Factor (EGF) (Invitrogen, PHG0311L) and MG132 (Sigma Aldrich, M8699). The antibodies used in the co-immunoprecipitation (co-immunoprecipitation) and/ or Western Blotting experiments were anti-β actin (Santa Cruz Biotechnology, SC1616), anti-LC3 (Novus, NB1002220), anti-p62

(Abnova, H0008878-M01), anti-EGFR (Santa Cruz Biotechnology, SC1005), anti-Beclin1 (Santa Cruz Biotechnology, SC48341), anti-GFP (Santa Cruz Biotechnology, SC9996), anti-Flag (Sigma-Aldrich, F3040), anti-Flag@ M2 Magnetic Beads (Sigma-Aldrich, M8823), protein A/G PLUS agarose beads (Santa Cruz Biotechnology, SC-2003) Anti-Mouse IgG-HRP (Sigma-Aldrich, A9044), Anti-Rabbit IgG-HRP (Sigma-Aldrich, A9169). The transfection reagents used in the study were Lipofectamine 2000 (Invitrogen™, 11668-019), Lipofectamine 3000 (Invitrogen™, L3000008). Opti-MEM reduced serum medium (Gibico™, 31985-062) were used for Lipofectamine and DNA plasmid dilution.

3.4.5. Immunoblot analysis

DNA plasmids were transfected into HEK 293T cells or HeLa cell stably expressing GFP-LC3. For co-immunoprecipitation experiment demonstrating UVRAG-endogenous Beclin1 interaction, FLAG-tagged UVRAG plasmids were transfected into HEK293T cells. For co-immunoprecipitation experiment demonstrating UVRAG/Atg14L-endogenous Beclin1 interaction, equal amounts of FLAG-tagged UVRAG mutant plasmids and GFP-tagged Atg14L plasmids or equal amounts of FLAG-tagged Atg14L plasmids and GFP-tagged UVRAG mutant plasmids were co-transfected into HEK293T cells to test their competitive binding to endogenous Beclin1. For immunoblotting assay of LC3-II, FLAG-tagged UVRAG mutant plasmids were transfected into HEK293T cells. For immunoblotting assay of

LC3-II and p62, FLAG-tagged UVRAG mutant plasmids were transfected into HeLa cell stably expressing GFP-LC3. For immunoblotting assay of EGFR degradation, FLAG-tagged UVRAG mutant plasmid were transfected into HEK293T cells or A549 cells. Cells were lysed in immunoprecipitation buffer (25 mM HEPES PH 7.5, 10 mM $MgCl_2$, 150 mM NaCl, 1 mM EDTA.2Na, 1% Nonidet P-40, 1% Triton X-100 and 2% glycerol) or Laemmli sample buffer (62.5 mM Tris-HCl, pH 6.8, 2% SDS, 25% glycerol, 5% β-mercaptoethanol) with freshly added EDTA-free protease inhibitor cocktail (Roche). For co-immunoprecipitation, Lysates were incubated with FLAG magnetic beads (Sigma) overnight at 4 °C. The beads were washed with 1× immunoprecipitation lysis buffer 5 times and then eluted with 2× SDS sample buffer.

3.4.6. EGFR degradation assay

Epidermal growth factor receptor (EGFR) is a 170 kDa protein expresses on the cell membrane. Expression of the protein is physiologically important to regulate cell growth and proliferation. Abnormally up-regulated expression or mutation of the protein lead to uncontrolled cell division, which have been associated with cancers including lung cancer and anal cancer (Walker et al., 2009). Binding of EGFR ligands epidermal growth factor (EGF) to EGFR trigger the transition of EGFR inactive monomer into active homodimer (Yarden and Schlessinger, 1987), which is rapidly internalized through endocytosis and translocated to early endosomes, where the complex are either recycled back to the cell membrane or maturated and passed to

lysosomes for degradation.

For measuring the EGFR degradation, cells were grown in 6-well plate to around 85% confluence. The cells were washed with PBS two times and serum-starved overnight in DMEM medium. EGFR endocytosis was induced by incubation with DMEM medium (with 20 mM HEPES and 0.2% BSA) containing 200ng/mL of EGF (Invitrogen). Cells were collected at different time points and lysed in Laemmli sample buffer (62.5 mM Tris-HCl, pH 6.8, 2% SDS, 25% glycerol, 5% β-mercaptoethanol). EGF treatment time point for HEK293 cell were 0 min, 30 min, 60 min, 90 min and 120 min. For A549 cells, the EGF treatment time point were 0 hour, 1 hour, 2 hour, 3 hour, 4 hour and 5 hour. 20 μg of protein lysate were resolved by 8% SDS-PAGE and transferred to 0.45 μm PVDF membrane (Bio-Rad) with Mini-Trans-Blot Electrophoretic Transfer Cell (Bio-Rad) at 300 mA for 120 min. The membrane was blocked and immunoblotted with anti-EGFR antibody (1:2000, Santa Cruz Biotechnology) that probe for total EGFR.

3.4.7. Autophagy assay by LC3

Microtubule-associated light chain 3 (LC3), a mammalian homolog of yeast Atg8 that ubiquitously distributed in mammalian tissues and cultured cells, is the mostly common used autophagy marker. The cytosolic unconjugated form of LC3 proteins are specifically cleaved at the carboxyl terminal by Atg4 to form LC3-I, which has an

exposed carboxyl terminal that conjugates to phosphatidylethanolamine to form LC3-II. Autophagy is accompanied with the redistribution of LC3-II to autophagosome to form cytoplasmic puncta, which is finally degraded in autolysosomes. Detection of puncta formation and LC3-II protein level therefore are the most experimentally straightforward way to monitoring autophagy.

Autophagy is a dynamic process. Autophagy flux is the flow of autophagosome formation, maturation, and the subsequently fusion with lysosome to breakdown cytoplasmic material and organelles and release of macromolecules. There are basically two means to monitor autophagy flux by LC3, one is to measure LC3-II protein level by western blot, as induced autophagy is accompanied with rapid transition of LC3-I to LC3-II; the other one is to count the number of GFP-LC3 puncta, which denotes the formation of autophagosome during autophagy induction. What is important in autophagy flux assay is the lysosome inhibitor has to be added in order to rule out the false positive caused by failure of autophagosome-lysosome fusion or lysosome malfunction(Mizushima et al., 2010). Bafilomycin A1 (Baf) blocks autophagosome-lysosome fusion by inhibiting vacuolar H^+ ATPase. Chloroquine (CQ) accumulation prevents acidification of lysosome that fuse with autophagosome, thereby preventing autolysosome formation and degradation.

Conversion of LC3-I to LC3-II

HeLa cell and HeLa cell with stable transfected of GFP-LC3 were used in measuring endogenous LC3 protein level and GFP-LC3 puncta formation, respectively. HeLa cell were seeded in 6-well plate and grown to 80% confluence. The cell were transfected with plasmid DNA (2.5 μg/well) by Lipofectamine 2000 (5 μl/well) (Invitrogen) or Lipofectamine 3000 (5 μl/well) (Invitrogen) for 24 hours according to the manufacture's instruction before different treatments with or without lysosome inhibitor CQ (50 μM) for 2 hours. After treatment, the cell were lysed with Laemmli sample buffer and 20 μg of protein lysate were resolved by 12% SDS-PAGE and transferred to 0.45 μm PVDF membrane (Bio-Rad) with Mini-Trans-Blot Electrophoretic Transfer Cell (Bio-Rad) at 300 mA for 90 min. The blot was probed by anti-LC3 antibody (1:2000, Novus). To observe the GFP-LC3 puncta formation, stable GFP-LC3 HeLa cell were seeded in 6-well plate with a piece of cover slip in the center and grown to 70% confluence. The cell were transfected with plasmid DNA for 24 hours before starvation treatment with or without lysosome inhibitor. The diagram shows LC3 turnover is in Figure 3.19.

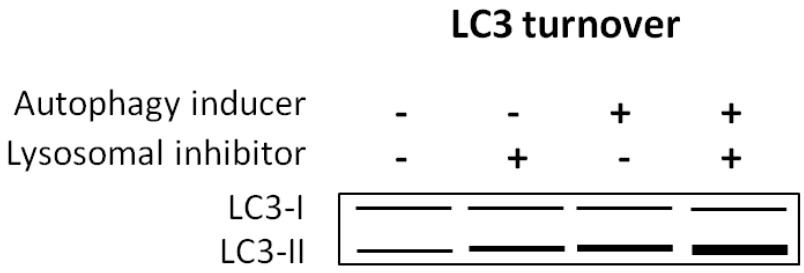

Figure 3.19 Scheme analysis of autophagy assay by LC3 turnover

LC3 turnover assay compares the LC3-II protein amount among two samples with or without lysosomal inhibitor.

GFP-LC3 puncta formation

Figure The GFP-LC3 puncta formation assay compares the number of punctate structures in cells with different treatments. HeLa cell with transiently or stably transfected with GFP-LC3 were treated with complete medium (Control) or starved with EBSS for 2 hours (EBSS starvation 2 hours). Cells were fixed with 4% paraformaldehyde (PFA) on ice for 20 minutes, washed with PBS 5 times and took the picture under a confocal microscope. EBSS starvation result in formation of significantly more GFP-LC3 punctas inside the cell, indicating the EBSS starvation induced autophagy (Figure 3.20).

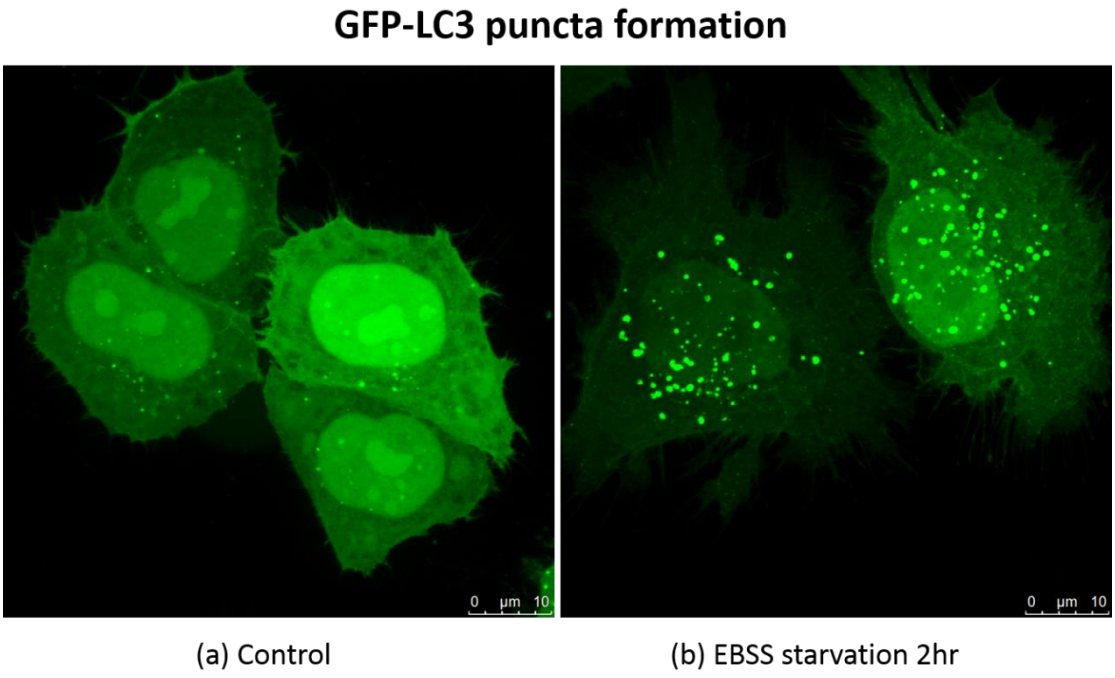

Figure 3.20 GFP-LC3 puncta formation under starvation

3.4.8. Autophagy assay by p62/SQSTM1

p62, also called sequestosome (SQSTM1), is an ubiquitin-binding protein that selectively incorporated into autophagosomes for degradation by directly binding to LC3(Bjørkøy et al., 2005). The protein serves as a link between the ubiquitinated-proteins and autophagy machinery, which is also used as a marker to study autophagy flux. Cells were treated the same as autophagy assay by LC3 except the blot was detect by an anti-p62/SQSTM1 antibody (1:3000, Abnova).

3.4.9. Isothermal titration calorimetry (ITC)

ITC is a technique to quantitative study the interactions of a wide variety of biomolecular interactions, such as protein-protein, protein-DNA/RNA, protein-compound, antibody-antigen, etc. ITC simultaneously measuring the heat transfer either released (exthothermic) or absorbed (endothothermic) during a biomolecular-binding event. The binding partners need no modifications and the binding affinity is measured in their native states, which allows determination of binding constants (Kd), entropy (ΔS), enthalpy (ΔH) and reaction stoichiometry (N). ITC goes beyond binding affinities determination by measuring dissociation constant of protein dimer, trimer and etc. There are some points in ITC experiments of protein sample. Firstly, the protein needs to be soluble in buffer and the buffer condition should be the same for both of the biomolecules. Secondly, negative controls, such as buffer to buffer or protein to buffer should be done before titration of protein samples, as these controls

would rule out abnormality of ITC machine or protein sample aggregation problem. Thirdly, accurate concentration determination of both titrant and sample in the cell are very important, as errors will directly impact on the thermodynamic results. Lastly, the molar concentration ratio of titrant in the syringe and sample in the cell has to be adjusted and optimized. For a binding of molar ratio 1:1(stoichiometry=1), the molar concentration of titrant is typically ten to tween times higher than the molar concentration of protein sample in the cell to make sure that protein in the cell be saturated at the end of the titration experiment.

In this study, Beclin1 coiled coil domain and UVRAG coiled coil domain wild type and mutants were purified from BL-21 D (DE3). Proteins were concentrated in Tris-NaCl buffer (50 mM Tris, PH 8.0, 150 mM NaCl). All the buffer and protein sample were centrifuged to remove particles and bubbles before ITC experiment by a MicroCal VP $ITC_{200.}$ Stapled peptide was dissolved in ddH_2O as stock (25 mM). The injection interval was 150 seconds to let the base line recover and stable. The volume for the first injection was set to 0.4 μL as the first data point has always to be discard due to equilibration artifact mostly seen in the first injection. Data analysis was done by using Origin 7 provided by the MicroCal VP-ITC_{200} manufacture.

3.4.9. Static light scattering (SLC)

Static light scattering was performed on Wyatt Dawn 8+ (Wyatt Technology)

that is connected to an ÄKTA FPLC system (GE Healthcare). The ÄKTA system was equipped with a size exclusion column (Superdex 200 10/30 GL, GE Healthcare), and equilibrated with at least one column-volume of Tris buffer until the light scattering signal become stable. Concentrated proteins after size exclusion chromatography were centrifuged to remove any bubbles and particles before loaded onto the size exclusion column at the flow rate of 0.5mL/min. Both UV signal and light scattering signal were plotted and analysed by software ASTRA.

3.4.10. Cell viability assay

3-(4,5-Dimethylthiazol-2-yl)-2,5-Diphenyltetrazolium Bromide solution (MTT) is used to assess cell viability as a function of redox potential. Actively respiring cells convert the water-soluble MTT to water- insoluble purple formazan. The formazan is then solubilized by DMSO and its concentration determined by optical density. Specifically, cells are seeded in a 96-well plate one day before treatment. After treatment, cells were incubated with 30 μL MTT (5mg/mL) for 4 hours to let formazan formation. The formazan was dissolved in 200 μL DMSO and read for absorbance by a plate reader (CLARIOstar, BMG LABTECH) at 570 nm with 650 nm as reference.

Chapter 4. Concluding remarks and future perspectives

4.1. Further effort to determine the structure of the UBA-Ub complex

Our work in chapter 2 studied the pS405 and pS409 on UBA-Ub interaction. We further solved the crystal structure of UBA S405E and S409E, and UBA S409E structure lead to the identification of K422 as a critical residue for UBA-Ub interaction.

Crystal structures of Ub or p62 UBA WT alone had been solved and reported (Senadhi Vuay-kumar, 1985; Shin Isogai, 2011). Complex structure of p62 UBA-Ub would be of great help to understand how p62 UBA interacts with Ub and the role of p62-Ub interaction in selective autophagy. We tried to crystalize different UBA mutants with enhanced Ub binding ability (single UBA mutant S405E, K422A or triple UBA mutant S405E & W414F & K422A) in complex with Ub. Equal or excess amount of UBA mutant was mixed with Ub for crystallization and some conditions readily yield crystals. Test of crystals on in house X-Ray beamline revealed that they are not complex crystals but UBA mutant alone or Ub alone. There are several reasons that make the crystallization of UBA-Ub complex difficult. Firstly, both UBA and Ub are quite easy to grow crystals, especially for the highly stable Ub. Secondly, UBA-Ub interaction is not strong enough to form crystal complex, even for the p62 UBA mutants. Thirdly, mutations on UBA dimer might destabilize UBA and prevent crystallization. Based on the above facts and predictions, we linked UBA and Ub

together with a (GS)*6 linker in the hope of locking the interaction complex as one unit for crystallization. UBA-Ub linker construct was expressed, purified and set tray for crystals. We do get small and single crystals for UBA K422A-(GS) *6-Ub (Figure 4.1), and the condition is now in optimization for large and better crystals.

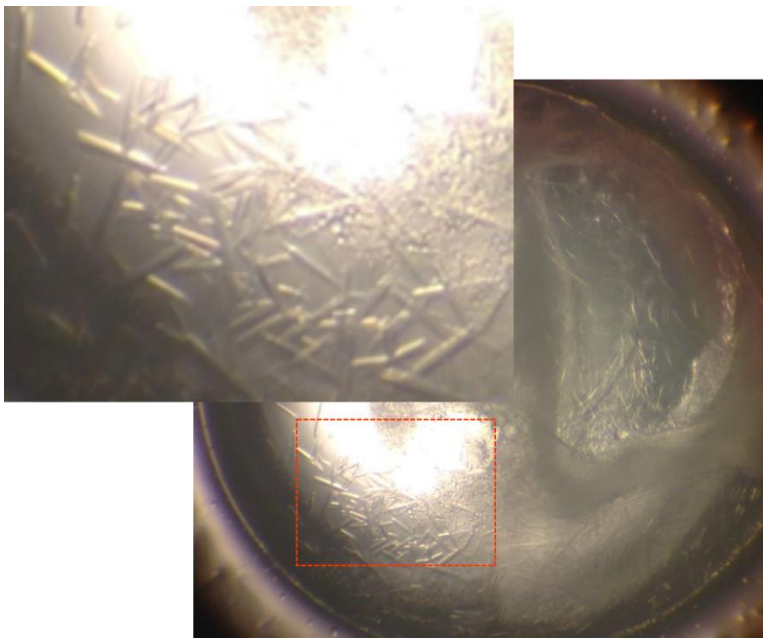

Figure 4.1 Crystals of UBA K422A-(GS) *6-Ub

Crystals grows up in 0.05 M Zinc acetate dihydrate, 20% w/v Polyethylene glycol 3,350 7 days after tray setting.

4.2. Future effort to optimize the potency of the stapled peptides and to test *in vivo* efficacy in EGFR-related cancer models

Our work in the second part studied how the potent Beclin1-UVRAG interaction promotes Vps34-dependent endocytic trafficking via their coiled-coil domain and how this interaction can be targeted by rationally designed stapled peptides for modulation.

The ongoing work are to optimize the potency of the stapled peptides for binding to Beclin1 coiled coil domain and test their efficacy in EGFR-related cancer models, where the efficacy of the stapled peptide on the context of an intact organism can be assessed. For potency optimization, we will optimize the current peptide design and also design some new peptides based on molecular dynamics (MD) simulation results of peptides to Beclin1 coiled coil domain. After confirming the strong binding of peptides to Beclin1 by ITC, we would like to test their efficacy in mouse model with, for example, EGFR overexpressed lung cancer.

Lung cancer is responsible for 30% of all cancer deaths due to its late detection and frequent local and distal metastases. 80% of lung cancers are non-small cell lung cancer (NSCLC) (Kwon and Berns, 2013). While 60% of NSCLCs express the epidermal growth factor receptor (EGFR), approximately 10% of patients in US and 35% patients in East Asia have tumor associated with mutated EGFR (Lynch et al., 2004; Paez et al., 2004; Pao et al., 2004). EGFR is a transmembrane protein with cytoplasmic kinase activity that transduces important growth factor signaling for cancer cell growth and proliferation. Inhibition the tyrosine kinase domain of EGFR by tyrosine kinase inhibitor (TKI) has been proved as an effective treatment for patients with EGFR that sensitive to TKI, but not to patients with TKI insensitive EGFR. We hope our stapled peptide could accelerate the degradation of EGFR and serve as an effective choice for cancer treatment.

References

Lida, A., Emi, M., Matsuoka R., Hiratsuka E., Okui K., Ohashi H., Inazawa J., Fukushima Y., Imai T., and Nakamura Y. (2000). Identification of a gene disrupted by inv(11)(q13.5;q25) in a patient with left-right axis malformation. Human Genetics *106*, 277-287.

Agarraberes, F.A., and Dice, J.F. (2001). A molecular chaperone complex at the lysosomal membrane is required for protein translocation. Journal of Cell Science *114*, 2491-2499.

Aita, V.M., Liang, X.H., Murty, V.V.V.S., Pincus, D.L., Yu, W., Cayanis, E., Kalachikov, S., Gilliam, T.C., and Levine, B. (1999). Cloning and Genomic Organization of Beclin 1, a Candidate Tumor Suppressor Gene on Chromosome 17q21. Genomics *59*, 59-65.

Alers, S., Löffler, A.S., Wesselborg, S., and Stork, B. (2012). Role of AMPK-mTOR-Ulk1/2 in the Regulation of Autophagy: Cross Talk, Shortcuts, and Feedbacks. Molecular and Cellular Biology *32*, 2-11.

Ali, A.B., Nin, D.S., Tam, J., and Khan, M. (2011). Role of Chaperone Mediated Autophagy (CMA) in the Degradation of Misfolded N-CoR Protein in Non-Small Cell Lung Cancer (NSCLC) Cells. PLoS One *6*, e25268.

Alvarez-Erviti, L., Rodriguez-Oroz, M.C., Cooper, J., and et al. (2010). CHaperone-mediated autophagy markers in parkinson disease brains. Archives of Neurology *67*, 1464-1472.

Alvarez-Erviti, L., Seow, Y., Schapira, A.H., Rodriguez-Oroz, M.C., Obeso, J.A., and Cooper, J.M. (2013). Influence of microRNA deregulation on chaperone-mediated autophagy and α-synuclein pathology in Parkinson's disease. Cell Death & Disease *4*, e545.

Anguiano, J., Garner, T.P., Mahalingam, M., Das, B.C., Gavathiotis, E., and Cuervo, A.M. (2013). Chemical modulation of chaperone-mediated autophagy by retinoic acid derivatives. Nature Chemical Biology *9*, 374-382.

Ashford, T.P., and Porter, K.R. (1962). CYTOPLASMIC COMPONENTS IN HEPATIC CELL LYSOSOMES. The Journal of Cell Biology *12*, 198-202.

Auteri, J.S., Okada, A., Bochaki, V., and Fred Dice, J. (1983). Regulation of intracellular protein degradation in IMR-90 human diploid fibroblasts. Journal of Cellular Physiology *115*, 167-174.

Avin-Wittenberg, T., Bajdzienko, K., Wittenberg, G., Alseekh, S., Tohge, T., Bock, R., Giavalisco, P., and Fernie, A.R. (2015). Global Analysis of the Role of Autophagy in Cellular Metabolism and Energy Homeostasis in Arabidopsis Seedlings under Carbon Starvation. The Plant Cell *27*, 306-322.

Baba, M., Takeshige, K., Baba, N., and Ohsumi, Y. (1994). Ultrastructural analysis of the autophagic

process in yeast: detection of autophagosomes and their characterization. The Journal of Cell Biology *124*, 903-913.

Backer, J.M., Bourret, L., and Dice, J.F. (1983). Regulation of catabolism of microinjected ribonuclease A requires the amino-terminal 20 amino acids. Proceedings of the National Academy of Sciences of the United States of America *80*, 2166-2170.

Backer, J.M., and Dice, J.F. (1986). Covalent linkage of ribonuclease S-peptide to microinjected proteins causes their intracellular degradation to be enhanced during serum withdrawal. Proceedings of the National Academy of Sciences *83*, 5830-5834.
Ballard, C., Gauthier, S., Corbett, A., Brayne, C., Aarsland, D., and Jones, E. (2011). Alzheimer's disease. The Lancet *377*, 1019-1031.

Bandyopadhyay, U., Kaushik, S., Varticovski, L., and Cuervo, A.M. (2008). The Chaperone-Mediated Autophagy Receptor Organizes in Dynamic Protein Complexes at the Lysosomal Membrane. Molecular and Cellular Biology *28*, 5747-5763.

Barnard, R.A., Wittenburg, L.A., Amaravadi, R.K., Gustafson, D.L., Thorburn, A., and Thamm, D.H. (2014). Phase I clinical trial and pharmacodynamic evaluation of combination hydroxychloroquine and doxorubicin treatment in pet dogs treated for spontaneously occurring lymphoma. Autophagy *10*, 1415-1425.

Beck, T., and Hall, M.N. (1999). The TOR signalling pathway controls nuclear localization of nutrient-regulated transcription factors. Nature *402*, 689-692.

Bekri, S., Adélaïde, J., Merscher, S., Grosgeorge, J., Caroli-Bosc, F., Perucca-Lostanlen, D., Kelley, P.M., Pébusque, M.J., Theillet, C., Birnbaum, D., *et al.* (1997). Detailed map of a region commonly amplified at 11q13→q14 in human breast carcinoma. Cytogenetic and Genome Research *79*, 125-131.

Bjørkøy, G., Lamark, T., Brech, A., Outzen, H., Perander, M., Øvervatn, A., Stenmark, H., and Johansen, T. (2005). p62/SQSTM1 forms protein aggregates degraded by autophagy and has a protective effect on huntingtin-induced cell death. The Journal of Cell Biology *171*, 603-614.

Bröcker, C., Kuhlee, A., Gatsogiannis, C., kleine Balderhaar, H.J., Hönscher, C., Engelbrecht-Vandré, S., Ungermann, C., and Raunser, S. (2012). Molecular architecture of the multisubunit homotypic fusion and vacuole protein sorting (HOPS) tethering complex. Proceedings of the National Academy of Sciences *109*, 1991-1996.

Chang, Y.-G., Song, A.-X., Gao, Y.-G., Shi, Y.-H., Lin, X.-J., Cao, X.-T., Lin, D.-H., and Hu, H.-Y. (2006). Solution structure of the ubiquitin-associated domain of human BMSC-UbP and its complex with ubiquitin. Protein Science : A Publication of the Protein Society *15*, 1248-1259.

Cheong, H., Nair, U., Geng, J., and Klionsky, D.J. (2008). The Atg1 Kinase Complex Is Involved in

the Regulation of Protein Recruitment to Initiate Sequestering Vesicle Formation for Nonspecific Autophagy in Saccharomyces cerevisiae. Mol Biol Cell *19*, 668-681.

Chiang, H.L., and Dice, J.F. (1988). Peptide sequences that target proteins for enhanced degradation during serum withdrawal. Journal of Biological Chemistry *263*, 6797-6805.

Choi, A.M.K., Ryter, S.W., and Levine, B. (2013). Autophagy in Human Health and Disease. New England Journal of Medicine *368*, 651-662.

Clark, S.L. (1957). Cellular differentiation in the kidneys of newborn mice studied with the electron microscope. The Journal of Biophysical and Biochemical Cytology *3*, 349-362.

Cuervo, A.M., and Dice, J.F. (1996). A Receptor for the Selective Uptake and Degradation of Proteins by Lysosomes. Science *273*, 501-503.

Cuervo, A.M., Knecht, E., Terlecky, S.R., and Dice, J.F. (1995). Activation of a selective pathway of lysosomal proteolysis in rat liver by prolonged starvation. American Journal of Physiology - Cell Physiology *269*, C1200-C1208.

Cuervo, A.M., Stefanis, L., Fredenburg, R., Lansbury, P.T., and Sulzer, D. (2004). Impaired Degradation of Mutant α-Synuclein by Chaperone-Mediated Autophagy. Science *305*, 1292-1295.

Cuervo, A.M., Terlecky, S.R., Dice, J.F., and Knecht, E. (1994). Selective binding and uptake of ribonuclease A and glyceraldehyde-3-phosphate dehydrogenase by isolated rat liver lysosomes. Journal of Biological Chemistry *269*, 26374-26380.

de Duve, C., and Wattiaux, R. (1966). Functions of Lysosomes. Annual Review of Physiology *28*, 435-492.

Deretic, V. (2011). Autophagy in Immunity and Cell-Autonomous Defense Against Intracellular Microbes. Immunological reviews *240*, 92-104.

Deter, R.L., Baudhuin, P., and de Duve, C. (1967). Participation of lysosomes in cellular autophagy induced in rat liver by glucagon. The Journal of Cell Biology 35, C11-C16.

Di Bartolomeo, S., Nazio, F., and Cecconi, F. (2010). The Role of Autophagy During Development in Higher Eukaryotes. Traffic *11*, 1280-1289.

Dice, J.F., Walker, C.D., Byrne, B., and Cardiel, A. (1978). General characteristics of protein degradation in diabetes and starvation. Proceedings of the National Academy of Sciences of the United States of America *75*, 2093-2097.

Ding, W.-X., Ni, H.-M., Gao, W., Yoshimori, T., Stolz, D.B., Ron, D., and Yin, X.-M. (2007).

Linking of Autophagy to Ubiquitin-Proteasome System Is Important for the Regulation of Endoplasmic Reticulum Stress and Cell Viability. The American Journal of Pathology *171*, 513-524.

Doelling, J.H., Walker, J.M., Friedman, E.M., Thompson, A.R., and Vierstra, R.D. (2002). The APG8/12-activating Enzyme APG7 Is Required for Proper Nutrient Recycling and Senescence in Arabidopsis thaliana. Journal of Biological Chemistry *277*, 33105-33114.

Dohi, E., Tanaka, S., Seki, T., Miyagi, T., Hide, I., Takahashi, T., Matsumoto, M., and Sakai, N. (2012). Hypoxic stress activates chaperone-mediated autophagy and modulates neuronal cell survival. Neurochemistry International *60*, 431-442.

Dos, D.S., Ali, S.M., Kim, D.-H., Guertin, D.A., Latek, R.R., Erdjument-Bromage, H., Tempst, P., and Sabatini, D.M. (2004). Rictor, a Novel Binding Partner of mTOR, Defines a Rapamycin-Insensitive and Raptor-Independent Pathway that Regulates the Cytoskeleton. Current Biology *14*, 1296-1302.

Duve, C.d. (1963). The lysosome. Scientific American *208*, 64-72.
Duve, C.D., Pressman, B., Gianetto, R., Wattiaux, R., and Appelmans, F. (1955). Tissue fractionation studies.6.Intracellular distribution patterns of enzymes in rat-liver tiddue. Biochemical Journal *60*, 604-617.

Duve, C.d., and Wattiaux, R. (1966). Functions of Lysosomes. Annual Review of Physiology *28*, 435-492.

Egan, D.F., Shackelford, D.B., Mihaylova, M.M., Gelino, S.R., Kohnz, R.A., Mair, W., Vasquez, D.S., Joshi, A., Gwinn, D.M., Taylor, R., *et al.* (2011). Phosphorylation of ULK1 (hATG1) by AMP-activated protein kinase connects energy sensing to mitophagy. Science (New York, NY) *331*, 456-461.

Emsley, P., and Cowtan, K. (2004). Coot: model-building tools for molecular graphics. Acta Crystallogr D Biol Crystallogr *60*, 2126-2132.

Epple, U.D., Suriapranata, I., Eskelinen, E.-L., and Thumm, M. (2001). Aut5/Cvt17p, a Putative Lipase Essential for Disintegration of Autophagic Bodies inside the Vacuole. Journal of Bacteriology *183*, 5942-5955.

Evans, P. (2006). Scaling and assessment of data quality. Acta Crystallogr D Biol Crystallogr *62*, 72-82.

Fahn, S. (2003). Description of Parkinson's Disease as a Clinical Syndrome. Annals of the New York Academy of Sciences *991*, 1-14.

Farr, J.-c., Mathewson, R.D., Manjithaya, R., and Subramani, S. (2010). Roles of Pichia pastoris Uvrag in vacuolar protein sorting and the phosphatidylinositol 3-kinase complex in phagophore

elongation in autophagy pathways. Autophagy *6*, 86-99.

Fred Dice, J. (1990). Peptide sequences that target cytosolic proteins for lysosomal proteolysis. Trends in Biochemical Sciences *15*, 305-309.

Frias, M.A., Thoreen, C.C., Jaffe, J.D., Schroder, W., Sculley, T., Carr, S.A., and Sabatini, D.M. (2006). mSin1 Is Necessary for Akt/PKB Phosphorylation, and Its Isoforms Define Three Distinct mTORC2s. Current Biology *16*, 1865-1870.

Fry, M.R., Thomson, J.M., Tomasini, A.J., and Dunn, W.A. (2006). Early and late molecular events of glucose-induced pexophagy in Pichia pastoris require Vac8. Autophagy *2*, 280-288.

Funderburk, S.F., Wang, Q.J., and Yue, Z. (2010). The Beclin 1-VPS34 complex - at the crossroads of autophagy and beyond. Trends Cell Biol *20*, 355-362.

Ganley, I.G., Lam, D.H., Wang, J., Ding, X., Chen, S., and Jiang, X. (2009). ULK1·ATG13·FIP200 Complex Mediates mTOR Signaling and Is Essential for Autophagy. The Journal of Biological Chemistry *284*, 12297-12305.

Gao, X., Zacharek, A., Salkowski, A., Grignon, D.J., Sakr, W., Porter, A.T., and Honn, K.V. (1995). Loss of Heterozygosity of the BRCA1 and Other Loci on Chromosome 17q in Human Prostate Cancer. Cancer Research *55*, 1002-1005.

Giatromanolaki, A., Koukourakis, M.I., Koutsopoulos, A., Chloropoulou, P., Liberis, V., and Sivridis, E. (2011). High Beclin 1 expression defines a poor prognosis in endometrial adenocarcinomas. Gynecologic Oncology *123*, 147-151.

Gill, S.C., and Hippel, P.H.v. (1989). Calculation of Protein Extinction Coefficients from Amino Acid Sequence Data. Analytical Biochemistry *182*, 8.

Glickman, M.H., and Ciechanover, A. (2002). The Ubiquitin-Proteasome Proteolytic Pathway: Destruction for the Sake of Construction. Physiological Reviews *82*, 373-428.

Haar, E.V., Lee, S.-i., Bandhakavi, S., Griffin, T.J., and Kim, D.-H. (2007). Insulin signalling to mTOR mediated by the Akt/PKB substrate PRAS40. Nature Cell Biology *9*, 316-323.

Hanada, T., Noda, N.N., Satomi, Y., Ichimura, Y., Fujioka, Y., Takao, T., Inagaki, F., and Ohsumi, Y. (2007). The Atg12-Atg5 Conjugate Has a Novel E3-like Activity for Protein Lipidation in Autophagy. Journal of Biological Chemistry *282*, 37298-37302.

Hanahan, D., and Weinberg, R.A. (2000). The Hallmarks of Cancer. Cell *100*, 57-70.
Hara, K., Maruki, Y., Long, X., Yoshino, K.-i., Oshiro, N., Hidayat, S., Tokunaga, C., Avruch, J., and Yonezawa, K. (2002). Raptor, a Binding Partner of Target of Rapamycin (TOR), Mediates TOR Action. Cell *110*, 177-189.

Hara, T., Takamura, A., Kishi, C., Iemura, S.-i., Natsume, T., Guan, J.-L., and Mizushima, N. (2008). FIP200, a ULK-interacting protein, is required for autophagosome formation in mammalian cells. The Journal of Cell Biology *181*, 497-510.

He, C., and Levine, B. (2010). The Beclin 1 interactome. Current Opinion in Cell Biology *22*, 140-149.

He, S., Zhao, Z., Yang, Y., O'Connell, D., Zhang, X., Oh, S., Ma, B., Lee, J.-H., Zhang, T., Varghese, B., *et al.* (2015). Truncating mutation in the autophagy gene UVRAG confers oncogenic properties and chemosensitivity in colorectal cancers. Nature Communications *6*, 7839.

Henry, E., Fung, N., Liu, J., Drakakaki, G., and Coaker, G. (2015). Beyond Glycolysis: GAPDHs Are Multi-functional Enzymes Involved in Regulation of ROS, Autophagy, and Plant Immune Responses. Plos genetics *11*, e1005199.

HL, C., SR, T., CP, P., and JF, D. (1989). A role for a 70-kilodalton heat shock protein in lysosomal degradation of intracellular proteins. Science *246*, 382-385.

Holen, I., Gordon, P.B., and Seglen, P.O. (1992). Protein kinase-dependent effects of okadaic acid on hepatocytic autophagy and cytoskeletal integrity. Biochemical Journal *284*, 633-636.

Hosokawa, N., Hara, T., Kaizuka, T., Kishi, C., Takamura, A., Miura, Y., Iemura, S.-i., Natsume, T., Takehana, K., Yamada, N., *et al.* (2009a). Nutrient-dependent mTORC1 Association with the ULK1–Atg13–FIP200 Complex Required for Autophagy. Mol Biol Cell *20*, 1981-1991.

Hosokawa, N., Sasaki, T., Iemura, S.-i., Natsume, T., Hara, T., and Mizushima, N. (2009b). Atg101, a novel mammalian autophagy protein interacting with Atg13. Autophagy *5*, 973-979.

Huangfu, L., Liang, H., Wang, G., Su, X., Li, L., Du, Z., Hu, M., Dong, Y., Bai, X., Liu, T., *et al.* (2015). miR-183 regulates autophagy and apoptosis in colorectal cancer through targeting of UVRAG. Oncotarget *7*.

Ichimura, Y., Kumanomidou, T., Sou, Y.-s., Mizushima, T., Ezaki, J., Ueno, T., Kominami, E., Yamane, T., Tanaka, K., and Komatsu, M. (2008). Structural Basis for Sorting Mechanism of p62 in Selective Autophagy. Journal of Biological Chemistry *283*, 22847-22857.

initiative, T.a.g. (2000). Analysis of the genome sequence of the flowering plant Arabidopsis thaliana. Nature *408*, 796-815.

Ionov, Y., Nowak, N., Perucho, M., Markowitz, S., and Cowell, J.K. (2004). Manipulation of nonsense mediated decay identifies gene mutations in colon cancer Cells with microsatellite instability. Oncogene *23*, 639-645.

Isogai, S., Morimoto, D., Arita, K., Unzai, S., Tenno, T., Hasegawa, J., Sou, Y.S., Komatsu, M., Tanaka, K., Shirakawa, M., *et al.* (2011). Crystal structure of the ubiquitin-associated (UBA) domain of p62 and its interaction with ubiquitin. The Journal of biological chemistry *286*, 31864-31874.

Itakura, E., Kishi, C., Inoue, K., and Mizushima, N. (2008). Beclin 1 Forms Two Distinct Phosphatidylinositol 3-Kinase Complexes with Mammalian Atg14 and UVRAG. Molecular biology of the cell *19*, 5360-5372.

Itakura, E., and Mizushima, N. (2009a). Atg14 and UVRAG: mutually exclusive subunits of mammalian Beclin 1-PI3K complexes. Autophagy *5*, 534-536.

Itakura, E., and Mizushima, N. (2009b). Atg14 and UVRAG: Mutually exclusive subunits of mammalian Beclin 1-PI3K complexes. Autophagy *5*, 534-536.

Jacinto, E., Facchinetti, V., Liu, D., Soto, N., Wei, S., Jung, S.Y., Huang, Q., Qin, J., and Su, B. (2006). SIN1/MIP1 Maintains rictor-mTOR Complex Integrity and Regulates Akt Phosphorylation and Substrate Specificity. Cell *127*, 125-137.

Janku, F., McConkey, D.J., Hong, D.S., and Kurzrock, R. (2011). Autophagy as a target for anticancer therapy. Nat Rev Clin Oncol *8*, 528-539.

Jung, C.H., Jun, C.B., Ro, S.-H., Kim, Y.-M., Otto, N.M., Cao, J., Kundu, M., and Kim, D.-H. (2009). ULK-Atg13-FIP200 Complexes Mediate mTOR Signaling to the Autophagy Machinery. Molecular biology of the cell *20*, 1992-2003.

Kabeya, Y., Mizushima, N., Ueno, T., Yamamoto, A., Kirisako, T., Noda, T., Kominami, E., Ohsumi, Y., and Yoshimori, T. (2000). LC3, a mammalian homologue of yeast Apg8p, is localized in autophagosome membranes after processing. The EMBO Journal *19*, 5720-5728.

Katsuragi, Y., Ichimura, Y., and Komatsu, M. (2015). p62/SQSTM1 functions as a signaling hub and an autophagy adaptor. FEBS Journal *282*, 4672-4678.

Kaushik, S., and Cuervo, A.M. (2012). Chaperone-mediated autophagy: a unique way to enter the lysosome world. Trends in cell biology *22*, 407-417.

Kiffin, R., Christian, C., Knecht, E., and Cuervo, A.M. (2004). Activation of Chaperone-mediated Autophagy during Oxidative Stress. Molecular biology of the cell *15*, 4829-4840.

Kihara, A., Kabeya, Y., Ohsumi, Y., and Yoshimori, T. (2001). Beclin–phosphatidylinositol 3-kinase complex functions at the trans-Golgi network. EMBO Reports *2*, 330-335.

Kim, B.Y., Krämer, H., Yamamoto, A., Kominami, E., Kohsaka, S., and Akazawa, C. (2001). Molecular Characterization of Mammalian Homologues of Class C Vps Proteins That Interact with Syntaxin-7. Journal of Biological Chemistry *276*, 29393-29402.

Kim, B.Y., Ueda, M., Kominami, E., Akagawa, K., Kohsaka, S., and Akazawa, C. (2003). Identification of mouse Vps16 and biochemical characterization of mammalian Class C Vps complex. Biochemical and Biophysical Research Communications *311*, 577-582.

Kim, E., Goraksha-Hicks, P., Li, L., Neufeld, T.P., and Guan, K.-L. (2008). Regulation of TORC1 by Rag GTPases in nutrient response. Nature cell biology *10*, 935-945.

Kim, J., Kundu, M., Viollet, B., and Guan, K.-L. (2011a). AMPK and mTOR regulate autophagy through direct phosphorylation of Ulk1. Nature cell biology *13*, 132-141.

Kim, M.S., Song, S.Y., Lee, J.Y., Yoo, N.J., and Lee, S.H. (2011b). Expressional and mutational analyses of ATG5 gene in prostate cancers. APMIS *119*, 802-807.

Kim, Y.C., and Guan, K.-L. (2015). mTOR: a pharmacologic target for autophagy regulation. The Journal of Clinical Investigation *125*, 25-32.

Kim, Y.M., Jung, C.H., Seo, M., Kim, E.K., Park, J.M., Bae, S.S., and Kim, D.H. (2015). mTORC1 phosphorylates UVRAG to negatively regulate autophagosome and endosome maturation. Molecular Cell *57*, 207-218.

Kim, Y.W., Grossmann, T.N., and Verdine, G.L. (2011c). Synthesis of all-hydrocarbon stapled alpha-helical peptides by ring-closing olefin metathesis. Nature Protocals *6*, 761-771.

Kirisako, T., Ichimura, Y., Okada, H., Kabeya, Y., Mizushima, N., Yoshimori, T., Ohsumi, M., Takao, T., Noda, T., and Ohsumi, Y. (2000). The Reversible Modification Regulates the Membrane-Binding State of Apg8/Aut7 Essential for Autophagy and the Cytoplasm to Vacuole Targeting Pathway. The Journal of Cell Biology *151*, 263-276.

Kirkin, V., McEwan, D.G., Novak, I., and Dikic, I. (2009). A Role for Ubiquitin in Selective Autophagy. Molecular Cell *34*, 259-269.

Knævelsrud, H., Ahlquist, T., Merok, M.A., Nesbakken, A., Stenmark, H., Lothe, R.A., and Simonsen, A. (2010). UVRAG mutations associated with microsatellite unstable colon cancer do not affect autophagy. Autophagy *6*, 863-870.

Komatsu, M., and Ichimura, Y. (2010). Physiological significance of selective degradation of p62 by autophagy. FEBS Letters *584*, 1374-1378.

Komatsu, M., Waguri, S., Ueno, T., Iwata, J., Murata, S., Tanida, I., Ezaki, J., Mizushima, N., Ohsumi, Y., Uchiyama, Y., *et al.* (2005). Impairment of starvation-induced and constitutive autophagy in Atg7-deficient mice. The Journal of Cell Biology *169*, 425-434.

Kon, M., Kiffin, R., Koga, H., Chapochnick, J., Macian, F., Varticovski, L., and Cuervo, A.M.

(2011). Chaperone-Mediated Autophagy Is Required for Tumor Growth. Science translational medicine *3*, 109ra117-109ra117.

Korolchuk, V.I., Menzies, F.M., and Rubinsztein, D.C. (2010). Mechanisms of cross-talk between the ubiquitin-proteasome and autophagy-lysosome systems. FEBS Letters *584*, 1393-1398.

Koukourakis, M.I., Giatromanolaki, A., Sivridis, E., Pitiakoudis, M., Gatter, K.C., and Harris, A.L. (2010). Beclin 1 over- and underexpression in colorectal cancer: distinct patterns relate to prognosis and tumour hypoxia. British Journal of Cancer *103*, 1209-1214.

Kraft, C., Deplazes, A., Sohrmann, M., and Peter, M. (2008). Mature ribosomes are selectively degraded upon starvation by an autophagy pathway requiring the Ubp3p/Bre5p ubiquitin protease. Nature Cell Biology *10*, 602-610.

Kuma, A., Hatano, M., Matsui, M., Yamamoto, A., Nakaya, H., Yoshimori, T., Ohsumi, Y., Tokuhisa, T., and Mizushima, N. (2004). The role of autophagy during the early neonatal starvation period. Nature *432*, 1032-1036.

Kuma, A., and Mizushima, N. (2010). Physiological role of autophagy as an intracellular recycling system: With an emphasis on nutrient metabolism. Seminars in Cell & Developmental Biology *21*, 683-690.

Kuma, A., Mizushima, N., Ishihara, N., and Ohsumi, Y. (2002). Formation of the ~350-kDa Apg12-Apg5·Apg16 Multimeric Complex, Mediated by Apg16 Oligomerization, Is Essential for Autophagy in Yeast. Journal of Biological Chemistry *277*, 18619-18625.

Kwon, M.-c., and Berns, A. (2013). Mouse models for lung cancer. Molecular Oncology *7*, 165-177.

Kwon, S.I., and Park, O.K. (2008). Autophagy in plants. Journal of Plant Biology *51*, 313-320.

Lamark, T., Perander, M., Outzen, H., Kristiansen, K., Øvervatn, A., Michaelsen, E., Bjørkøy, G., and Johansen, T. (2003). Interaction Codes within the Family of Mammalian Phox and Bem1p Domain-containing Proteins. Journal of Biological Chemistry *278*, 34568-34581.

Lee, G., Liang, C., Park, G., Jang, C., Jung, J.U., and Chung, J. (2011a). UVRAG is required for organ rotation by regulating Notch endocytosis in Drosophila. Developmental biology *356*, 588-597.

Lee, H.K., Mattei, L.M., Steinberg, B.E., Alberts, P., Lee, Y.H., Chervonsky, A., Mizushima, N., Grinstein, S., and Iwasaki, A. (2010). In Vivo Requirement for Atg5 in Antigen Presentation by Dendritic Cells. Immunity *32*, 227-239.

Lee, S., Sato, Y., and Nixon, R.A. (2011b). Lysosomal proteolysis inhibition selectively disrupts axonal transport of degradative organelles and causes an Alzheimer's-like axonal dystrophy. The Journal of Neuroscience *31*, 7817-7830.

Lemasters, and J., J. (2005). Selective Mitochondrial Autophagy, or Mitophagy, as a Targeted Defense Against Oxidative Stress, Mitochondrial Dysfunction, and Aging. Rejuvenation Research *8*, 3-5.

Leslie, A.G. (2006). The integration of macromolecular diffraction data. Acta Crystallogr D Biol Crystallogr *62*, 48-57.

Levine, B., and Klionsky, D.J. (2004). Development by Self-Digestion: Molecular Mechanisms and Biological Functions of Autophagy. Developmental Cell *6*, 463-477.

Levine, B., and Kroemer, G. (2008). Autophagy in the Pathogenesis of Disease. Cell *132*, 27-42.

Levine, B., Mizushima, N., and Virgin, H.W. (2011). Autophagy in immunity and inflammation. Nature *469*, 323-335.

Li, C., Capan, E., Zhao, Y., Zhao, J., Stolz, D., Watkins, S.C., Jin, S., and Lu, B. (2006). Autophagy Is Induced in CD4+ T Cells and Important for the Growth Factor-Withdrawal Cell Death. The Journal of Immunology *177*, 5163-5168.

Li, F., Chung, T., and Vierstra, R.D. (2014). AUTOPHAGY-RELATED11 Plays a Critical Role in General Autophagy- and Senescence-Induced Mitophagy in Arabidopsis. The Plant Cell *26*, 788-807.

Li, W.-w., Li, J., and Bao, J.-k. (2012a). Microautophagy: lesser-known self-eating. Cell Mol Life Sci *69*, 1125-1136.

Li, X., He, L., Che, K.H., Funderburk, S.F., Pan, L., Pan, N., Zhang, M., Yue, Z., and Zhao, Y. (2012b). Imperfect interface of Beclin1 coiled-coil domain regulates homodimer and heterodimer formation with Atg14L and UVRAG. Nature Communications *3*, 662.

Li, X., He, L., Che, K.H., Funderburk, S.F., Pan, L., Pan, N., Zhang, M., Yue, Z., and Zhao, Y. (2012c). Imperfect interface of Beclin1 coiled-coil domain regulates homodimer and heterodimer formation with Atg14L and UVRAG. Nature Communications *3*, 662.

Liang, C., Feng, P., Ku, B., Dotan, I., Canaani, D., Oh, B.-H., and Jung, J.U. (2006a). Autophagic and tumour suppressor activity of a novel Beclin1-binding protein UVRAG. Nature Cell Biology *8*, 688-698.

Liang, C., Feng, P., Ku, B., Dotan, I., Canaani, D., Oh, B.H., and Jung, J.U. (2006b). Autophagic and tumour suppressor activity of a novel Beclin1-binding protein UVRAG. Nature Cell Biology *8*, 688-699.

Liang, C., Feng, P., Ku, B., Oh, B.H., and Jung, J.U. (2007). UVRAG: a new player in autophagy and tumor cell growth. Autophagy *3*, 69-71.

Liang, C., Lee, J.-s., Inn, K.-S., Gack, M.U., Li, Q., Roberts, E.A., Vergne, I., Deretic, V., Feng, P., Akazawa, C., *et al.* (2008a). Beclin1-binding UVRAG targets the class C Vps complex to coordinate autophagosome maturation and endocytic trafficking. Nature cell biology *10*, 776-787.

Liang, C., Lee, J.S., Inn, K.S., Gack, M.U., Li, Q., Roberts, E.A., Vergne, I., Deretic, V., Feng, P., Akazawa, C., *et al.* (2008b). Beclin1-binding UVRAG targets the class C Vps complex to coordinate autophagosome maturation and endocytic trafficking. Nature Cell Biology *10*, 776-787.

Liang, C., Sir, D., Lee, S., Ou, J.-h.J., and Jung, J.U. (2008c). Beyond autophagy: The role of UVRAG in membrane trafficking. Autophagy *4*, 817-820.

Liang, C., Sir, D., Lee, S., Ou, J.H., and Jung, J.U. (2008d). Beyond autophagy: the role of UVRAG in membrane trafficking. Autophagy *4*, 817-820.

Liang, X.H., Jackson, S., Seaman, M., Brown, K., Kempkes, B., Hibshoosh, H., and Levine, B. (1999). Induction of autophagy and inhibition of tumorigenesis by beclin 1. Nature *402*, 672-676.

Lilienbaum, A. (2013). Relationship between the proteasomal system and autophagy. International Journal of Biochemistry and Molecular Biology *4*, 1-26.

Lim, J., Lachenmayer, M.L., Wu, S., Liu, W., Kundu, M., Wang, R., Komatsu, M., Oh, Y.J., Zhao, Y., and Yue, Z. (2015). Proteotoxic Stress Induces Phosphorylation of p62/SQSTM1 by ULK1 to Regulate Selective Autophagic Clearance of Protein Aggregates. PLoS Genetics *11*, e1004987.

Liu, H., He, Z., von Rütte, T., Yousefi, S., Hunger, R.E., and Simon, H.-U. (2013). Down-Regulation of Autophagy-Related Protein 5 (ATG5) Contributes to the Pathogenesis of Early-Stage Cutaneous Melanoma. Science translational medicine *5*, 202ra123-202ra123.

Long, J., Gallagher, T.R., Cavey, J.R., Sheppard, P.W., Ralston, S.H., Layfield, R., and Searle, M.S. (2008a). Ubiquitin recognition by the ubiquitin-associated domain of p62 involves a novel conformational switch. The Journal of biological chemistry *283*, 5427-5440.

Long, J., Gallagher, T.R.A., Cavey, J.R., Sheppard, P.W., Ralston, S.H., Layfield, R., and Searle, M.S. (2008b). Ubiquitin Recognition by the Ubiquitin-associated Domain of p62 Involves a Novel Conformational Switch. Journal of Biological Chemistry *283*, 5427-5440.

Long, J., Garner, T.P., Pandya, M.J., Craven, C.J., Chen, P., Shaw, B., Williamson, M.P., Layfield, R., and Searle, M.S. (2010a). Dimerisation of the UBA domain of p62 inhibits ubiquitin binding and regulates NF-kappaB signalling. Journal of molecular biology *396*, 178-194.

Long, J., Garner, T.P., Pandya, M.J., Craven, C.J., Chen, P., Shaw, B., Williamson, M.P., Layfield, R., and Searle, M.S. (2010b). Dimerisation of the UBA Domain of p62 Inhibits Ubiquitin Binding and Regulates NF-κB Signalling. Journal of Molecular Biology *396*, 178-194.

Lowry, O.H., Rosebrough, N.J., Farr, A.L., and Randall, R.J. (1951). Protein measurement with the folin phenol reagent. Journal of Biological Chemistry *193*, 265-275.

Lv, L., Li, D., Zhao, D., Lin, R., Chu, Y., Zhang, H., Zha, Z., Liu, Y., Li, Z., Xu, Y., *et al.* (2011). Acetylation Targets the M2 Isoform of Pyruvate Kinase for Degradation through Chaperone-Mediated Autophagy and Promotes Tumor Growth. Molecular Cell *42*, 719-730.

Lynch, T.J., Bell, D.W., Sordella, R., Gurubhagavatula, S., Okimoto, R.A., Brannigan, B.W., Harris, P.L., Haserla , S.M., Supko, J.G., Haluska, F.G., *et al.* (2004). Activating Mutations in the Epidermal Growth Factor Receptor Underlying Responsiveness of Non–Small-Cell Lung Cancer to Gefitinib. New England Journal of Medicine *350*, 2129-2139.

Müller, O., Neumann, H., Bayer, M.J., and Mayer, A. (2003). Role of the Vtc proteins in V-ATPase stability and membrane trafficking. Journal of Cell Science *116*, 1107-1115.

Müller, O., Sattler, T., Flötenmeyer, M., Schwarz, H., Plattner, H., and Mayer, A. (2000). Autophagic Tubes: Vacuolar Invaginations Involved in Lateral Membrane Sorting and Inverse Vesicle Budding. The Journal of Cell Biology *151*, 519-528.

Massey, A.C., Kaushik, S., Sovak, G., Kiffin, R., and Cuervo, A.M. (2006). Consequences of the selective blockage of chaperone-mediated autophagy. Proceedings of the National Academy of Sciences of the United States of America *103*, 5805-5810.

Matsumoto, G., Wada, K., Okuno, M., Kurosawa, M., and Nukina, N. (2011a). Serine 403 phosphorylation of p62/SQSTM1 regulates selective autophagic clearance of ubiquitinated proteins. Molecular cell *44*, 279-289.

Matsunaga, K., Saitoh, T., Tabata, K., Omori, H., Satoh, T., Kurotori, N., Maejima, I., Shirahama-Noda, K., Ichimura, T., Isobe, T., *et al.* (2009b). Two Beclin 1-binding proteins, Atg14L and Rubicon, reciprocally regulate autophagy at different stages. Nature Cell Biology *11*, 385-396.

Matsuura, A., Tsukada, M., Wada, Y., and Ohsumi, Y. (1997). Apg1p, a novel protein kinase required for the autophagic process in Saccharomyces cerevisiae. Gene *192*, 245-250.

McCoy, A.J. (2007). Solving structures of protein complexes by molecular replacement with Phaser. Acta Crystallogr D Biol Crystallogr *63*, 32-41.

Mercer, C.A., Kaliappan, A., and Dennis, P.B. (2009). A novel, human Atg13 binding protein, Atg101, interacts with ULK1 and is essential for macroautophagy. Autophagy *5*, 649-662.

Merz, E.A., Brinster, R.L., Brunner, S., and Chen, H.Y. (1981). Protein degradation during preimplantation development of the mouse. Journal of Reproduction and Fertility *61*, 415-418.

Michaeli, S., Galili, G., Genschik, P., Fernie, A.R., and Avin-Wittenberg, T. (2015). Autophagy in Plants - What's New on the Menu? Trends in Plant Science *21*, 134-144.

Minina, E.A., Bozhkov, P.V., and Hofius, D. (2014). Autophagy as initiator or executioner of cell death. Trends in Plant Science *19*, 692-697.

Minina, E.A., Filonova, L.H., Fukada, K., Savenkov, E.I., Gogvadze, V., Clapham, D., Sanchez-Vera, V., Suarez, M.F., Zhivotovsky, B., Daniel, G., *et al.* (2013). Autophagy and metacaspase determine the mode of cell death in plants. The Journal of Cell Biology *203*, 917-927.

Mizushima, N. (2007). Autophagy: process and function. Genes&Development *21*, 2861-2873.

Mizushima, N. (2010). The role of the Atg1/ULK1 complex in autophagy regulation. Current Opinion in Cell Biology *22*, 132-139.

Mizushima, N., and Komatsu, M. (2011). Autophagy: Renovation of Cells and Tissues. Cell *147*, 728-741.

Mizushima, N., Kuma, A., Kobayashi, Y., Yamamoto, A., Matsubae, M., Takao, T., Natsume, T., Ohsumi, Y., and Yoshimori, T. (2003). Mouse Apg16L, a novel WD-repeat protein, targets to the autophagic isolation membrane with the Apg12-Apg5 conjugate. Journal of Cell Science *116*, 1679-1688.

Mizushima, N., and Levine, B. (2010). Autophagy in mammalian development and differentiation. Nature cell biology *12*, 823-830.

Mizushima, N., Sugita, H., Yoshimori, T., and Ohsumi, Y. (1998). A New Protein Conjugation System in Human: the counterpart of the yeast apg12p conjugation system essential for autophagy. Journal of Biological Chemistry *273*, 33889-33892.

Mizushima, N., Yamamoto, A., Hatano, M., Kobayashi, Y., Kabeya, Y., Suzuki, K., Tokuhisa, T., Ohsumi, Y., and Yoshimori, T. (2001). Dissection of Autophagosome Formation Using Apg5-Deficient Mouse Embryonic Stem Cells. The Journal of Cell Biology *152*, 657-668.

Mizushima, N., Yamamoto, A., Matsui, M., Yoshimori, T., and Ohsumi, Y. (2004). In Vivo Analysis of Autophagy in Response to Nutrient Starvation Using Transgenic Mice Expressing a Fluorescent Autophagosome Marker. Molecular Biology of the Cell *15*, 1101-1111.

Mizushima, N., Yoshimori, T., and Levine, B. (2010). Methods in Mammalian Autophagy Research. Cell *140*, 313-326.

Mizushima, N., Yoshimori, T., and Ohsumi, Y. (2011). The Role of Atg Proteins in Autophagosome Formation. Annual Review of Cell and Developmental Biology *27*, 107-132.

Moscat, J., Diaz-Meco, M.T., and Wooten, M.W. (2007). Signal integration and diversification through the p62 scaffold protein. Trends in Biochemical Sciences *32*, 95-100.

Murshudov, G.N., Vagin, A.A., and Dodson, E.J. (1997). Refinement of macromolecular structures by the maximum-likelihood method. Acta Crystallogr D Biol Crystallogr *53*, 240-255.

Myung Park, J., Tougeron, D., Huang, S., Okamoto, K., and Sinicrope, F.A. (2014). Beclin 1 and UVRAG Confer Protection from Radiation-Induced DNA Damage and Maintain Centrosome Stability in Colorectal Cancer Cells. PLoS One *9*, e100819.

Nakamura, N., Hirata, A., Ohsumi, Y., and Wada, Y. (1997). Vam2/Vps41p and Vam6/Vps39p Are Components of a Protein Complex on the Vacuolar Membranes and Involved in the Vacuolar Assembly in the Yeast Saccharomyces cerevisiae. Journal of Biological Chemistry *272*, 11344-11349.

Nakatogawa, H. (2013). Two ubiquitin-like conjugation systems that mediate membrane formation during autophagy. Essays In Biochemistry *55*, 39-50.

Narendra, D., Tanaka, A., Suen, D.-F., and Youle, R.J. (2008). Parkin is recruited selectively to impaired mitochondria and promotes their autophagy. The Journal of Cell Biology *183*, 795-803.

Nixon, R.A. (2013). The role of autophagy in neurodegenerative disease. Nat Med *19*, 983-997.

Noda, T., and Ohsumi, Y. (1998). Tor, a phosphatidylinositol kinase homologue, controls autophagy in yeast. Journal of Biological Chemistry *273*, 3963-3966.

Novikoff, A.B. (1959). The Proximal Tubule Cell in Experimental Hydronephrosis. The Journal of Biophysical and Biochemical Cytology *6*, 136-138.

Novikoff AB, E.E., Quintana N (1964). Golgi apparatus and lysosomes. Federation Proceedings *23*, 13.

Orenstein, S.J., Kuo, S.-H., Tasset, I., Arias, E., Koga, H., Fernandez-Carasa, I., Cortes, E., Honig, L.S., Dauer, W., Consiglio, A., *et al.* (2013). Interplay of LRRK2 with chaperone-mediated autophagy. Nature Neuroscience *16*, 394-406.

Pérez-Pérez, M.E., Florencio, F.J., and Crespo, J.L. (2010). Inhibition of Target of Rapamycin Signaling and Stress Activate Autophagy in Chlamydomonas reinhardtii. Plant Physiology *152*, 1874-1888.

Paez, J.G., Jänne, P.A., Lee, J.C., Tracy, S., Greulich, H., Gabriel, S., Herman, P., Kaye, F.J., Lindeman, N., Boggon, T.J., *et al.* (2004). EGFR Mutations in Lung Cancer: Correlation with Clinical Response to Gefitinib Therapy. Science *304*, 1497-1500.

Pang, S., Chen, D., Zhang, A., Qin, X., and Yan, B. (2012). Genetic analysis of the LAMP-2 gene

promoter in patients with sporadic Parkinson's disease. Neuroscience Letters *526*, 63-67.

Pankiv, S., Clausen, T.H., Lamark, T., Brech, A., Bruun, J.-A., Outzen, H., Øvervatn, A., Bjørkøy, G., and Johansen, T. (2007). p62/SQSTM1 Binds Directly to Atg8/LC3 to Facilitate Degradation of Ubiquitinated Protein Aggregates by Autophagy. Journal of Biological Chemistry *282*, 24131-24145.

Pao, W., Miller, V., Zakowski, M., Doherty, J., Politi, K., Sarkaria, I., Singh, B., Heelan, R., Rusch, V., Fulton, L., *et al.* (2004). EGF receptor gene mutations are common in lung cancers from "never smokers" and are associated with sensitivity of tumors to gefitinib and erlotinib. Proceedings of the National Academy of Sciences of the United States of America *101*, 13306-13311.

Pearce, Laura R., Huang, X., Boudeau, J., Pawłowski, R., Wullschleger, S., Deak, M., Ibrahim, Adel F M., Gourlay, R., Magnuson, Mark A., and Alessi, Dario R. (2007). Identification of Protor as a novel Rictor-binding component of mTOR complex-2. The Biochemical Journal *405*, 513-522.

Peplowska, K., Markgraf, D.F., Ostrowicz, C.W., Bange, G., and Ungermann, C. The CORVET Tethering Complex Interacts with the Yeast Rab5 Homolog Vps21 and Is Involved in Endo-Lysosomal Biogenesis. Developmental Cell *12*, 739-750.

Perelman, B., Dafni, N., Naiman, T., Eli, D., Yaakov, M., Feng, T.L.Y., Sinha, S., Weber, G., Khodaei, S., Sancar, A., *et al.* (1997). Molecular Cloning of a Novel Human Gene Encoding a 63-kDa Protein and Its Sublocalization within the 11q13 Locus. Genomics *41*, 397-405.

Peterson, G.L. (1979). Review of the folin phenol protein quantitation method of lowry, rosebrough, farr and randall. Analytical Biochemistry *100*, 201-220.

Pfeifer, U. (1977). Inhibition by insulin of the physiological autophagic breakdown of cell organelles. Acta biologica et medica Germanica *36*, 4.

PO, S., PB, G., and I, H. (1990). Non-selective autophagy. Seminars in Cell Biology *1*, 441-448.

Potterton, L., McNicholas, S., Krissinel, E., Gruber, J., Cowtan, K., Emsley, P., Murshudov, G.N., Cohen, S., Perrakis, A., and Noble, M. (2004). Developments in the CCP4 molecular-graphics project. Acta Crystallogr D Biol Crystallogr *60*, 2288-2294.

Pua, H.H., Dzhagalov, I., Chuck, M., Mizushima, N., and He, Y.-W. (2007). A critical role for the autophagy gene Atg5 in T cell survival and proliferation. The Journal of Experimental Medicine *204*, 25-31.

Pyo, J.-O., Yoo, S.-M., Ahn, H.-H., Nah, J., Hong, S.-H., Kam, T.-I., Jung, S., and Jung, Y.-K. (2013). Overexpression of Atg5 in mice activates autophagy and extends lifespan. Nature Communications *4*.

Qu, X., Yu, J., Bhagat, G., Furuya, N., Hibshoosh, H., Troxel, A., Rosen, J., Eskelinen, E.-L.,

Mizushima, N., Ohsumi, Y., *et al.* Promotion of tumorigenesis by heterozygous disruption of the beclin 1 autophagy gene. The Journal of Clinical Investigation *112*, 1809-1820.

Qu, X., Yu, J., Bhagat, G., Furuya, N., Hibshoosh, H., Troxel, A., Rosen, J., Eskelinen, E.-L., Mizushima, N., Ohsumi, Y., *et al.* (2003). Promotion of tumorigenesis by heterozygous disruption of the beclin 1 autophagy gene. Journal of Clinical Investigation *112*, 1809-1820.

Ramundo, S., Casero, D., Mühlhaus, T., Hemme, D., Sommer, F., Crèvecoeur, M., Rahire, M., Schroda, M., Rusch, J., Goodenough, U., *et al.* (2014). Conditional Depletion of the Chlamydomonas Chloroplast ClpP Protease Activates Nuclear Genes Involved in Autophagy and Plastid Protein Quality Control. The Plant Cell *26*, 2201-2222.

Reggiori, F., and Klionsky, D.J. (2013). Autophagic Processes in Yeast: Mechanism, Machinery and Regulation. Genetics *194*, 341-361.

Richardson, S.C.W., Winistorfer, S.C., Poupon, V., Luzio, J.P., and Piper, R.C. (2004). Mammalian Late Vacuole Protein Sorting Orthologues Participate in Early Endosomal Fusion and Interact with the Cytoskeleton. Mol Biol Cell *15*, 1197-1210.
Rosenfeldt, M.T., and Ryan, K.M. (2011). The multiple roles of autophagy in cancer. Carcinogenesis *32*, 955-963.

Rubinsztein, David C., Mariño, G., and Kroemer, G. (2011). Autophagy and Aging. Cell *146*, 682-695.

Saha, T. (2012). LAMP2A overexpression in breast tumors promotes cancer cell survival via chaperone-mediated autophagy. Autophagy *8*, 1643-1656.

Saito, H., Inazawa, J., Saito, S., Kasumi, F., Koi, S., Sagae, S., Kudo, R., Saito, J., Noda, K., and Nakamura, Y. (1993). Detailed Deletion Mapping of Chromosome 17q in Ovarian and Breast Cancers: 2-cM Region on 17q21.3 Often and Commonly Deleted in Tumors. Cancer Research *53*, 3382-3385.

Sakoh-Nakatogawa, M., Matoba, K., Asai, E., Kirisako, H., Ishii, J., Noda, N.N., Inagaki, F., Nakatogawa, H., and Ohsumi, Y. (2013). Atg12–Atg5 conjugate enhances E2 activity of Atg3 by rearranging its catalytic site. Nature Structural & Molecular Biology *20*, 433-439.

Salvador, N., Aguado, C., Horst, M., and Knecht, E. (2000). Import of a Cytosolic Protein into Lysosomes by Chaperone-Mediated Autophagy depends on its Folding State. Journal of Biological Chemistry.

Sancak, Y., Peterson, T.R., Shaul, Y.D., Lindquist, R.A., Thoreen, C.C., Bar-Peled, L., and Sabatini, D.M. (2008). The Rag GTPases bind raptor and mediate amino acid signaling to mTORC1. Science (New York, NY) *320*, 1496-1501.

Sancak, Y., Thoreen, C.C., Peterson, T.R., Lindquist, R.A., Kang, S.A., Spooner, E., Carr, S.A., and Sabatini, D.M. (2007). PRAS40 Is an Insulin-Regulated Inhibitor of the mTORC1 Protein Kinase. Molecular Cell *25*, 903-915.

Schapira, A.H.V. (2008). Mitochondria in the aetiology and pathogenesis of Parkinson's disease. The Lancet Neurology *7*, 97-109.

Scott, R.C., Schuldiner, O., and Neufeld, T.P. (2004). Role and Regulation of Starvation-Induced Autophagy in the Drosophila Fat Body. Developmental Cell *7*, 167-178.

Seglen, P.O., and Gordon, P.B. (1982). 3-Methyladenine: Specific inhibitor of autophagic/lysosomal protein degradation in isolated rat hepatocytes. Proceedings of the National Academy of Sciences of the United States of America *79*, 1889-1892.

Senadhi Vuay-kumar, C.E.B., Keith D. Wilkinson, WilliamJ Cook (1985). Three-dimentional structure of Ubiquitin at 2.8A resolution. Proceedings of the National Academy of Sciences *82*, 3582-3585.

Shaid, S., Brandts, C.H., Serve, H., and Dikic, I. (2013). Ubiquitination and selective autophagy. Cell Death and Differentiation *20*, 21-30.

Shemi, A., Ben-Dor, S., and Vardi, A. (2015). Elucidating the composition and conservation of the autophagy pathway in photosynthetic eukaryotes. Autophagy *11*, 701-715.

Shin Isogai, D.M., Kyohei Arita, Satoru Unzai, Takeshi Tenno, Jun Hasegawa, Yu-shin Sou, Masaaki Komatsu, Keiji Tanaka, Masahiro Shirakawa, and Hidehito Tochio (2011). Crystal Structure of the Ubiquitin-associated (UBA) Domain of p62 and Its Interaction with Ubiquitin. The Journal of Biological Chemistry *286*.

Shintani, T., Mizushima, N., Ogawa, Y., Matsuura, A., Noda, T., and Ohsumi, Y. (1999). Apg10p, a novel protein-conjugating enzyme essential for autophagy in yeast. The EMBO Journal *18*, 5234-5241.

Shoji-Kawata, S., Sumpter, R., Leveno, M., Campbell, G.R., Zou, Z., Kinch, L., Wilkins, A.D., Sun, Q., Pallauf, K., MacDuff, D., *et al.* (2013). Identification of a candidate therapeutic autophagy-inducing peptide. Nature *494*, 201-206.

Shvets, E., Fass, E., Scherz-Shouval, R., and Elazar, Z. (2008). The N-terminus and Phe52 residue of LC3 recruit p62/SQSTM1 into autophagosomes. Journal of Cell Science *121*, 2685-2695.

Singh, R., Kaushik, S., Wang, Y., Xiang, Y., Novak, I., Komatsu, M., Tanaka, K., Cuervo, A.M., and Czaja, M.J. (2009). Autophagy regulates lipid metabolism. Nature *458*, 1131-1135.

Stitzel, M.L., and Seydoux, G. (2007). Regulation of the Oocyte-to-Zygote Transition. Science *316*,

407-408.

Stolz, A., Ernst, A., and Dikic, I. (2014). Cargo recognition and trafficking in selective autophagy. Nature Cell Biology *16*, 495-501.

Suzuki, K. (2013). Selective autophagy in budding yeast. Cell Death and Differentiation *20*, 43-48.

Suzuki, K., and Ohsumi, Y. (2007). Molecular machinery of autophagosome formation in yeast, Saccharomyces cerevisiae. FEBS Letters *581*, 2156-2161.
Takeshige, K., Baba, M., Tsuboi, S., Noda, T., and Ohsumi, Y. (1992). Autophagy in yeast demonstrated with proteinase-deficient mutants and conditions for its induction. The Journal of Cell Biology *119*, 301-311.

Takeshige；, K., Baba；, M., Tsuboi；, S., Noda；, T., and Ohsumi, Y. (1992). Autophagy in yeast demonstrated with proteinase-deficient mutants and conditions for its induction. The Journal of Cell Biology *119*, 301-311.

Terlecky, S.R., Chiang, H.L., Olson, T.S., and Dice, J.F. (1992). Protein and peptide binding and stimulation of in vitro lysosomal proteolysis by the 73-kDa heat shock cognate protein. Journal of Biological Chemistry *267*, 9202-9209.

Thedieck, K., Polak, P., Kim, M.L., Molle, K.D., Cohen, A., Jenö, P., Arrieumerlou, C., and Hall, M.N. (2007). PRAS40 and PRR5-Like Protein Are New mTOR Interactors that Regulate Apoptosis. PLoS One *2*, e1217.

Tian, Y., Li, Z., Hu, W., Ren, H., Tian, E., Zhao, Y., Lu, Q., Huang, X., Yang, P., Li, X., *et al.* (2010). C. elegans Screen Identifies Autophagy Genes Specific to Multicellular Organisms. Cell *141*, 1042-1055.

Trinh, J., and Farrer, M. (2013). Advances in the genetics of Parkinson disease. Nature Reviews Neurology *9*, 445-454.

Tsukada, M., and Ohsumi, Y. (1993). Isolation and characterization of autophagy-defective mutants of Saccharomyces cerevisiae. FEBS Letters *333*, 169-174.

Tsukamoto, S., Kuma, A., Murakami, M., Kishi, C., Yamamoto, A., and Mizushima, N. (2008). Autophagy Is Essential for Preimplantation Development of Mouse Embryos. Science *321*, 117-120.

Uttenweiler, A., Schwarz, H., and Mayer, A. (2005). Microautophagic Vacuole Invagination Requires Calmodulin in a Ca2+-independent Function. Journal of Biological Chemistry *280*, 33289-33297.

Valente, E.M., Abou-Sleiman, P.M., Caputo, V., Muqit, M.M.K., Harvey, K., Gispert, S., Ali, Z., Del Turco, D., Bentivoglio, A.R., Healy, D.G., *et al.* (2004). Hereditary Early-Onset Parkinson's Disease Caused by Mutations in PINK1. Science *304*, 1158-1160.

Valente, E.M., Bentivoglio, A.R., Dixon, P.H., Ferraris, A., Ialongo, T., Frontali, M., Albanese, A., Wood, and Nicholas, W. (2001). Localization of a Novel Locus for Autosomal Recessive Early-Onset Parkinsonism, PARK6, on Human Chromosome 1p35-p36. American Journal of Human Genetics *68*, 895-900.

Vincow, E.S., Merrihew, G., Thomas, R.E., Shulman, N.J., Beyer, R.P., MacCoss, M.J., and Pallanck, L.J. (2013). The PINK1–Parkin pathway promotes both mitophagy and selective respiratory chain turnover in vivo. Proceedings of the National Academy of Sciences of the United States of America *110*, 6400-6405.

Virgin, H.W., and Levine, B. (2009). Autophagy genes in immunity. Nature immunology *10*, 461-470.

Walker, F., Abramowitz, L., Benabderrahmane, D., Duval, X., Descatoire, V., Hénin, D., Lehy, T., and Aparicio, T. (2009). Growth factor receptor expression in anal squamous lesions: modifications associated with oncogenic human papillomavirus and human immunodeficiency virus. Human Pathology *40*, 1517-1527.

Wang, C.-W., and Klionsky, D.J. (2003). The Molecular Mechanism of Autophagy. Molecular Medicine *9*, 65-76.

Wang, L., Harris, T.E., Roth, R.A., and Lawrence , J.C. (2007). PRAS40 Regulates mTORC1 Kinase Activity by Functioning as a Direct Inhibitor of Substrate Binding. Journal of Biological Chemistry *282*, 20036-20044.

Wang, R.C., Wei, Y., An, Z., Zou, Z., Xiao, G., Bhagat, G., White, M., Reichelt, J., and Levine, B. (2012). Akt-mediated regulation of autophagy and tumorigenesis through Beclin 1 phosphorylation. Science *338*, 956-959.

Wei, Y., Zou, Z., Becker, N., Anderson, M., Sumpter, R., Xiao, G., Kinch, L., Koduru, P., Christudass, C.S., Veltri, R.W., *et al.* (2013). EGFR-mediated Beclin 1 phosphorylation in autophagy suppression, tumor progression, and tumor chemoresistance. Cell *154*, 1269-1284.

Weidberg, H., Shvets, E., and Elazar, Z. (2011). Biogenesis and Cargo Selectivity of Autophagosomes. Annual Review of Biochemistry *80*, 125-156.

White, E. (2012). Deconvoluting the context-dependent role for autophagy in cancer. Nature reviews Cancer *12*, 401-410.

Wong, P.-M., Feng, Y., Wang, J., Shi, R., and Jiang, X. (2015). Regulation of autophagy by coordinated action of mTORC1 and protein phosphatase 2A. Nature Communications *6*.

Wurzer, B., Zaffagnini, G., Fracchiolla, D., Turco, E., Abert, C., Romanov, J., and Martens, S.

(2015). Oligomerization of p62 allows for selection of ubiquitinated cargo and isolation membrane during selective autophagy. eLife *4*, e08941.

XB, W., XJ, F., MY, C., J, X., PY, H., L, G., XY, W., J, X., ZJ, L., Y, Z., *et al.* (2010). Elevated Beclin 1 expression is correlated with HIF-1alpha in predicting poor prognosis of nasopharyngeal carcinoma. Autophagy *3*, 395-404.

Xia, P., Wang, J.-J., Zhao, B.-B., and Song, C.-L. (2013). The role of beclin-1 expression in patients with gastric cancer: a meta-analysis. Tumor Biology *34*, 3303-3307.

Xie, Q., Michaeli, S., Peled-Zehavi, H., and Galili, G. (2015). Chloroplast degradation: one organelle, multiple degradation pathways. Trends in Plant Science *20*, 264-265.

Yang, Z., and Klionsky, D.J. (2007). Permeases Recycle Amino Acids Resulting from Autophagy. Autophagy *3*, 149-150.

Yarden, Y., and Schlessinger, J. (1987). Epidermal growth factor induces rapid, reversible aggregation of the purified epidermal growth factor receptor. Biochemistry *26*, 1443-1451.

YH, S., ZB, D., J, Z., SJ, Q., and J, F. (2009). Prognostic significance of Beclin 1-dependent apoptotic activity in hepatocellular carcinoma. Autophagy *5*.

Yin, X., Cao, L., Kang, R., Yang, M., Wang, Z., Peng, Y., Tan, Y., Liu, L., Xie, M., Zhao, Y., *et al.* (2011). UV irradiation resistance-associated gene suppresses apoptosis by interfering with BAX activation. EMBO Reports *12*, 727-734.

Yue, J., Sun, H., Zhang, W., Pei, D., He, Y., and Wang, H. (2015). Wheat homologs of yeast ATG6 function in autophagy and are implicated in powdery mildew immunity. BMC Plant Biology *15*, 95.

Yue, Z., Jin, S., Yang, C., Levine, A.J., and Heintz, N. (2003). Beclin 1, an autophagy gene essential for early embryonic development, is a haploinsufficient tumor suppressor. Proceedings of the National Academy of Sciences of the United States of America *100*, 15077-15082.

Zhang, Y., Yan, L., Zhou, Z., Yang, P., Tian, E., Zhang, K., Zhao, Y., Li, Z., Song, B., Han, J., *et al.* (2009). SEPA-1 Mediates the Specific Recognition and Degradation of P Granule Components by Autophagy in C. elegans. Cell *136*, 308-321.

Zhao, Z., Oh, S., Li, D., Ni, D., Pirooz, Sara D., Lee, J.-H., Yang, S., Lee, J.-Y., Ghozalli, I., Costanzo, V., *et al.* (2012). A Dual Role for UVRAG in Maintaining Chromosomal Stability Independent of Autophagy. Developmental Cell *22*, 1001-1016.

Zhong, Y., Wang, Q.J., Li, X., Yan, Y., Backer, J.M., Chait, B.T., Heintz, N., and Yue, Z. (2009). Distinct regulation of autophagic activity by Atg14L and Rubicon associated with Beclin 1-phosphatidylinositol-3-kinase complex. Nature Cell Biology *11*, 468-476.

Zhu, H., and He, L. (2014). UVRAG: A Multifunctional Protein with Essential Roles in the Heart. Cardiology & Current Research *1*.